2007-01-12

Kinetics, catalysis and mechanism of methane steam reforming

James Liu
Worcester Polytechnic Institute

Kinetics, catalysis and mechanism of methane steam reforming

Thesis

Submitted to the Faculty

Of the

WORCESTER POLYTECHNIC INSTITUTE

Department of Chemical Engineering

In partial fulfillment of the requirements for the

Degree of Master of Science in Chemical Engineering

by

James A. Liu

January 3, 2006

Professor Ravindra Datta, Advisor
WPI Chemical Engineering Department

Professor Ilie Fishtik, Co-Advisor
WPI Chemical Engineering Department

Professor David DiBiasio, Dept. Head
WPI Chemical Engineering Department

ABSTRACT

The search for an alternative clean and renewable energy source has become an urgent matter. One such energy-saving technology is a fuel cell; it uses fuel as the source of energy to produce electricity directly and the byproducts formed are not as voluminous and environmentally harmful. The conventional low temperature fuel cells use hydrogen as the fuel which is produced from conventional fuels via reforming. However, developing reformers for hydrocarbon fuels requires AN understanding of the fundamental mechanisms and kinetics studies. In this study, simple hydrocarbon fuel, namely methane, in external reforming or internal reforming within a solid oxide fuel cell has been studied because of its importance and with the hope that it will ultimately lead to an understanding of reforming of higher hydrocarbons, such as logistic fuels like JP-8.

For this purpose, methane was used the starting point and building block for the progressive understanding of reforming of complex hydrocarbons. Methane steam reforming (MSR), $CH_4 + 2H_2O = CO_2 + 4H_2$ is, in fact, the most common method of producing commercial bulk hydrogen along with the hydrogen used in ammonia plants. United States alone produces 9 million tons of hydrogen per year. The overall MSR reaction $CH_4 + 2H_2O = CO_2 + 4H_2$ is in fact composed of two reactions, the water gas shift reaction, $CO + H_2O = CO_2 + H_2$, which has recently been investigated by a former Ph.D. student in our group, Caitlin Callaghan. Here, the first reaction $CH_4 + H_2O = CO + 3H_2$, i.e., methane reforming, is analyzed using a reaction route network approach to obtain the overall methane steam reforming network and kinetics.

Kinetics providing detailed information of elementary reaction steps for this system, namely micro-kinetics, has not yet been fully addressed. Employing the theory of Reaction Route Network Theory, recently developed by Fishtik and Datta, and using the Unity Bond Index-Quadratic Exponential Potential (UBI-QEP) method of Shustorovich to predict elementary step kinetics coupled with transition-state theory, a detailed microkinetic model of steam and dry reforming of methane has been developed for Rh(111) and Ni(111) in this thesis.

While there is extensive literature on it, the standard reference on the mechanism and kinetics of MSR is that of Xu and Froment, who proposed a 13 step mechanism.

Based on the assumption of rate limiting steps for these overall reactions, Xu and Froment derived rate expressions for overall kinetics with fitted parameters. Here a more detailed micro-kinetic model of steam reforming of methane has been developed by adding 3 steps pertinent to carbon formation on the catalyst to Xu and Froment's mechanism. The complete set as well as the dominant reaction routes has been identified. This was accomplished first by enumerating the list of reaction routes and drawing this network. A program was written in Maple and was used to assist in creating the list of full routes, empty routes and intermediate nodes. This program reduces the amount of repetitive work that was needed in an earlier Matlab program when computing the list.

After drawing the complete reaction network it was than converted into an equivalent electrical circuit and Multisim analysis was performed. Further, the resistances of various reaction steps were compared. From the reduced graph, it was determined that reaction steps pertaining to desorption of carbon dioxide, i.e., step s_4, and intermediate methylene forming intermediate methylidyne, s_{11}, are the rate limiting steps. Further, through simulation with Multisim, it was determined that in fact only 2 overall reactions are needed. Adding a third overall reaction results in a nodal balance error. A rate expression was developed based on assuming the above two rate determining steps, with remaining steps at pseudo equilibrium along with the quasi-steady state approximation. The rate expression however produced a substantial error in conversion when compared to the overall microkinetic model.

In addition to computing the micro-kinetic model, experimental work for methane steam reforming was conducted. A steam to carbon ratio of 2:1 was fed to the packed bed reactor, where experimental conversion data were obtained. These data points for Ni and Rh catalyst were plotted against the model to see how well the simulation predicted the experimental results. Reasonable agreement was obtained.

ACKNOWLEDGMENT

I would like to thank the following individuals for their assistance, support, guidance and inspiration.

My Advisors:

- Prof. Ravindra Datta, Advisor
- Prof. Ilie Fishtik, Co-Advisor

My Labmates:

- Dr. Caitlin Callaghan
- Saurabh Vilekar
- Amanda Simpson

I would like to acknowledge the Department of Chemical Engineering for providing me this opportunity, Office of Naval Resurch/University Laboratory Initiative, for funding this project.

I would like to thank

- Giacomo P. Ferraro
- Doug White

for assisting me in technical issues with the equipment setup.

Last but not least, I would like to thank my parents, Chin Wen Liu and Whei Chue Shih for supporting me throughout my life.

TABLE OF CONTENTS

TABLE OF FIGURES

TABLE OF TABLES

Chapter 1 Introduction

Since the beginning of the industrial revolution in the 18th century, "fossil fuels in the form of coal, oil, and natural gas have powered the technology and transportation networks that drive society." This threatens the supply of energy and causes enormous strains to the environment[1].

"Worldwide population growth and industrial expansion has led to a seven-fold increase in oil consumption in the past 50 years [1]." In addition, the international energy agency projects a 33% increase in oil consumption by 2020, which would affect the use and number of automobiles in the world. As of June 2002, the US has 2% of the world's oil reserves, and consumes 26% of the world's oil, with only 5% of the world's population living in the US. In addition to this problem, petroleum is becoming increasingly expensive. It is also the current primary source of cheap energy that powers the modern industrial civilization. At the rate that oil and natural gas usage is going, known oil and fossil fuel reserves are not expected to last into the year 2038 [1].

In general, power plants, automobile exhausts, factory smokestacks, and other waste vents of the human environment contribute about 22 billion tons of carbon dioxide (CO_2) and other greenhouse gases into the earth's atmosphere each year. The atmospheric concentration of CO_2 has increased by 31% above pre-industrial levels. These emissions are one of the reasons why global warming is occurring [2].

One promising alternative to fossil fuels is hydrogen, which can mitigate the problems of energy supply and the ill effects of using hydrocarbons. The reaction of hydrogen with oxygen can release energy explosively in heat engines and quietly in fuel cells to produce water as the byproduct. In 2004, 50 million metric tons of hydrogen equivalent to 170 million tons of oil, were produced. Since, hydrogen storage and transport is expensive, most hydrogen is currently produced locally, and used immediately [3].

It has been suggested that fuel cells would be a good way in diminishing the emissions while efficiently utilizing the fossil as well as renewable energy resources that are available. In addition, hydrogen may be produced locally within a reformer to be used in fuel cells rather than transported and stored. Recently, fuel cells have seen remarkable

growth in their technology along with potential applications in transportation, as well as stationary and portable power generation. [2]

In 1838, Swiss scientist Christian Friedrich Schönbein discovered the principle of fuel cells. A few years later, Welsh scientist Sir William Grove developed the first fuel cell using these principles. A fuel cell is an electrochemical device similar to a battery that directly converts the chemical energy of its fuel into electricity. A basic fuel cell is constructed with a thin layer of electrolyte between a cathode and an anode electrode. Typical reactants used in a fuel cell are hydrogen on the anode side and oxygen or air on the cathode side as shown in Figure 1.

There are three main components within a fuel cell: a cathode (air electrode), an anode (fuel electrode) and an electrolyte as seen in Figure 2. In a fuel cell, the hydrogen combustion reaction is split into two electrochemical half reactions, where the spatial separation of these reactions allow electrons from the fuel to flow through an external circuit to perform work before completing the reaction. The electrolyte is to allow ions to flow but not electrons[4].

Hydrogen based fuel cells are considered to be attractive in modern applications for their high efficiency and ideally emission-free use, in contrast to conventional methods of producing electricity than more common fuels such as methane or natural gas that generate substantial carbon dioxide. Fuel cells are devices that can continuously produce electric energy as long as fuel and an oxidant are fed to the electrodes. The chemical energy is directly converted to electricity and heat without involving combustion cycles. The overall efficiency in fuel cells to produce profitable energy is about twice that of conventional combustion engines. For this reason alone, fuel cells are attractive, even if hydrogen is derived from fossil fuels such as methane.

Two fundamental technical problems with fuel cells are: [5]

- Slow reaction rate with impure hydrogen, leading to low currents and power
- The availability of pure hydrogen fuel.

To solve these problems, different fuel cell types have been investigated and there are six classes of fuel cell that have emerged. These systems are summarized in Table 1. PEM fuel cells running on hydrogen may be termed *zero-emission*, because the only emission from this type of fuel cell is water. Unfortunately, hydrogen does not occur

naturally as a gaseous fuel, and so for practical fuel cell systems, it usually has to be generated from whatever fuel source is available, fossil or renewable.

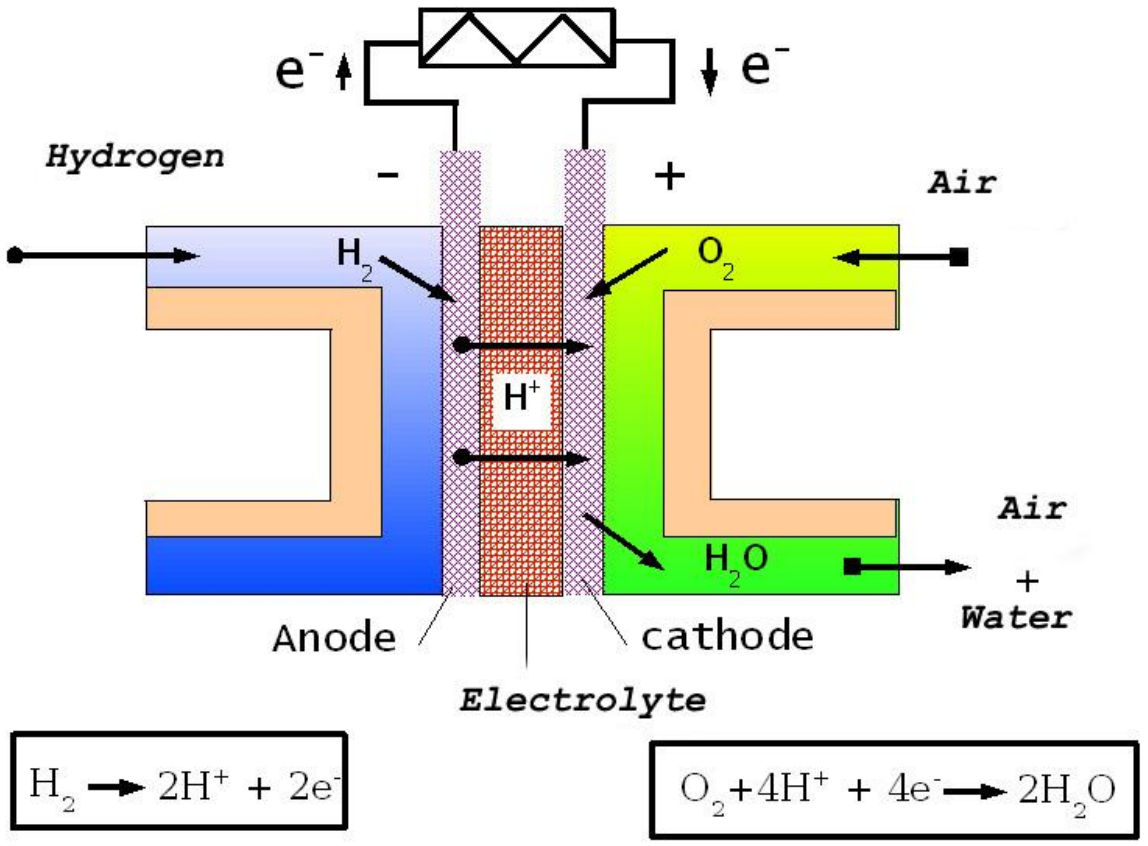

Figure 1 Illustration showing the makeup of a fuel cell and the reaction it uses to produce electricity [6]

Table 1 Comparison for different types of fuel cells [5]

Fuel cell Type	Mobile ion	Operating temperature	Applications and notes
Alkaline (AFC)	OH^-	50-200°C	Used in space vehicles e.g. Apollo, shuttle.
Proton exchange membrane(PEMFC)	H^+	30-100°C	Vehicles and mobile applications
Direct methanol (DMFC)	H^+	20-90°C	Suitable for portable electronic systems of low power, running for long times
Phosphoric acid (PAFC)	H^+	~220°C	
Molten carbonate (MCFC)	CO_3^{2-}	~650°C	Suitable for medium to large – scale systems
Solid oxide (SOFC)	O^{2-}	500-1000°C	Suitable for all sizes of systems

The hybrid fuel cell uses hydrogen as the preferred fuel due to its high reactivity for the electrochemical anode reaction, and its environmentally benign byproduct (water) when hydrogen undergoes oxidation. However, due to lack of ready availability of hydrogen, it is difficult to use fuel cells in most applications. Since this is a dilemma, other types of fuel cells have been developed that utilize conventional fuels directly. The one that stands out the most is solid oxide fuel cell.[5] It does not require pure hydrogen to operate. It is a simple, highly efficient system that can tolerate impurities, and can at least partially internally reform hydrocarbon fuels. Solid oxide fuel cells has the ability to operate at high temperatures in the range of 700-1000^{o}C. The electrolyte of a SOFC is a solid making it better than molten carbonate fuel cell systems that also operate at high temperatures (650^{o}C) and can tolerate impurities. Various fuel options are considered feasible for SOFC operation, which include natural gas (methane), methanol, ethanol, and gasoline.[7]

Solid oxide fuel cells employ a solid ion-conducting ceramic material as the electrolyte and an electronic insulator. Under operation, molecular oxygen is reduced to oxygen anions using electrons supplied from an external circuit at the cathode through the following reaction:

$$O_2\,(g) + 4e^- \rightarrow 2O^{2-} \qquad (1)$$

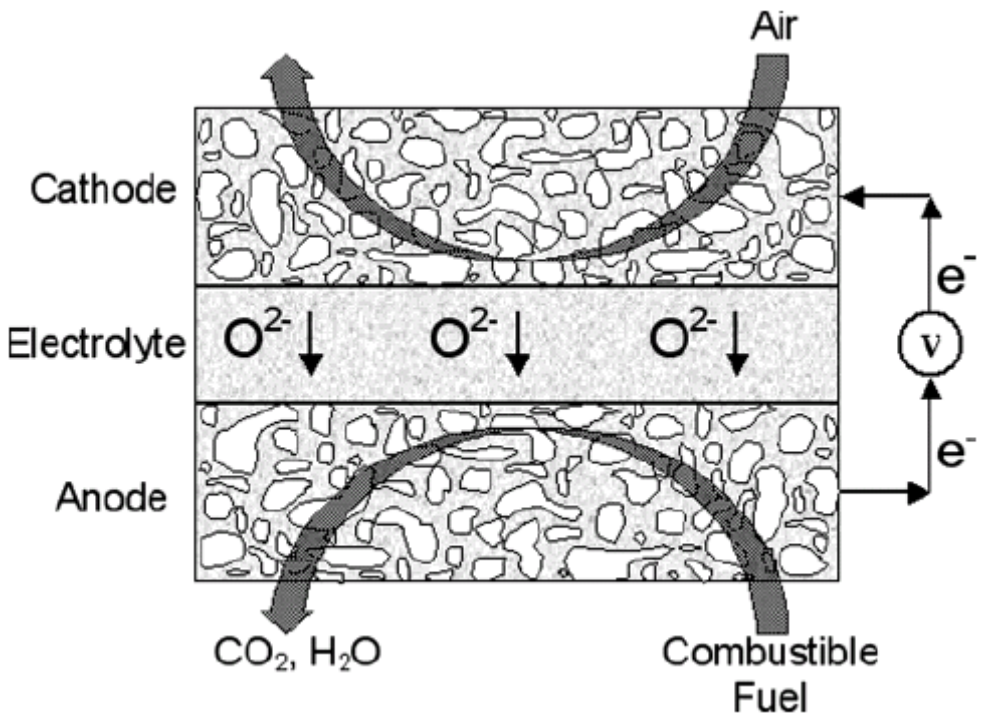

Figure 2 Schematic of SOFC [5]

Since most fuel cells are powered by hydrogen, one major issue is in which way hydrogen will be generated. The most likely solution to generate hydrogen is by extracting it from available fuels ($C_nH_mO_p$), or hydrocarbon fuels such as natural gas (NG), methanol, gasoline or ethanol by a process known as reforming.[5] There are two different kinds of reforming: external reforming, which is carried out before the fuel reaches the fuel cell, and internal reforming, which takes place within the fuel cell anode. In addition, there are three principal pathways that reforming can take and they are steam reforming, partial oxidation, and autothermal reforming. These principal pathways are discussed further in the next chapter.[2]

The generation of hydrogen, or hydrogen-rich product streams, by reforming of hydrocarbons or alcohols, could be categorized into two different processes. The first process is an endothermic method known as steam reforming in which hydrocarbon or alcohol is reacted with steam. The heat required for this reaction is supplied from an external source. [5] The other process is exothermic known as partial oxidation, where the feed reacts with air or pure oxygen. The overall process becomes net heat producing.

For many years, researchers have known that the electrochemical reaction in a stack can provide enough heat to sustain the internal endothermic reforming of low molecular weight hydrocarbons. [5] This has provided many internal reforming concepts that have been applied to molten carbonate and solid oxide fuel cells, on account for their high operating temperatures. In contrast to the steam reforming reactions, the fuel cell reactions are exothermic, because of heat production within the cell caused by the internal resistances. In general there are two approaches to internal reforming, and these are usually referred to as direct (DIR) and indirect (IIR) internal reforming. [5]

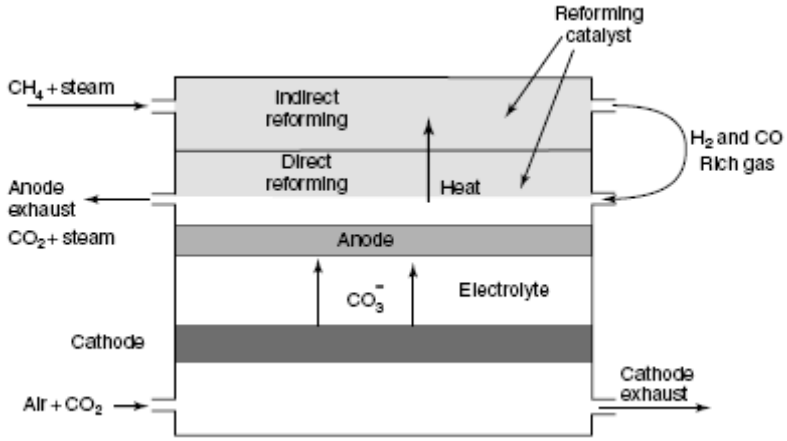

Figure 3 Schematic representation of direct and indirect internal reforming[5]

Indirect internal reforming, also known as integrated reforming, positions the reformer catalyst in a separate chamber in close thermal contact with the stack, which allows the heat production from the exothermic reaction to reform the fuel in the reformer. In direct internal reforming, the reforming reactions are carried out within the anode compartment of the stack. The reforming catalysts are placed within the channels of the fuel cell. For SOFC's, the reactions can be performed directly on the anode catalyst as well, although the reactions are limited by the amount of catalyst. [5]

Chapter 2 provides an overview of steam reforming and reforming processes. In addition, discussion of several studies related to types of catalysts used in steam reforming and the performance of these catalysts will be provided. A review of the effect of the active metal, and support on the performance of the catalyst is presented. Additionally, reaction mechanism and kinetic details of steam-reforming are provided.

Chapter 3 is an overview of microkinetics and reaction route graph theory. Details of the theories used to predict the energetic parameters of the elementary steps are provided. These include the Unity Bond Index-Quadratic Exponential Potential (UBI-QEP) to determine the activation energy and reaction enthalpies, along with the transition-state theory to estimate the pre-exponential factors of the elementary reactions. Some of the reaction route graph theories are also presented here. Chapter 5 utilizes these theoretical tools to provide examples of calculations of methane steam reforming full routes, empty routes and intermediate nodes. Further, a reaction route graph of methane steam reforming is presented here.

Chapter 6 introduces the methane steam reforming microkinetic model by analyzing, simplifying and reducing with the reaction route graph theory. The results of Chapter 6 are experimentally validated using the experimental results described in Chapter 4. Chapter 7 provides conclusion and suggestions that are needed to extend the research.

Chapter 2 Catalytic Reforming

A hydrogen economy has become an interest of the world. Steam reforming reactions will play a key role in new applications of synthesis gas and in a future hydrogen economy. In this chapter, types of reforming processes to obtain hydrogen are discussed. In addition, some recent studies on types of catalysts, properties of the catalytically active metal and the catalytic role of the support are addressed. Further, the reaction mechanisms and some kinetic details of methane steam reforming are consulted.

2.1 Steam Reforming, Autothermal Reforming and Partial Oxidation

In broad terms, steam reforming (SR) is a process of producing hydrogen by combining steam and hydrocarbon and reacting in a reformer at temperatures above 500^{o}C in the presence of a metal-based catalyst. [5] In principle, there are three types of reforming processes:

- Steam Reforming
- Partial Oxidation
    - (Non-Catalytic) Partial Oxidation (POX)
    - Catalytic Partial Oxidation (CPO)
- Autothermal Reforming

Often times, autothermal reforming is grouped under partial oxidation, because partial oxidation may be carried by a combination of non-catalytic oxidation and steam reforming[8]. The advantage of partial oxidation and autothermal reforming is that these processes are self-sustaining and do not require external provision of heat. However, they are less efficient in producing hydrogen.

Steam Reforming

Steam reforming of methane consists of three reversible reactions: the strongly endothermic reforming reactions, 2 and 4, and the moderately exothermic water-gas shift (WGS) reaction 3. [5]

$CH_4 + H_2O \leftrightarrows CO + 3H_2$ [ΔH = +206 kJ mol-1] (2)
$CO + H_2O \leftrightarrows CO_2 + H_2$ [ΔH = -41 kJ mol-1] (3)
$CH_4 + 2H_2O \leftrightarrows CO_2 + 4H_2$ [ΔH = +165 kJ mol^{-1}] (4)

The basic reforming reaction for a generic hydrocarbon C_nH_m may be written as:

$$C_nH_m + nH_2O \leftrightarrows nCO + (\frac{m}{2} + n)H_2 \quad (5)$$

Reactions 2 and 5 have also been termed "oxygenolysis" for the corresponding "pyrolysis" and "hydrogenolysis" of hydrocarbons.[9] CO_2 is not only produced through the shift reaction 3, but also directly through the steam reforming reaction 4. In fact reaction 4 results from the combination of reaction 2 and 3. Because of the endothermic behavior of steam reforming, high temperature is favored. In addition, because volume expansion occurs, low pressure is favored. In contrast, reaction 3 the exothermic reaction is favored by low temperature, while changes in pressure have no effect. Reforming reactions 2 and the associated water gas shift reaction 3 are carried out normally over a supported nickel catalyst at elevated temperatures, typically above 500^oC.

Reactions 2 and 4 are reversible and normally reach equilibrium over an active catalyst, at high temperatures. The overall product gas is a mixture of carbon monoxide, carbon dioxide, hydrogen, and unconverted methane and steam. The temperature of the reactor, the operating pressure, the composition of the feed gas, and the proportion of steam fed to the reactor governs the product from the reformer.

The amount of carbon monoxide produced through steam reforming of methane is quite high; because the water gas shift reaction, shown in equation 3, is thermodynamically favorable at higher temperatures. The amount of carbon monoxide in the final product from the steam reforming of methane is determined by the thermodynamics and kinetics of the reaction within the reformer. This also determines the downstream processes necessary to reduce CO concentration, which is desired by proton-exchange membrane. This is accomplished by a combination of WGS reactions at lower temperatures and the preferential oxidation reaction. For solid oxide fuel cell, the

CO concentration has to be reduced so additional hydrogen may be produced providing high WGS activity at the anode side. [10]

Steam reforming is the most important route for large scale manufacture of synthesis gas for ammonia, methanol, and other petrochemicals and for the manufacture of hydrogen for refineries. In general, reforming reactions are catalyzed by group 8-10 metals with nickel as the preferred metal for industrial application because of its activity ready availability and low cost. Methane is activated on the nickel surface. The resulting CH_x species then reacts with OH species adsorbed on the nickel or on the support.[8]

Steam reforming process is divided into two steps: a section at high temperature and pressure (typically 800-1000C and 30-40 bar) in which the reforming and shift reaction occurs, followed by an additional two-step shift section at a lower temperature (typically at 200-400C) in order to maximize the CO conversion.

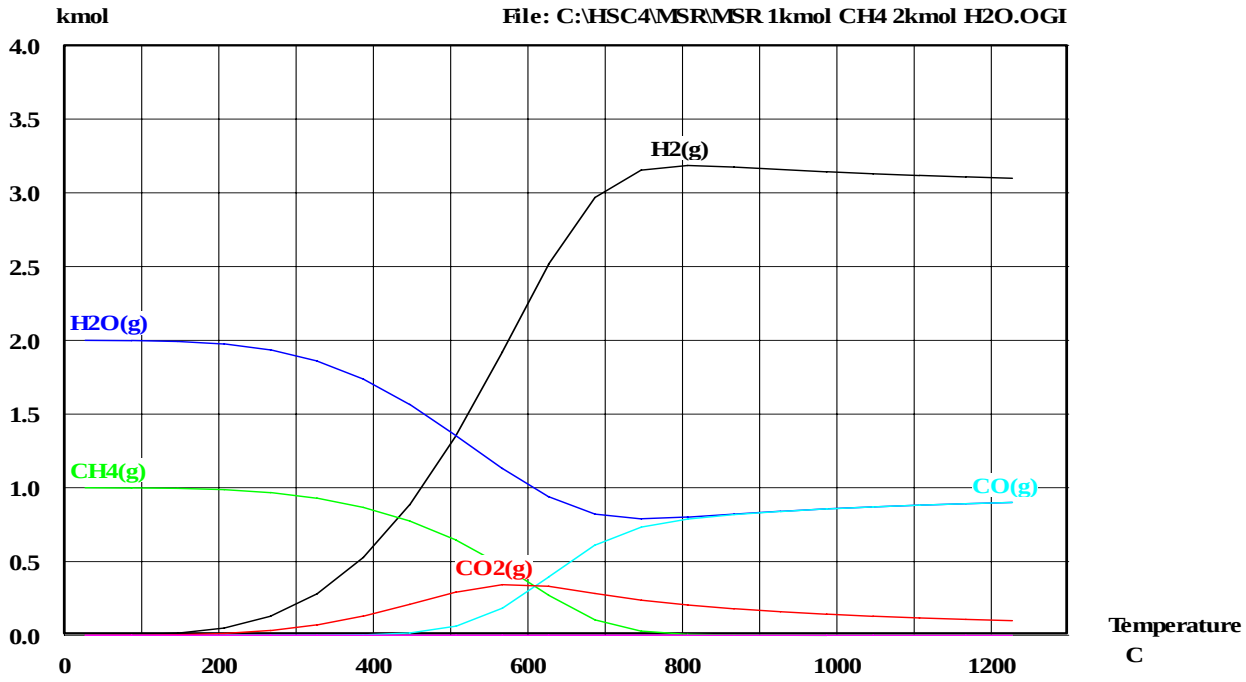

Figure 4 Theoretical Thermodynamic Calculation of MSR 2:1 S/C

This is done because thermodynamics of the WGS reaction are more favorable at lower temperatures, also WGS activities declines rapidly with temperature. Typically, a 3:1 ratio of steam to carbon (S/C) is used to obtain high methane conversion and carbon monoxide and carbon dioxide selectivity. Joensen and Rostrup-Nielsen showed a typical

equilibrium conversion graph of steam reforming of methane against temperature, pressure and steam/carbon ratio.[11] It can be observed from the graph that in order to maintain a high methane conversion, it is necessary to operate the system at high temperature, low pressure, and relatively high steam to carbon ratio.

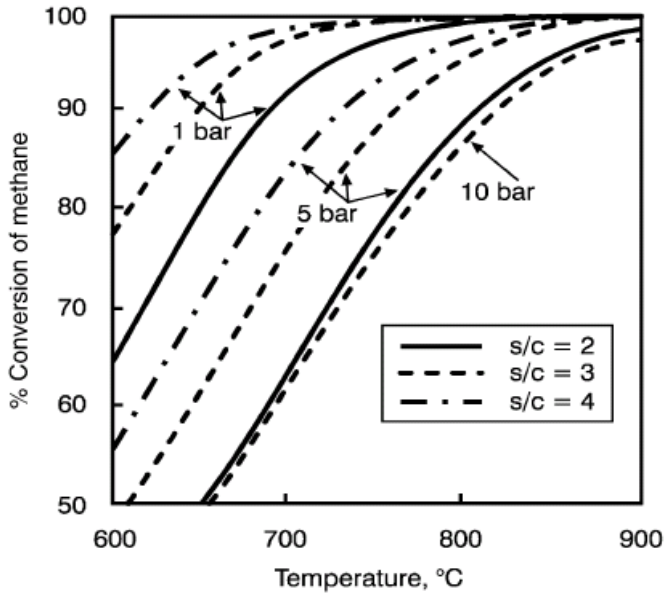

Figure 5 Equilibrium conversion of steam reforming of methane against temperature, pressure and steam/carbon ratio.[11]

At high temperatures about 920 K, the hydrocarbons may react in parallel to reaction 1 by thermal cracking causing formation of coke. [9]

Ming et al. [12] conducted a 300 h continuous test using a proprietary catalyst by InnovaTek for steam reforming of iso-octane at 800^{o}C with a steam/carbon ratio of 3.6. Figure 6 displays the product composition of steam reforming of iso-octane at different temperature with 8.0g of catalyst. Ming also used the catalyst for steam reforming of hexadecane for 73h, shown in Figure 7, as well as natural gas for over 150h continuously without deactivation or carbon deposition shown in Figure 8. These figures provide typical behavior of steam reforming process.

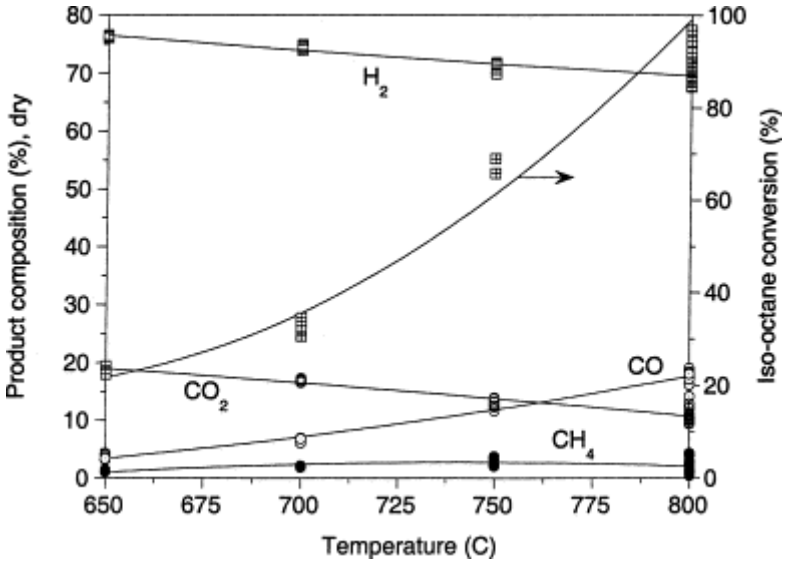

Figure 6 Product composition (H_2, CO, CO_2, and CH_4) and iso-octane conversion for steam reformed iso-octane at different reaction temperatures using 8.0 g ITC catalyst; ratio of $H_2O/C = 3.6$ at a feed rate of 0.28g/min [12]

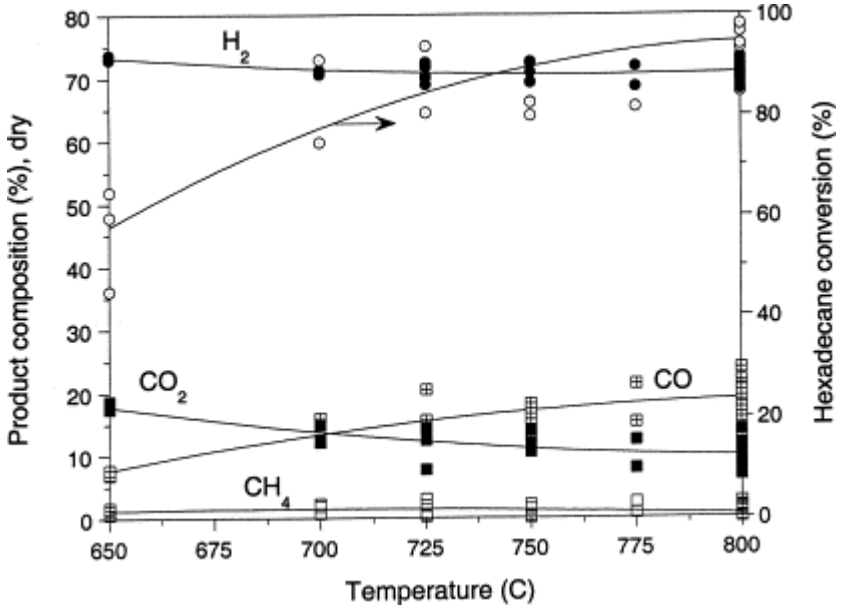

Figure 7 Product composition and hexadecande conversion for steam reformed hexadecane at different temperatures using 5.0 g ITC catalyst at different reaction temperatures; ratio of H2)/C pf 2.7 with a feed rate of 0.14 g/min. [12]

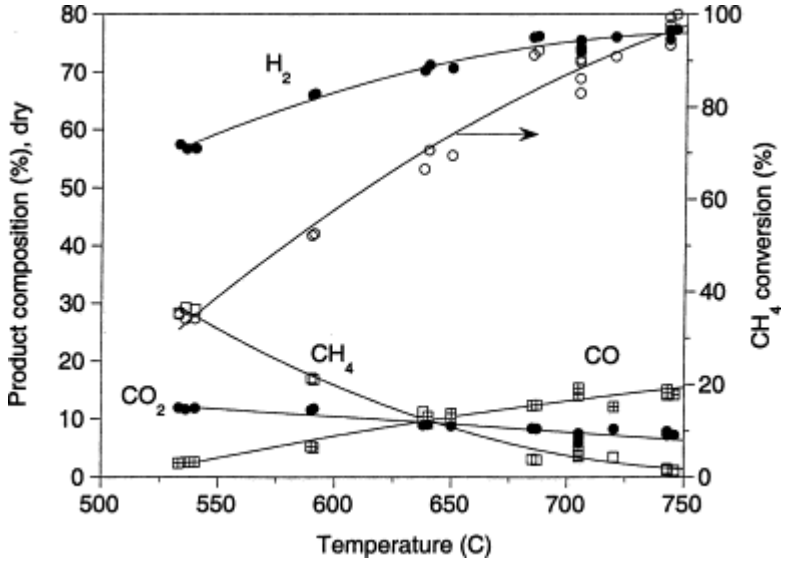

Figure 8 Product composition (H2, CO, CO2, and CH4) for steam reformed methane at different temperatures using 1.45 g ITC catalyst; ratio of H2O/C was 3.0; methane feed rate was 300 ml/min. [12]

In the past, much attention has been placed on the preparation of catalysts and the evaluation of the process and equipment with little work being done on the kinetics and mechanism of the reaction. As a result, kinetic data are lacking and contradictory mechanisms have been proposed. Some early groups, such as Temkin and Xu and Froment, have worked on methane steam reforming have investigated the kinetics mainly with Ni catalysts.

Temkin [13] studied reforming kinetics on nickel foil at atmospheric pressure in circulation flow system. These experiments were conducted in the temperature range of 470-900^{o}C. At 900^{o}C the rate of the reforming reaction is a first-order equation $=W = k \times P_{CH_4}$, where P_{CH_4} is the partial pressure of the methane and k the rate constant. They also discovered that the ratio of the partial pressures in the exit mixture was approximately close to the equilibrium constant of the water gas shift reaction at 800^{o}C. A retardation of the rate of the reforming by hydrogen was observed at 470-530^{o}C.

To take this consideration of retardation, Xu and Froment improved the model of rate of the reforming. Xu and Froment [14] studied steam reforming on Ni/$MgAl_2O_4$ catalysts, with nickel surface area of 9.3 m^2/g and void fractions of 0.528. They mixed 0.4g of catalyst with about 8 mL of α-alumina diluent. A molar ratio feed of 5 H_2O/CH_4, molar ratio of 1.25 H_2/CH_4 were used for testing the activity of the steam reforming. Xu and Froment noticed an immediate drop of activity within the first 24 hours, but then much more gradually. The kinetic study commenced after 70 hrs. This same procedure was used to for the reverse water-gas shift with a molar ratio of 1 H_2/CH_4 [14]. The set of conditions used are presented in Figure 9[14].

Pres. bar	H_2O/CH_4 molar	H_2/CH_4 molar	Temp. K
Steam Reforming			
5.0	5.0		
5.0	3.0		
10.0	3.0	1.25	773, 798, 823, 848
15.0	5.0		
3.0	5.0		
3.0	3.0		
Pres. bar		H_2/CO_2 molar	Temp. K
Reverse of Water-Gas Shift and Methanation			
8.0			
10.0		1.0, 0.5	573, 598, 623, 648, 673
3.0			
10.0			

Figure 9 Xu and Froment's experimental conditions [14]

In addition, Xu and Froment provided rate expressions with fitted parameters. These rate expressions are provided in section 2.5. From these rate expressions, Xu and Froment observed that the predicted rates would become infinite as the partial pressure of hydrogen is zero. The cause of this can be traced back to the reaction mechanism of hydrogen adsorption; however, in the application of the equation would not be a problem since feed generally contains some hydrogen or higher hydrocarbons that rapidly transform into hydrogen.

A more recent group that have been quite active in the area of methane steam reforming have used isotopic tracer and kinetic studies to probe the identity and reversibility of elementary steps on supported noble clusters and turnover rate on catalytically relevant noble metals. Wei and Iglesia [15]came up with a simple mechanistic proposal for reaction of CH_4 with CO_2 and H_2O for its decomposition on Pt cluster and water gas shift reactions. They noticed that the reforming and decomposition rates were first order in CH_4 concentration and are solely limited by C-H bond activation on metal cluster surfaces. They observed that higher dispersion of Pt produces higher CH_4 turnover rates for CO_2 reforming, H_2O reforming, and CH_4 decomposition reactions. The effects of the support influences the dispersion of the noble metal rather then the turnover rates.

Partial Oxidation

An alternative to reforming is partial oxidation, which is endothermic. It may be carried out through catalytic partial oxidation (CPO) or by non-catalytic partial oxidation (POX) or by autothermal reforming (ATR). [11] The general form of partial oxidation is:

$$CH_4 + \frac{1}{2} O_2 \rightarrow CO + 2H_2 \qquad [\Delta H = -247 \text{ kJ mol}^{-1}] \qquad (6)$$

$$CH_4 + 2O_2 \rightarrow CO_2 + 2H_2O \qquad [\Delta H = -801 \text{ kJ mol}^{-1}] \qquad (7)$$

Catalytic partial oxidation (CPO) uses catalysts to activate the reaction as opposed to non-catalytic partial oxidation (POX) that is carried out at high temperatures, typically 1200 to 1500^{o}C without a catalyst. Non-catalytic oxidation has an advantage over catalytic process in that material such as sulphur compounds do not need to be removed, until a later stage. Catalytic partial oxidation does not require operating at very high temperature, but entails the removal of sulfur which poisons the catalyst. [5]

High temperature partial oxidation can also handle much heavier petroleum fractions than catalytic processes and is therefore attractive for processing diesels, logistic fuels, and residual fractions. These fuels have removed in large scale operations, however it is difficult to scale down, and control the process. The common catalysts used for this process have been supported platinum-metal or nickel based catalysts. [5]

Comparing reaction 6 to reaction 4, it is seen that partial oxidation produces less hydrogen per molecule of methane. This means that partial oxidation is less efficient than steam reforming for fuel cell applications. Partial oxidation is an exothermic reaction that can be used to provide heat for the endothermic steam reforming reaction in autothermal reforming. A commonly used method in fuel processing is the autothermal reforming method, in which both steam and oxidant are fed with the fuel to a catalytic reactor. Therefore it can be considered as a combination of partial oxidation and the steam reforming process. The endothermic steam reforming reaction and the exothermic partial oxidation reaction occur together, so that no heat needs to be supplied or removed from the system.

Autothermal Reforming

Autothermal reforming combines the heat effects of the exothermic partial oxidation and endothermic steam reforming reactions by feeding fuel, water, and air together into the reactor. The steam reforming reaction absorbs part of the heat generated by the oxidation reaction, limiting the maximum temperature in the reactor. [11] This method, hence needs less steam compared to conventional reforming and practically all of the heat for the reforming reaction is provided by partial combustion of the fuel, so that external heating is not required. [5]

$$CH_4 + \frac{3}{2} O_2 \rightarrow CO + 2H_2O \qquad [\Delta H = -519 \text{ kJ mol}^{-1}] \qquad (8)$$

Dreyer et al. [16] performed autothermal steam reforming of higher hydrocarbons such as n-decane, n-hexadecande, and JP-8 fuel with Rh as the catalyst and observed that for carbon to oxygen ratios of 0.7 to 1.5 and for steam to carbon feed ratios from 0.0 to 4.0, the reactor operated autothermally while H_2 to CO ratio increased from ~1 to ~4.0. Their experimental results are displayed in Figure 10 and Figure 11.

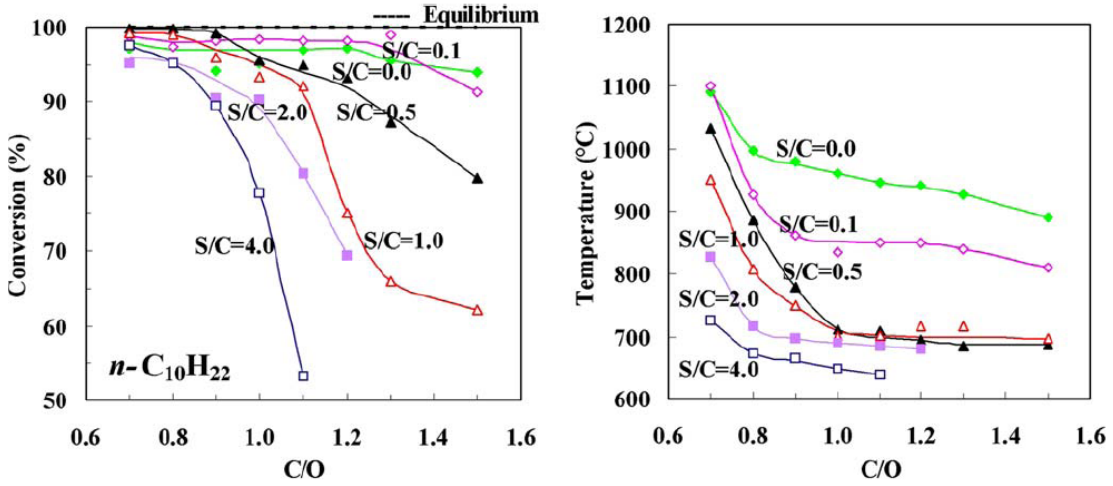

Figure 10 Effect of *n*-decane/oxygen (C/O) and steam/*n*-decane (S/C) ratio on the fuel conversion in autothermal reforming [16]

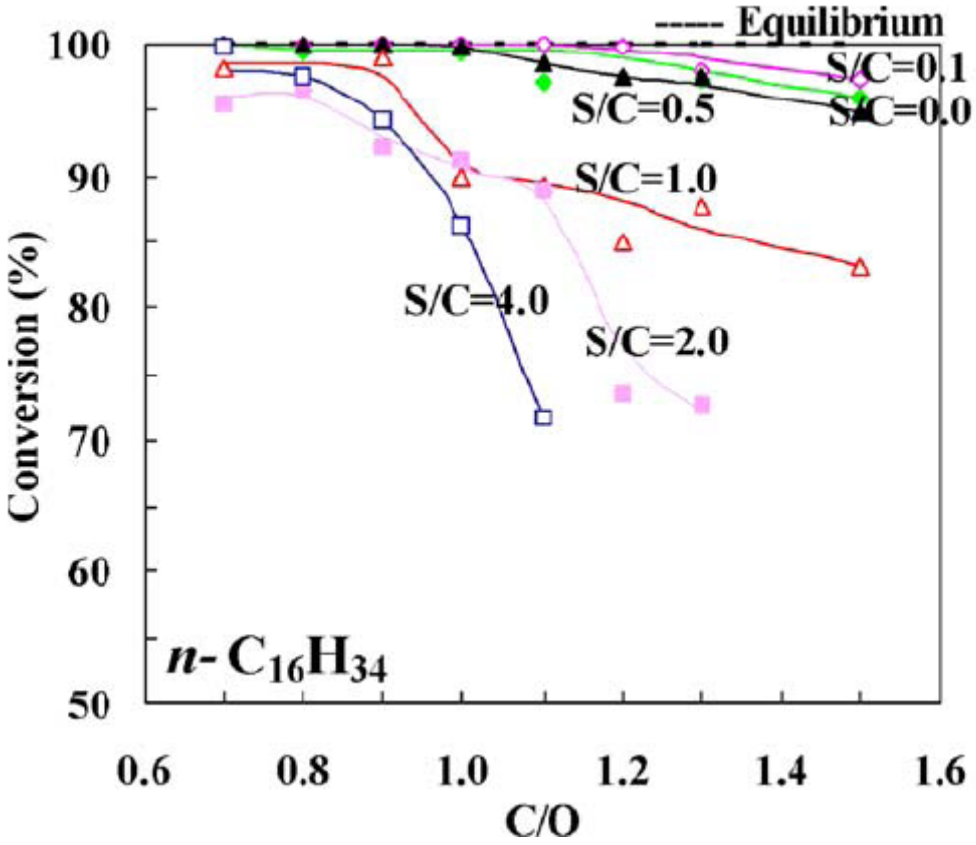

Figure 11 Effect of *n*-hexadecane/oxygen (C/O) and steam/*n*-hexadecane (S/C) ratio on the fuel conversion in autothermal reforming [16]

2.2 Steam Reforming and Partial Oxidation Catalysts

There has been extensive amount of work on steam reforming catalysts; however, in this chapter of the literature review, a few more current steam reforming catalysts used in fuel processing technology and in fuel cells are highlighted. Further reading of earlier literature may be found elsewhere. Recent work on various catalysts is summarized below.

2.2.1 Rhodium Catalyst

Rhodium coated α-Al_2O_3 foam monoliths were used by Horn, et al. [17] to investigate the mechanism of catalytic partial oxidation of CH_4 by measuring and comparing the species and temperature profiles with numerical simulations. The α-Al_2O_3 foams were 10mm in length, and 16.5mm in diameter; with 80 pores per linear inch. A loading of ~6wt% Rh by wet incipient method was used. The reaction was carried out in a quartz tube, where carbon to oxygen (C/O) ratios of 0.7, 1.0, and 1.3 were used under autothermal operation.

They demonstrated that the 2D numerical simulation compared relatively well to the measured profiles for all experimental conditions. Complete O_2 conversion was achieved within 2 mm of the catalyst entrance for all C/O ratios and flow. Further, H_2 and CO were found to be formed after O_2 was fully converted by steam reforming and partly in the oxidation zone. With a C/O of 0.7, some water gas shift was observed, while at other ratios CO_2 was formed at small amounts in the oxidation zone and remained constant thereafter.

Ce-ZrO_2-supported Rh catalyst was studied by Kusakabe et al. [18] to determine whether or not this catalyst is highly active and stable in membrane reactor for methane conversion and CO selectivity for a temperature range of 500-800^oC. The highest activity, where methane conversion was 28.1% at 500^oC, was obtained with 3 wt% Rh/ $Ce_{0.15}Zr_{0.85}O_2$ catalyst.

Wanat et al. [19] studied ethanol as a renewable, portable, and non-toxic liquid fuel for the possible source of hydrogen for PEM fuel cells. They used Rh and Rh-Ce across an auto-thermal wall for ethanol steam reforming, while using Pt-Ce catalyst for water-gas shift part of the steam reforming. It was observed that complete conversion of

ethanol with 90% selectivity could be achieved at 800°C.[20] Further, using Rh catalyst for steam reforming and Pt/Ce catalyst for water-gas shift, an effluent stream with an H_2/CO ratio of 42/1 was obtained. [21] Wanat et al. found a steam/carbon ratio of 3/1 to give a conversion of 99% for ethanol along with a H_2/CO ratio of 3/1.

Liguras et al. [20] studied the catalytic performance of supported noble metal catalysts for the steam reforming of ethanol in the temperature range of 600-850°C with respect to the nature of the active metallic phase, the nature of the support and the metal loading. They observed that Pt is not as active as Rh, which is significantly more active and selective for hydrogen formation compared to Ru and Pd.

2.2.2 Nickel Catalyst

Ce-ZrO_2-supported Ni catalysts were studied by Kusakabe et al [18]. They performed methane conversion and CO selectivity tests at temperatures of 500-800°C to see if $Ce_{1-x}Zr_xO_2$ supported with 10 wt% Ni loading is active and stable in membrane reactor.

The catalyst showed the highest CH_4 conversion at 500-600°C and a high H_2/CO ratio caused by the oxidation of CO through water-gas shift reaction.

Activity tests of steam reforming of methane, at 673-823 K under atmospheric pressure in a continuous-flow reactor, on catalysts prepared by Huang et al [10] were conducted on 2 wt% Ni supported on samaria-doped ceria, gadolinia-doped ceria, and α-Al_2O_3, as well as SDC-supported Ni-Cu catalysts with 0.5 wt % Ni or Cu and addition of 0.01-0.1 wt % Cu or Ni. Gadolinia-doped ceria, yttria-doped ceria and the samaria-doped ceria were prepared by a coprecipitation method. A gel was formed when an atomic molar ratio 1:9 of Gd/Ce, Y/Ce, or Sm/Ce dissolved in deionized water undergoes hydrolysis of metal salt to hydroxide by dropping the solution into NH_4OH while stirring to keep the pH of the solution greater than 9. Doped-ceria-supported nickel catalyst was prepared by impregnating the doped-ceria prepared above with nickel nitrate. Both samaria-doped ceria supported Ni-Cu catalyst and α-Al_2O_3 supported nickel catalyst were prepared the same way as the doped-ceria-supported catalysts, by impregnation [10].

The results indicated that the weighting of the WGS activity decreases with increasing temperature. Variation of the WGS weighting is larger with doped ceria as the support than with α-Al_2O_3. The addition of Cu to Ni catalyst enhances the activity of WGS[10].

Often times, ceramic-supported nickel catalysts are used in steam reforming, and because of this, the supported catalyst would suffer from deactivation by particle sintering or by reaction with supports, thermal deterioration of the support, and carbon deposition. It has been reported by Rostrup-Nielsen et al that porous supports can affect the sintering process and the morphology of the support can change under sintering conditions. Because of this, Rakass, et al. [22] studied steam reforming of methane over unsupported nickel powder catalysts as a catalyst in internal or external reforming of solid oxide fuel cell systems.

The unsupported Ni catalyst (Inco Ni 255) is a pure nickel powder with a BET surface area of 0.44 m^2g^{-1}. The catalytic activity was conducted in a seven-cell differential reactor system. The partial pressure of water in the gas was used to regulate the CH_4:H_2O ratio. It was observed that CH_4 conversion increased and coke deposition decreases significantly with a decrease of CH_4:H_2O ratio. Thermodynamic equilibrium was achieved at a CH_4:H_2O ratio of 1:2. CH_4 conversion of 98±2 % was achieved at 700^o C and no coke was generated. This compares favorably with supported Ni catalyst systems. In conclusion, a ratio of 1:2 of fuel to water showed that unsupported Ni catalyst exhibited high catalytic activity and stability during the reforming of methane at low-mid temperature range.

2.2.3 Ruthenium Catalyst

Ru-added Ni catalysts supported on Al_2O_3 or $MgAl_2O_4$ were prepared by Jeong et al. [23] for methane steam reforming to investigate Ru-induced effects on the catalytic activity.

Berman et al [24] performed kinetic studies of methane steam reforming on Ru/(α-Al_2O_3 + MnO_x) catalysts in a flow reactor operated in a differential mode in the temperature range of 500-900^{o}C and total pressure of 1-7 atm. They observed an unchanged activity of the catalyst in steam reforming of methane at 1100^{o}C for 100 h.

Ishihara et al. [25] studied the effect of the addition of ruthenium on nickel steam reforming catalysts supported by MgO, La_2O_3, and Al_2O_3. Using m-cresol as fuel, they discovered that the presence of ruthenium enhances the catalytic performance of the Ni-based catalyst when the loading of ruthenium was increased up to 15 wt%. In addition, did a study of loading Ni up to 15% onto a Ru-based catalyst, and found that it too enhanced the catalytic activity of the catalyst. Further, they developed a bimetallic catalyst consisting of 2 wt% Ru – 15 wt% Ni and found a reasonably high resistance to carbon deposition.

2.2.4 Platinum Catalyst

Souza et al. [26] studied autothermal reforming of methane, by combining partial oxidation and reforming of methane with CO_2 or steam, carried out on Pt/Al_20_3, Pt/ZrO_2 and Pt/CeO_2 catalysts, in a temperature range of 300-900 ^oC. They prepared the catalyst through incipient wetness impregnation of the calcinated γ-alumina (Engelhard Corporation Catalyst), zirconium hydroxide (MEL Chemicals) and cerium ammonium nitrate (Aldrich) supports. The study took place within a fixed bed flow type quartz reactor, where a total feed flow rate of 200 cm^3/min with He. Carbon deposition was measured through thermogravimetric analysis (TGA).

It was observed that the support played an important role in the activity of the catalyst. Pt/ZrO_2 catalyst showed the highest initial activity but deactivated very fast due to coking; however Pt/CeO_2 had higher stability with coking resistance due to the support and Pt interaction allowing CO_2 dissociation to occur on the surface. They observed a two-step mechanism that many authors have proposed for the partial oxidation of methane with CO_2 reforming and partial oxidation of methane. In the first step of the mechanism, methane combustion takes place producing CO_2 and H_2O; followed by the second step where synthesis gas is produced through CO_2 and steam reforming of un-reacted methane.

McMinn et al. [27]studied the catalyst deactivation in steam reforming of trichloroethylene on $Pt/\gamma\text{-}Al_2O_3$. In general, coking occurs as a product of CH_4 decomposition, hydrocarbon hydrogenolysis, and CO disproportionation. Cracking,

condensation, and hydrogen abstraction occurs on the support γ-Al_2O_3. When coking occurs, the catalytic sites are covered, pores are plugged, and the catalyst will fracture. They showed that chlorine decreases the water gas shift activity.

2.2.5 Palladium Catalyst

Chin et al. [28] investigated methanol steam reforming over highly active Pd/ZnO catalyst. They prepared the catalyst through impregnation using $Pd(NO_3)_2$ solution containing 20.19 wt% Pd onto ZnO powder with a solution to solid ratio of 0.58 ml/g. Various catalyst characterization techniques such as TEM, TPR, chemisorption, and XRD were used to evaluate the performance of the catalyst. They noticed high activity and very low selectivity of CO.

Agrell et al. [29] studied partial oxidation of methanol over ZnO supported catalysts. The catalyst was prepared by microemulsion technique. Berol 02 (nonylphenolethoxylate, NP-5) was used as both precipitation and deposition medium. Pd^{2+} was reproduced by using hydrazine, followed by deposition of Pd onto ZnO by chemical destabilization of the suspension. After the preparation, they performed the effect of the catalytic activity and product distribution studies of various Pd particle sizes between 230-300^oC while providing stoichiometric feeds. A correlation between CO selectivity and Pd particle size was seen. This correlation was higher CO selectivity with increasing particle size.

Most studies done on palladium have been with methanol; however, Goula et al. [30] performed steam reforming of ethanol on alumina supported palladium catalyst. The catalysts used were from Precious Metal Corporation, with 5 wt% Pd on Al_2O_3 and are between 300-500μm in particle size. The catalytic performance was conducted in the temperature range of 220-770^oC. They observed hydrogen selectivity of up to 95% when temperature values were close to 650^oC. When the ratio of steam to ethanol is equal to the stoichiometric one, carbon formation becomes negligible and when the steam to ethanol ratio is below the stoichiometric value, the usual carbon formation occured and deactivated the catalyst.

2.3 Active Metal Surface

Metals of group VIII of the periodic table are active for steam reforming reactions [9]. Liguras et al. [20] suggest that the noble metals have an activity of this order: Rh>Pt>Pd>Ru; however, Rostrup-Nielsen [31] has observed an activity sequence of Ru, Rh>Ir>Ni, Pt, Pd. It has also been said that nickel at higher loadings is equally effective with Rh, Pt, and Pd [27].

In general, the activity of a catalyst is related to its metal surface area i.e., the number of active sites. The catalytic activity of a given metal benefits from a high dispersion of the metal particles. For Ni catalysts, the dispersion of the metal particle is 2-5%, with metal particles of 20-50 nm. It has been shown that a loading of 15-20 wt% of Ni does not produce any increase in activity[9].

Apart from the amount of available metal surface area, the structure of the available surface area strongly influences the catalyst activity. It has been noticed that close packed (111) surface of nickel is less active than the more open (110) surface. Smith et al, [32] has shown that some lattice distortion is required to play a role in the catalytic reaction. Wei and Iglesia et al [33] investigated catalytic activity of catalysts with different loadings of Rh on Al_2O_3 and ZrO_2 supports. They found that methane turnover rates increased with decreasing Rh clusters [33]. Unsaturated Rh surface atoms prevalent in smaller clusters activate C-H bonds more effectively than atoms on lower-index surfaces.

Rostrup-Nielsen concluded that the activity per unit metal surface area decreases with increasing dispersion[9]. The reason for this is due to a decrease of large ensemble landing sites on the smaller particles. It can also be explained as a change in electronic state of the metal particles. Yokota et al. showed this by studying dry reforming reaction using methane and carbon dioxide on Rh supported on various metal oxides. [34] They saw that Rh-based catalysts with high dispersion may result in a less metallic and less reactive character for Rh particles.

2.4 Catalyst Support

It is often found that the support plays an important direct or indirect role in the reaction steps involved in a catalytic process. As discussed in chapter 2, the same active metal on different support produces different conversion and yields. The support determines the dispersion of the catalytically active metal particles and the catalyst's resistance to sintering. In general, the role of the support is literally to provide a surface support for dispersing the catalytically active metal, in order to obtain a stable and high activity metal surface. Most common supports for methane reforming are α- and γ-Al_2O_3, MgO, $MgAl_2O_4$, SiO_2, ZrO_2 and TiO_2. These supports have good porosity, which allows larger surface area. Support plays a crucial role since it determine the final particle size of the metal, with its pore structure, morphology, and phase transitions that it can undergo. In addition, a support can have a chemical role as well, by activating one or more reaction steps.

Wang et al. showed that strong interaction between metal and support would make a catalyst more resistant to sintering and coking, which would create a more stable catalyst[35].

Bradford et al. [36] found that Ni-Ni bonds for Ni/MgO catalysts can be stabilized by NiO-MgO solid solution. In addition it can prevent carbon diffusion into nickel particles. In addition, they noticed that the support influences the catalyst activity by varying the electron donating ability of the reduced nickel surfaces. With the Ni/TiO_2 study, they found that a strong metal-support interaction occurs, which would cause blockage of the active nickel sites. These blockages are due to the migration of TiO_x-species from the TiO_2-carrier [36].

These few examples show the influence of the support on catalysts. However, a support can also participate in catalytic reactions. Supports with a basic nature, such as MgO, are known to enhance the activation of steam, and dissociation of steam into OH and H species. Carbon deposits can lead to active site blocking and affect the catalyst reactivity and stability. The support can also play a role in suppressing carbon deposition. ZrO_2 and CeO_2 have been known to be able to oxidize deposited carbon. Further, they are capable of participating in the catalytic reaction by oxidizing or reducing reaction intermediates.

Dong et al. studied methane reforming over $Ni/Ce_{0.15}Zr_{0.85}O_2$ catalysts[37]. They observed that there were two kinds of active sites that exist, one for methane activation and one for steam or oxygen activation. Ceria, has the ability to store, release, and transfer oxygen species, which results in an enhanced ability to prevent carbon formation. They also found that part of the Ni incorporates in the surface of the $Ce_xZr_{1-x}O_2$ support and the resulting strong interaction between NiO and the $Ce_xZr_{1-x}O_2$ matrix inhibits the reduction of NiO.

2.5 Reaction Mechanisms and Kinetic Details of Steam-Reforming

The reaction mechanism of steam reforming is dependent on the catalysts, primarily on the active metal and the nature of the support. Early work on the kinetics of the steam reforming of methane was based on the assumption that the methane adsorption. Khomenko et al. avoided the discussion of rate determining step by using the quasi steady-state approximation in terms of the Temkin identity. He was able to come up a rate expression for the temperature range of 470-700^{o}C. [38]

$$r = \frac{k \cdot P_{CH_4} \cdot P_{H_2O}\left(1 - \dfrac{P_{CO}P_{H_2}^3}{K_{eq}P_{CH_4}P_{H_2O}}\right)}{f\left(P_{H_2O}, P_{H_2}\right)\left(1 + \dfrac{K_{H_2O}P_{H_2O}}{P_{H_2}}\right)} \tag{9}$$

where, K_{eq} is the equilibrium constant for the overall reaction and $f(P_{H_2O}, P_{H_2})$ is a polynomial in P_{H_2}, and P_{H_2O}.

One of the earliest proposed rate expressions based on detailed reaction mechanism were provided by Xu and Froment[14]. They studied the kinetic and mechanistic details on a $Ni/MgAl_2O_4$ catalyst and arrived at the following mechanistic:

s_1: $CH_4 + S = CH_4{\cdot}S$
s_2: $H_2O + S = O{\cdot}S + H_2$
s_3: $CO{\cdot}S = CO + S$
s_4: $CO_2{\cdot}S = CO_2 + S$

s_5: $H{\cdot}S + H{\cdot}S = H_2{\cdot}S + S$

s_6: $H_2{\cdot}S = H_2 + S$

s_7: $CH_4{\cdot}S + S = CH_3{\cdot}S + H{\cdot}S$

s_8: $CH_3{\cdot}S + S = CH_2{\cdot}S + H{\cdot}S$

s_9: $CH_2{\cdot}S + O{\cdot}S = CH_2O{\cdot}S + S$

s_{10}: $CH_2O{\cdot}S + S = CHO{\cdot}S + H{\cdot}S$

s_{11} : $CHO{\cdot}S + S = CO{\cdot}S + H{\cdot}S$ (rate determining step)

s_{12} : $CHO{\cdot}S + O{\cdot}S = CO_2{\cdot}S + H{\cdot}S$ (rate determining step)

s_{13}: $CO{\cdot}S + O{\cdot}S = CO_2{\cdot}S + S$ (rate determining step)

with S as the surface catalyst. The rate equations that were obtained based on the rate determining steps are for $CH_4 + H_2O = 3H_2 + CO$

$$r_1 = \frac{k_1}{p_{H_2}^{2.5}}\left(p_{CH_4} p_{H_2O} - \frac{p_{H_2}^3 p_{CO}}{K_1} \right) / (DEN)^2 \tag{10}$$

for $CO + H_2O = H_2 + CO_2$

$$r_2 = \frac{k_2}{p_{H_2}}\left(p_{CO} p_{H_2O} - \frac{p_{H_2} p_{CO_2}}{K_2} \right) / (DEN)^2 \tag{11}$$

for $CH_4 + 2H_2O = 4H_2 + CO_2$

$$r_3 = \frac{k_3}{p_{H_2}^{3.5}}\left(p_{CH_4} p^2{}_{H_2O} - \frac{p_{H_2}^4 p_{CO_2}}{K_3} \right) / (DEN)^2 \tag{12}$$

$$DEN = 1 + K_{CO} P_{CO} + K_{H_2} P_{H_2} + K_{CH_4} P_{CH_4} + K_{H_2O} P_{H_2O} / P_{H_2}$$

Many other groups have followed the work of Xu and Froment and proposed their own mechanisms. Rostrup-Nielson proposed a model like this [39, 40]:

s_1: $CH_4 + 2{\cdot}S = CH3{\cdot}S + H{\cdot}S$

s_2: $CH_3{\cdot}S + S = CH_2{\cdot}S + H{\cdot}S$

s_3: $CH_2{\cdot}S + S = CH{\cdot}S + H{\cdot}S$

s_4: $H_2 + 2{\cdot}S = 2H{\cdot}S$

where S represents a catalyst surface site. Another complex mechanism has been presented in Compton's book, for methane with steam on a nickel surface, where S is the catalyst surface site and the final two steps, 5 and 6, are in equilibrium and is designated by the symbol ≈ [40].

s_1: $CH_4 + S = S{\cdot}CH_2 + H_2$

s_2: $S{\cdot}CH_2 + H_2O = S{\cdot}CHOH + H_2$

s_3: $S{\cdot}CHOH = S{\cdot}CO + H_2$

s_4: $S{\cdot}CO = S + CO$

s_5: $S + H_2O \approx S{\cdot}O + H_2$

s_6: $S{\cdot}O + CO \approx S + CO_2$

Another mechanism had been proposed by Wei et al. [33] He investigated the reactions of CH_4 with CO_2 and H_2O on Rh clusters and he found that the reaction rates were proportional to CH_4 partial pressure, but independent of CO_2 and H_2O pressures, which led them to the conclusion of sole kinetic relevance of C-H bond activation steps. They discovered that the Rh surface may be uncovered by reactive intermediates, due to the fast steps of the activation of the co-reactant and CH_4 activation through the foraging of chemisorbed carbon intermediates. The activation of C-H bonds has also been shown to be irreversible and that recombinative desorption steps of H atoms with OH groups form H_2 or H_2O.

s_1: $CH_4 + 2{\cdot}S \rightarrow CH_3{\cdot}S + H{\cdot}S$ (rate determining step)

s_2: $CH_3{\cdot}S + S \rightarrow CH_2{\cdot}S + H{\cdot}S$

s_3: $CH2{\cdot}S + S \rightarrow CH{\cdot}S + H{\cdot}S$

s_4: $CH{\cdot}S + S \rightarrow CS + H{\cdot}S$

s_5: $CO_2 + 2{\cdot}S \leftrightarrow CO{\cdot}S + O{\cdot}S$

s_6: $CS + O{\cdot}S \leftrightarrow CO{\cdot}S + O{\cdot}S$

s_7: $CO{\cdot}S \leftrightarrow CO + S$

s_8: $H{\cdot}S + H{\cdot}S \leftrightarrow H_2{\cdot}S + S$

s_9: $H{\cdot}S + O{\cdot}S \leftrightarrow OH{\cdot}S + S$

s_{10}: $OH{\cdot}S + H{\cdot}S \leftrightarrow H_2O{\cdot}S + S$

s_{11} : $H_2O{\cdot}S \leftrightarrow H_2O + S$

Comparing Wei et al [33] mechanism and to Xu and Froment's [14] mechanism, shows that the first mechanism indicates that reactions of carbon intermediates with oxygen are rate determining steps. This means that oxygen plays a large role in the reaction kinetics. Further this shows that importance of oxygen conducting support such as ceria. The mechanism of Wei et al. [33] indicates that the reactivity of the metal towards C-H bond breaking governs the overall reaction kinetics.

Chapter 3 Theory

A deeper understanding of the mechanisms and kinetics on the surface of the catalysts can be developed by applying a recently developed method known as the reaction route network formulated by Fishtik and Datta. In addition, the Unity Bond Index-Quadratic Exponential Potential (UBI-QEP) method developed by Shustorovich is used here to evaluate the energetic of the elementary reactions, while the pre-exponential factors are estimated from the transition state theory.

The theory has been provided on detail by us in a recent paper [41-43] and also by Callaghan, in her thesis [44]. Therefore, only an outline of the relevant notations and definitions are presented here.

For the general case of a heterogeneous catalytic chemical reaction system, the species participating in the elementary reactions of the catalytic mechanism are divided into: 1) active sites on the surface of the catalyst S; 2) intermediates (surface) species I_1, I_2, ….I_q; and 3) terminal (gas phase reactants and products) species T_1, T_2,…, T_n. The mechanism is described by the following set of *p* elementary reaction denoted by s_ρ [45]

$$s_\rho = \alpha_{\rho 0}\,\mathrm{S} + \sum_{k=1}^{q} \alpha_{\rho k} I_k + \sum_{i=1}^{n} \beta_{\rho i} T_i = 0; \qquad \rho = 1,2,...p \tag{13}$$

where, the stoichiometric coefficents $\alpha_{\rho 0}, \alpha_{\rho s}$ and $\beta_{\rho i}$ take on positive for products and negative for reactants. Each elementary reactions are characterized by its affinity A_ρ (ρ = 1, 2,…*p*) that is defined as [41, 45]

$$-\frac{1}{RT} A_\rho = -\ln K_\rho + \alpha_{\rho 0} \ln \theta_0 + \sum_{k=1}^{q} \alpha_{\rho k} \ln \theta_k + \sum_{i=1}^{n} \beta_{\rho i} \ln P_i \;;\; \rho = 1,2,...p \tag{14}$$

where, $K_j = \vec{k}_\rho / \overleftarrow{k}_\rho$ is the equilibrium constant of the *j*th elementary reaction, $\vec{k}_\rho$ and $\overleftarrow{k}_\rho$ are rate constants of the *ρ*th forward and reverse reaction, θ_0 is the fraction of the free (uncovered) surface of the catalyst, θ_k is the fraction of the surface occupied by the intermediate I_k and, P_i is the partial pressure of the terminal species T_i. [45]

The elementary reactions may be written in the form of

$$\vec{\alpha}_{\rho 0}\,\mathrm{S} + \sum_{k=1}^{q} \vec{\alpha}_{\rho k} I_k + \sum_{i=1}^{n} \vec{\beta}_{\rho i} T_i = \overleftarrow{\alpha}_{\rho 0}\,\mathrm{S} + \sum_{k=1}^{q} \overleftarrow{\alpha}_{\rho k} I_k + \sum_{i=1}^{n} \overleftarrow{\beta}_{\rho i} T_i \;; \qquad \rho = 1,2,...p \tag{15}$$

for kinetic considerations, where the arrows → and ← represents the reactants and the products, respectively. The rates of the elementary reaction then can be represented as

$$r_\rho = \vec{r}_\rho - \overleftarrow{r}_\rho = \vec{r}_\rho \left[1 - \exp\left(\frac{-A_\rho}{RT} \right) \right] \tag{16}$$

where

$$\vec{r}_\rho = \vec{A}_\rho e^{\frac{-\vec{E}_\rho}{RT}} \theta_o^{\vec{\alpha}_{\rho o}} \prod_{k=1}^{q} \theta_k^{\vec{\alpha}_{\rho k}} \prod_{i=1}^{n} P_i^{\vec{\beta}_{\rho k}} \tag{17}$$

where $\vec{A}_\rho$ and $\vec{E}_\rho$ are the pre-exponential factors and the activation energy and determining these values will be explained here.

A reaction route (RR) is defined as a linear combination of the elementary reactions s_ρ, such that a certain number of species, either terminal or intermediate, are canceled thus producing a new reaction referred to as an overall reaction (OR). By eliminating all the intermediate species, an OR results and it is called a full route (FR). If all the species are eliminated in a Reaction Route, an empty route (ER) is formed where all the stoichiometric coefficients are equal to zero. Further explanation on how to enumerate the full routes, empty routes, intermediate nodes, and terminal nodes may be found in Callaghan's thesis [44].

Ideally, reaction energetics should be determined by using quantum mechanical methods, such as first principles *ab initio* or density functional theory (DFT). However, this is computationally intensive still and of limited accuracy. Therfore, here we utilize the UBI-QEP method of Shustorobich. The UBI-QEP method provides, heats of adsorption and reaction activation barriers with a typical accuracy of 1-3 kcal[46, 47]. It is based on four postulates:

1. The interaction of the energy of two bodies will have a minimum and approach zero monotonically as the distance between them increases.
2. The forces between two bodies are spherical and depend on the interbody distance *r*.
3. The bond index is an exponential variable expressing the two body interaction as a polynomial function,

$$x(r) = \exp\left[\frac{-(r - r_0)}{b} \right] \tag{18}$$

$$E(x(r)) = a\left[x^2(r) - 2x(r)\right] \quad (19)$$

where r is the distance of the bond of interest, a is the bond energy, r_0 is the equilibrium distance, and b is the distance scaling constant.

4. Potential energy is the summation of the nearest pair-wise interaction of a group of atoms that may be considered as a single molecule. [46, 47]

$$E = \sum_i a_i \left[x^2(r_i) - 2x(r_i)\right] \quad (20)$$

The UBI-QEP method is limited to elementary reactions of the forms:

1) AB(g) + S = ABS
2) AB(g) + S = AS + BS
3) AS + BCS = ABS + CS

where S represents the vacant site on the surface of the catalyst. The activation energy of the reaction in the forward direction is determined by using

$$\vec{E} = \frac{1}{2}\left[\Delta H + \frac{Q_{AB}Q_C}{Q_{AB} + Q_C}\right] \quad (21)$$

where Q_i are the heats of chemisorption for reactants and products. Further, $\Delta H = \vec{E} - \overleftarrow{E}$

Estimating the pre-exponential factors using the transition state theory accounts for the loss of entropy that occurs when molecules unite to form an activated complex. Dumesic, et al provides the guidelines from which pre-exponential factors may be estimated through transition state theory. Further, Lund [48] has also provided additional insight on the evaluation of the reverse pre-exponential factor. The most important assumption of the transition state theory is that equilibrium is reached between the reactants and the activated complex. This method is better at estimating rate constants because it allows details of molecular structure to be incorporated[49].

Considering bimolecular gas-phase reaction, A + B→C + D, where a transition state is formed when old bonds are weakened and new bonds begin to form or the old bonds break first to form the transition state and then the new bond form after. This intermediate known as the activated complex is unstable and is a high-energy species that must be formed before the reaction can occur. The potential energy surface for the reaction shows reactants smoothly transforming into products. The point at which the lowest energy barrier to convert reactants to products is at the saddle point. The rate of

the chemical reaction, r_{AB}, is equal to the concentration of activated complex times a frequency factor[49]

$$r_{AB} = \frac{k_B T}{h} K n_A^{\pm} n_B \tag{22}$$

where $k_B T/h$ is the frequency factor, k_B is Boltzmann's constant, h is Planck's constant, and K is the equilibrium constant for this formation of the activated complex [49].

$$K^{\pm} = \frac{n^{\pm}{}_{AB}}{n_A n_B} \tag{23}$$

The macroscopic formulation of transition-state theory is written by writing K in terms of standard entropy and enthalpy of formation of the activated complex,[49]

$$r_{AB} = \frac{k_B T}{h} \exp\left(\frac{\Delta S}{k_B}\right) \exp\left(-\frac{\Delta H}{k_B T}\right) n_A n_B \tag{24}$$

while the microscopic formulation of transition-state theory is obtained by writing K in terms of molecular partition functions per unit volume, Q_i'''.

$$r_{AB} = \frac{k_B T}{h} \frac{Q_{AB}'''}{Q_A''' Q_B'''} \exp\left(\frac{\Delta E^0}{k_B T}\right) n_A n_B \tag{25}$$

ΔE is the change in energy at absolute zero temperature. The product of the frequency factor and the ratio of the molecular partition function for the activated complex and the individual reactants give the corresponding preexponential factor, Λ.[49]

$$\Lambda = \frac{k_B T}{h} \frac{Q_{AB}'''}{Q_A''' Q_B'''} \tag{26}$$

Molecular partition function is a product of contributions from translational, rotational, and vibrational degrees of freedom, q_{it}''', q_{ir}, and q_{iv}.

$$Q_i''' = q_{it}''' q_{ir} q_{iv} \tag{27}$$

Translational degree of freedom is defined as:

$$q_{it}''' = \frac{(2\pi m_i k_B T)^{3/2}}{h^3} \tag{28}$$

where m_i is the mass of the molecule. The rotational partition function is given by

$$q_{ir} = \frac{8\pi^2 I_i k_B T}{\sigma_r h^2} \qquad \text{(linear molecule)} \tag{29}$$

$$q_{ir} = \frac{8\pi^2\sqrt{8\pi^3 I_{i1}I_{i2}I_{i3}}\left(k_B T\right)^{3/2}}{\sigma_r h^3} \qquad \text{(nonlinear molecule)} \tag{30}$$

where I_i is the moment of inertia about the molecular axis of a linear molecule, $I_{i1,}$ $I_{i2,}$ and I_{i3} are the moments of inertia about the three principal axes of the molecule; σ_r is the rotational symmetry number, and the vibrational partition function is [49]

$$q_{iv} = \prod_j \frac{1}{1-\exp\left(-\frac{hv_{ij}}{k_B T}\right)} \tag{31}$$

where v_{ij} are the frequencies of the $_j$ normal modes of vibration (the number of vibrational modes equal to $3N_i$-5 or $3N_i$-6 for a linear or nonlinear molecule, where N_i is the number of atoms in the molecule).

Initial estimates of rate constants could be accomplished by using the following order of magnitude estimates for the frequency factor and the partition function [49].

$$\frac{k_B T}{h} = 10^{13}\, s^{-1} \tag{32}$$

$$q_{it}''' = 5\times 10^{8}\, cm^{-1} \tag{33}$$

$$q_{ir} = 10 \tag{34}$$

$$q_{iv} = 1 \tag{35}$$

The rate of adsorption of species such as A is given by the reaction A(g) ↔ $A^{‡}$ → A*, with the rate of reaction of[49]

$$r_{AB} = \frac{k_B T}{h}\frac{Q_{A_+^+}''}{Q_{A(g)}'''}\exp\left(\frac{\Delta E^{0_+^+}}{k_B T}\right)n_A \tag{36}$$

with

$$Q_{A_+^+}'' = q_{A_+^+t}'' q_{A_+^+r} q_{A_+^+v} \tag{37}$$

and

$$q_{A_+^+t}'' = \frac{2\pi m_A k_B T}{h^2} \tag{38}$$

where $Q_{i_+^+}''$ is a partition function per unit area with an approximation of 1015cm^{-2}. Substitution into the preexponential equation for an immobile transition state gives a value of $\vec{\Lambda} = 10^{1}$ Pa^{-1}s^{-1}. [49]

In the case of desorption process, A* ↔ $A^{‡}$ → A(g), the rate expression is given as

$$r_{AB} = \frac{k_B T}{h} \frac{Q_{A_+^+}''}{Q_{A^*}''} \exp\left(\frac{\Delta E^{0_+^+}}{k_B T} \right) \rho_A \qquad (39)$$

where ρ_A is the concentration of species A on the surface. For an immobile transition state, the preexponential factor for desorption can be approximated to be $10^{13} s^{-1}$.[49]

For surface reactions $A^* + B^* \leftrightarrow AB^{\ddagger} \rightarrow C^* + D^*$, has a rate expression of

$$r_{AB} = \frac{k_B T}{h} \frac{Q_{AB_+^+}''}{Q_{A^*}'' Q_{B^*}''} \exp\left(\frac{\Delta E^{0_+^+}}{k_B T} \right) \rho_A \rho_B \qquad (40)$$

with a preexponential factor of $10^{13} s^{-1}$ for immobile transition state. These estimates are used in the following analysis.

Chapter 4 Experiments

4.1 Reaction Kinetics Apparatus

Figure 12 shows the reactor apparatus that was used for the study. It was constructed with 1/8 inch SS tubing and corresponding Swagelok fittings. A bypass was inserted around the furnace allowing sampling of the feed conditions. A conventional condenser surrounded by an ice bed was attached to the junction of the bypass outlet and the furnace outlet, where excess steam could be condensed before the product gas enters the GC. A pressure gauge (Ashcroft Test Gauge, 0-100 psi range, model #Q-4907) was installed prior to the reactor to monitor the system pressure[44, 47].

The flow rates of the inlet gas, hydrogen, carbon monoxide, carbon dioxide, nitrogen and methane are set by MKS1179 mass flow controllers and MKS 247-C mass flow controller readout boxes. The flow rate of the steam was controlled through an ISCO Model 100D syringe pump, where the water is evaporated through heating coil tape around the 1/8 inch SS tubing [44, 47].

A Lindberg/Blue M single-zone tube furnace (model #TF55035A-1, upper temperature limit 1100°C) was used to start and maintain the catalyst bed temperature in the reactor. The reactor was made of stainless steel with dimensions of 18 inch long, 0.75 inch OD (0.625 inch ID). A 1-2 inch catalyst bed was packed in between fiberglass packing within the center of the reactor, where reactions of methane and steam occur to produce hydrogen, carbon monoxide and carbon dioxide. The dry gases then proceed into the SRI Instruments 8610C Gas Chromatograph (GC) through a Carboxen 1000 column at a temperature of 125°C where their concentrations were measured and presented as area peaks by the data acquisition system. The 8610C Gas Chromatograph is controlled by the free program PeakSimple. A total of four samples were run for each condition at each furnace temperature [44, 47].

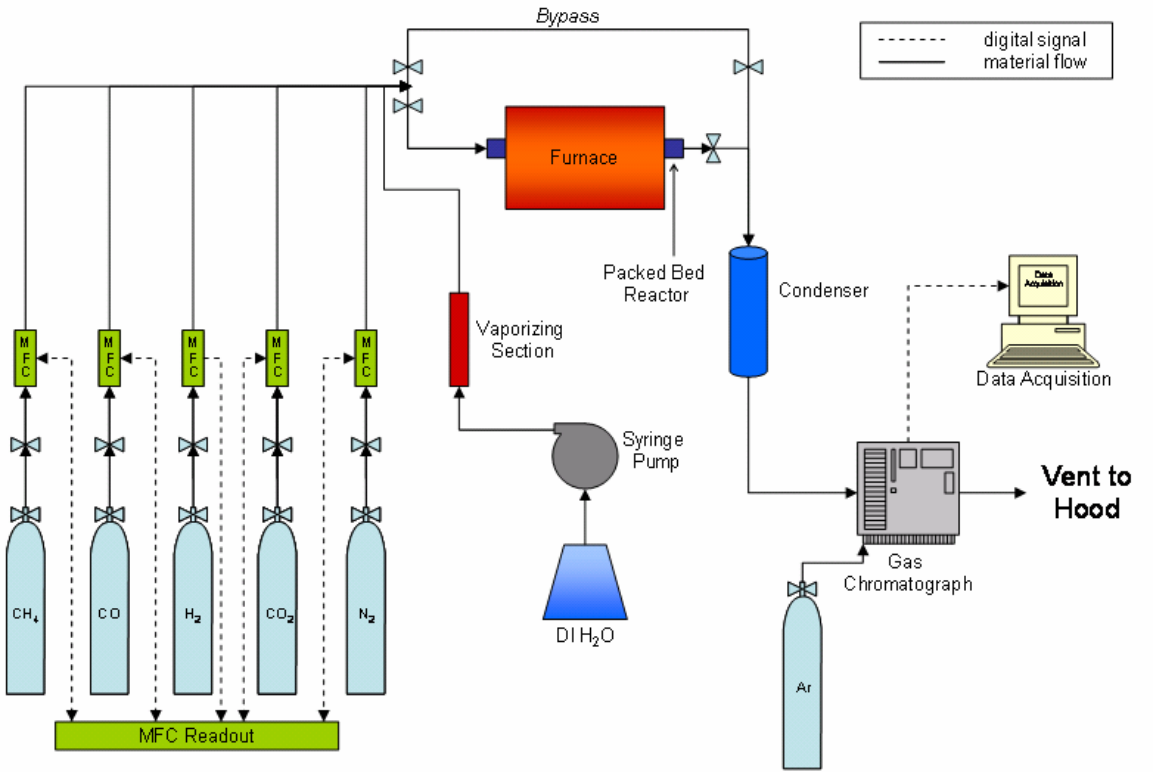

Figure 12 Schematic Drawing of the experimental setup

4.2 Calibrations

Calibrations were done for the mass flow controllers in the range of flow necessary for the desired feed conditions. An Alltech Digital Flow Bubble Meter (Model 4068) and compared the readout to the readout of MKS 247C readout. Calibration curves are shown in Appendix C.

The plots for GC calibrations are displayed in the Appendix C. These calibrations were performed using a constant flow rate of 100 sccm comprised of different concentrations of individual gas phase species balanced with inert nitrogen. Plots relating the volume ratio of gas species: volume of nitrogen to the ratio of their respective peak areas were generated and used to correlate the results to the real values of product stream composition.

4.3 Experimental Procedure

Forward reaction conditions of 2:1 steam to carbon ratio were conducted to see how well the experimental data fit with the simulation. The feed conditions used are presented in Table 2

Table 2 Experimental reactor feed conditions

Reaction Condition	Volume fraction					
	H_2O	CH_4	CO	CO_2	H_2	N_2
1	0.40	0.20	0.00	0.00	0.00	0.40

The line temperature was kept at a temperature above 130^{o}C to prevent condensation of the water vapor, while the vaporizing section and gas preheating section were held at 300^{o}C. Within the apparatus setup, a series of type-K thermal couples connected to a compatible multi-channel readout (Omega Monogram, 10-channel model #DPH6-KC) were placed strategically to monitor the temperature of the inlet, outlet and other locations along the line.

The bed within the reactor was packed with 8 micron fiberglass followed be an approximate estimation of 7 cm^3 of catalyst and then a final section of fiberglass. The nickel catalyst used were sized to 12-18 mesh and dispersed with silicon dioxide particles of similar sizes to achieve the total bed volume. In the case of the precious metal rhodium, the precious metal was dispersed over γ-alumina support. A total of 5 wt% of rhodium was used and it was estimated that about 2% of it had been deposited onto the alumina support. The rhodium catalyst preparation is described later on.

The catalysts were reduced using a 3% H_2/N_2 mixed gas flowing at 100 sccm for Nickel, and 6% H_2/N_2 mixed gas flowing at 30 sccm for Rhodium. The reactor temperature was raised slowly from over 250-300^{o}C temperature range during a 10-12 hour period for the nickel catalyst. For the rhodium catalyst, the reactor temperature was rasied to 450^{o}C and held for duration of 10-12 hour period.

To check that the flow rate that is flowing through the system is correct, the bypass section was left open, while the reactor sector was closed. The sample is then analyzed by the GC and checked if the results correspond to the calibration curve. After this, the bypass section was closed again and the reactor section opened. Before each run

was conducted, a 15 minute period was provided to confirm steady state and flush out any residual reducing gas before GC sampling began. In addition, the GC kept a record of the temperature of the reactor bed and the feed conditions under the comments option in printout.

4.4 Catalyst Pretreatment Procedure

Metals of Group VIII of the periodic system have been frequently found to be active for the steam reforming reaction. A great number of oxides have been proposed as promoters for improved activity or the ability to prevent formation of coke. [50] Two catalysts were considered for experimentation. Rhodium catalysts were prepared by wet incipient impregnation method. Rhodium (III) Chloride, anhydrous, 99.9% (metals basis), Rh 49.22% from Alfa Aeser were mixed in 25mL of DI H_2O. The mixture of Rhodium solution was pipetted onto 7.00 g of γ-Aluminum Oxide pellets from Alfa Aeser, while allowing air drying to occur at 70^{o}C for approximately 3 hrs. The catalysts were reduced in H_2 at 450^{o}C for 12 hrs.

Characterization of this catalyst was done through Scanning Electron Microscopy (SEM) and Energy Dispersive X-ray Spectroscopy (EDS). SEM provides an image of the sample, by an electron beam scanned across the sample's surface. The electrons will generate a variety of signals, in which the detection of the signal produces the image. EDS can provide rapid qualitative, or with adequate standards, quantitative analysis of elemental composition with sampling depth of 1-2 microns. The x-ray can also be used to form maps or line profiles, showing the elemental distribution in a sample surface, as shown in Figure 13.

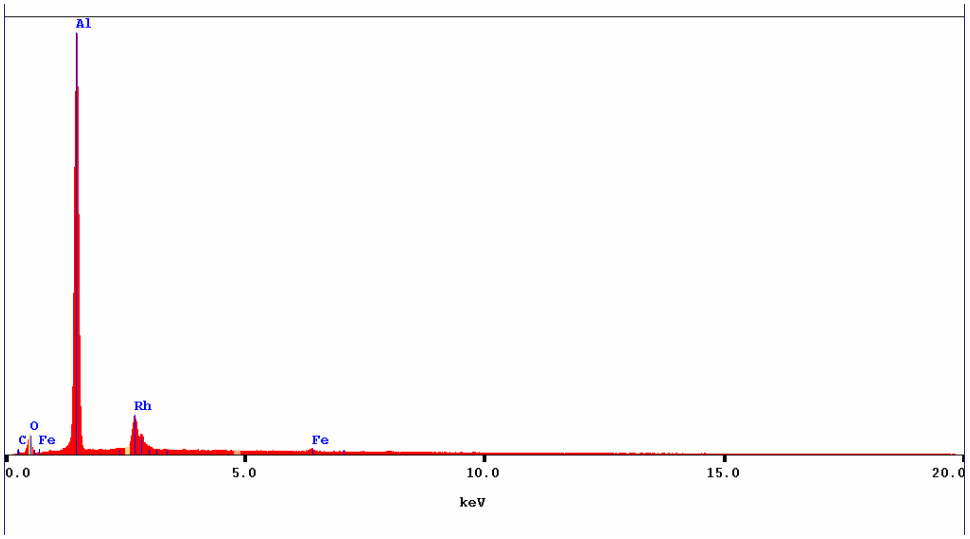

Figure 13 EDS mapping of rhodium on γ-alumina

Further, Brunauer, Emmett, and Teller (BET) was used to measure the surface area from the physical adsorption of a gas onto the solid surface. In our case, the gas that was used was hydrogen. However, due to the limited amount of catalyst available, we were unable to get a precise and accurate reading of the surface area. During the microkinetic study, the active surface area, number of active sites, and catalyst density were estimated to be similar to Ni with values of 3.43 x 10^5 cm^2/g, 1.41 x 10^{15} $sites/cm^2$, and 0.5 g/cm^3, respectively.

Chapter 5 RR Graph of Methane Steam Reforming

Using some of the theory present in Chapter 3 and along with the reation route graph theory dexcribed by Callaghan [44] and Fishtik et al [41], a reaction route graph for methane steam reforming using Froment and Xu's set of elementary reaction with 3 additional elementary steps in bold (crucial for carbon formation) is presented here.

s_1: $CH_4 + S = CH_4{\cdot}S$
IR_1: $H_2O + S = O{\cdot}S + H_2$
s_3: $CO{\cdot}S = CO + S$
s_4: $CO_2{\cdot}S = CO_2 + S$
s_5: $H{\cdot}S + H{\cdot}S = H_2{\cdot}S + S$
s_6: $H_2{\cdot}S = H_2 + S$
s_9: $CH_4{\cdot}S + S = CH_3{\cdot}S + H.S$
s_{10}: $CH_3{\cdot}S + S = CH_2{\cdot}S + H.S$
s_{11}: $CH_2{\cdot}S + S = CH{\cdot}S + H{\cdot}S$
s_{12}: $CH{\cdot}S + S = C{\cdot}S + H{\cdot}S$
s_{13}: $C{\cdot}S + OS = CO{\cdot}S + S$
s_{14}: $CH_2{\cdot}S + O{\cdot}S = CH_2O{\cdot}S + S$
s_{15}: $CH_2O{\cdot}S + S = CHO{\cdot}S + H.S$
s_{16}: $CHO{\cdot}S + S = CO{\cdot}S + H.S$
s_{17}: $CO{\cdot}S + O{\cdot}S = CO_2{\cdot}S + S$
s_{18}: $CHO{\cdot}S + O{\cdot}S = CO_2{\cdot}S + H{\cdot}S$

For the MSR mechanism, our starting point for the stoichiometric analysis is a list of species (reactants, intermediates, and products), which for this system includes: H_2O and CH_4 as reactants, $CH_4{\cdot}S$, $CH_3{\cdot}S$, $CH_2{\cdot}S$, $CH{\cdot}S$, $O{\cdot}S$, $CO{\cdot}S$, $CO_2{\cdot}S$, $H{\cdot}S$, $H_2{\cdot}S$, $CH_2O{\cdot}S$, $CHO{\cdot}S$, $C{\cdot}S$ (q = 12) as the independent surface intermediates, and CO, CO_2 and H_2 as products (i.e., n = 5). [44, 47] Considering the intermediate matrix [41, 44]

$$\alpha = \begin{array}{c} \begin{matrix} CH_4S & CH_3S & CH_2S & CHS & OS & COS & CO_2S & HS & H_2S & CH_2OS & CHOS & CS \end{matrix} \\ \begin{bmatrix} 1 & 0 & 0 & 0 & 0 & 0 & 0 & 0 & 0 & 0 & 0 & 0 \\ 0 & 0 & 0 & 0 & 1 & 0 & 0 & 0 & 0 & 0 & 0 & 0 \\ 0 & 0 & 0 & 0 & 0 & -1 & 0 & 0 & 0 & 0 & 0 & 0 \\ 0 & 0 & 0 & 0 & 0 & 0 & -1 & 0 & 0 & 0 & 0 & 0 \\ 0 & 0 & 0 & 0 & 0 & 0 & 0 & -2 & 1 & 0 & 0 & 0 \\ 0 & 0 & 0 & 0 & 0 & 0 & 0 & 0 & -1 & 0 & 0 & 0 \\ -1 & 1 & 0 & 0 & 0 & 0 & 0 & 1 & 0 & 0 & 0 & 0 \\ 0 & -1 & 1 & 0 & 0 & 0 & 0 & 1 & 0 & 0 & 0 & 0 \\ 0 & 0 & -1 & 0 & -1 & 0 & 0 & 0 & 0 & 1 & 0 & 0 \\ 0 & 0 & 0 & 0 & 0 & 0 & 0 & 1 & 0 & -1 & 1 & 0 \\ 0 & 0 & 0 & 0 & 0 & 1 & 0 & 1 & 0 & 0 & -1 & 0 \\ 0 & 0 & 0 & 0 & -1 & 0 & 1 & 1 & 0 & 0 & -1 & 0 \\ 0 & 0 & 0 & 0 & -1 & -1 & 1 & 0 & 0 & 0 & 0 & 0 \\ 0 & 0 & -1 & 1 & 0 & 0 & 0 & 1 & 0 & 0 & 0 & 0 \\ 0 & 0 & 0 & -1 & 0 & 0 & 0 & 1 & 0 & 0 & 0 & 1 \\ 0 & 0 & 0 & 0 & -1 & 1 & 0 & 0 & 0 & 0 & 0 & -1 \end{bmatrix} \end{array} \begin{matrix} s_1 \\ IR_1 \\ s_3 \\ s_4 \\ s_5 \\ s_6 \\ s_9 \\ s_{10} \\ s_{14} \\ s_{15} \\ s_{16} \\ s_{18} \\ s_{17} \\ s_{11} \\ s_{12} \\ s_{13} \end{matrix}$$

This intermediate matrix has a rank of 12. Since the surface intermediates are linearly independent, a direct RR involves no more than $q + 1 = 13 = 12 + 1$ elementary reactions. So the total number of RRs does not exceed the number of ways 13 elementary reactions may be selected from the 16 elementary steps of the mechanism. 16!/13!/3! = 560. [44, 47]

In enumerating the reaction routes, we may face three different scenarios, and these are illustrated here. The first scenario is enumerating the full route.

FR(s_1,IR$_2$,s_3,s_4,s_5,s_6,s_9,s_{10},s_{14},s_{15},s_{17},s_{11},s_{12})

$$
\begin{array}{c}
\begin{matrix} CH_4S & CH_3S & CH_2S & CHS & OS & COS & CO_2S & HS & H_2S & CH_2OS & CHOS & CS \end{matrix} \\
\left|\begin{array}{cccccccccccc|c}
1 & 0 & 0 & 0 & 0 & 0 & 0 & 0 & 0 & 0 & 0 & 0 & s_1 \\
0 & 0 & 0 & 0 & 1 & 0 & 0 & 0 & 0 & 0 & 0 & 0 & IR_1 \\
0 & 0 & 0 & 0 & 0 & -1 & 0 & 0 & 0 & 0 & 0 & 0 & s_3 \\
0 & 0 & 0 & 0 & 0 & 0 & -1 & 0 & 0 & 0 & 0 & 0 & s_4 \\
0 & 0 & 0 & 0 & 0 & 0 & 0 & -2 & 1 & 0 & 0 & 0 & s_5 \\
0 & 0 & 0 & 0 & 0 & 0 & 0 & 0 & -1 & 0 & 0 & 0 & s_6 \\
-1 & 1 & 0 & 0 & 0 & 0 & 0 & 1 & 0 & 0 & 0 & 0 & s_9 \\
0 & -1 & 1 & 0 & 0 & 0 & 0 & 1 & 0 & 0 & 0 & 0 & s_{10} \\
0 & 0 & -1 & 0 & -1 & 0 & 0 & 0 & 0 & 1 & 0 & 0 & s_{14} \\
0 & 0 & 0 & 0 & 0 & 0 & 0 & 1 & 0 & -1 & 1 & 0 & s_{15} \\
0 & 0 & 0 & 0 & -1 & -1 & 1 & 0 & 0 & 0 & 0 & 0 & s_{17} \\
0 & 0 & -1 & 1 & 0 & 0 & 0 & 1 & 0 & 0 & 0 & 0 & s_{11} \\
0 & 0 & 0 & -1 & 0 & 0 & 0 & 1 & 0 & 0 & 0 & 1 & s_{10}
\end{array}\right|
\end{array}
$$

= s_2 - s_3 + s_4 + s_{17}

In a more conventional format, this RR may be represented as

		σ_ρ
s_2:	-H2O - S + OS + H2 = 0	1
s_3:	-COS + CO + S = 0	-1
s_4:	-CO2S + CO2 + S = 0	1
s_{17}:	-COS – OS + CO2S + S = 0	1

OR: $H_2O + CO = CO_2 + H_2$

This FR(s_1,IR$_2$,s_3,s_4,s_5,s_6,s_9,s_{10},s_{14},s_{15},s_{17},s_{11},s_{12}) results in an OR and is known as a FR. This OR is the WGS reaction. The enumeration of the elementary reactions s_1,s_3,s_4,s_5,s_6,s_9,s_{10},s_{14},s_{15},s_{16},s_{18},s_{17},s_{11}, and s_{12} is an empty route(ER).

ER(s_1,s_3,s_4,s_5,s_6,s_9,s_{10},s_{14},s_{15},s_{16},s_{18},s_{17},s_{11},s_{12})

$$
\begin{array}{c}
\begin{array}{cccccccccccc}
CH_4S & CH_3S & CH_2S & CHS & OS & COS & CO_2S & HS & H_2S & CH_2OS & CHOS & CS
\end{array} \\
= \left|\begin{array}{cccccccccccc}
1 & 0 & 0 & 0 & 0 & 0 & 0 & 0 & 0 & 0 & 0 & 0 \\
0 & 0 & 0 & 0 & 0 & -1 & 0 & 0 & 0 & 0 & 0 & 0 \\
0 & 0 & 0 & 0 & 0 & 0 & -1 & 0 & 0 & 0 & 0 & 0 \\
0 & 0 & 0 & 0 & 0 & 0 & 0 & -2 & 1 & 0 & 0 & 0 \\
0 & 0 & 0 & 0 & 0 & 0 & 0 & 0 & -1 & 0 & 0 & 0 \\
-1 & 1 & 0 & 0 & 0 & 0 & 0 & 1 & 0 & 0 & 0 & 0 \\
0 & -1 & 1 & 0 & 0 & 0 & 0 & 1 & 0 & 0 & 0 & 0 \\
0 & 0 & -1 & 0 & -1 & 0 & 0 & 0 & 0 & 1 & 0 & 0 \\
0 & 0 & 0 & 0 & 0 & 0 & 0 & 1 & 0 & -1 & 1 & 0 \\
0 & 0 & 0 & 0 & 0 & 1 & 0 & 1 & 0 & 0 & -1 & 0 \\
0 & 0 & 0 & 0 & -1 & 0 & 1 & 1 & 0 & 0 & -1 & 0 \\
0 & 0 & 0 & 0 & -1 & -1 & 1 & 0 & 0 & 0 & 0 & 0 \\
0 & 0 & -1 & 1 & 0 & 0 & 0 & 1 & 0 & 0 & 0 & 0 \\
0 & 0 & 0 & -1 & 0 & 0 & 0 & 1 & 0 & 0 & 0 & 1
\end{array}\right|
\begin{array}{c}
s_1 \\ s_3 \\ s_4 \\ s_5 \\ s_6 \\ s_9 \\ s_{10} \\ s_{14} \\ s_{15} \\ s_{16} \\ s_{18} \\ s_{17} \\ s_{11} \\ s_{12}
\end{array}
\end{array}
$$

$= 0s_1 + 0s_3 + 0s_4 + 0s_5 + 0s_6 + 0s_9 + 0s_{10} + 0s_{14} + 0s_{15} + s_{16} - s_{18} + s_{17}$

$= s_{16} - s_{18} + s_{17}$

Or

		σ_ρ
s_{11}:	$-CHO^{\cdot}S - S + CO^{\cdot}S + H^{\cdot}S = 0$	1
s_{12}:	$-CHO^{\cdot}S - O^{\cdot}S + CO_2{}^{\cdot}S + H^{\cdot}S = 0$	-1
s_{13}:	$-CO^{\cdot}S - O^{\cdot}S + CO_2{}^{\cdot}S + S = 0$	1
Net:	$0 = 0$	

The full routes and empty routes calculated for this set of mechanism can be found in Appendix B.

The intermediate nodes are also enumerated using the equations presented in Callaghan's thesis [44]. The system includes twelve linearly independent intermediates, with some QSS conditions presented as

$Q1$:	$r_1 - r_9 = 0$	$CH_4{}^{\cdot}S$
$Q2$:	$r_9 - r_{10} = 0$	$CH_3{}^{\cdot}S$

and can be represented in terms of the intermediate matrix. By linearly combining all the *QSS* so as to eliminate at least q - 1 = 12 - 1 = 11 rates, a direct QSS condition may be obtained. The complete lists of intermediate nodes are presented in the Appendix.

After examining the list of direct FR and ERs, the RR graph is constructed by first considering the three empty routes then attaching the rest of the steps according to the direct FRs. For an example, we take a look at the first empty route and we see $ER_1 = s_{16} - s_{18} + s_{17}$. This empty route should be drawn as.

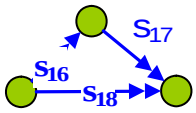

Similarly $ER_2 = s_{15} + s_4 + s_{16} - s_{13} - s_{12} - s_{11}$

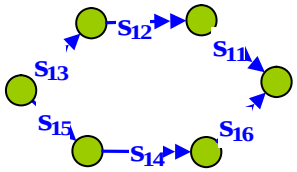

and $ER_3 = s_{15} + s_4 + s_{18} - s_{13} - s_{12} - s_{11} - s_{17}$

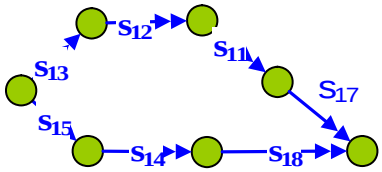

when all three of these ER's are combined, we get

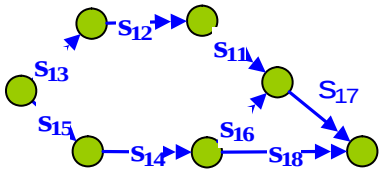

It is seen that some full routes have stoichiometric numbers of ±2, requiring us to draw a subgraph where empty cycles are drawn symmetrically.

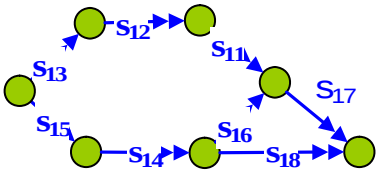

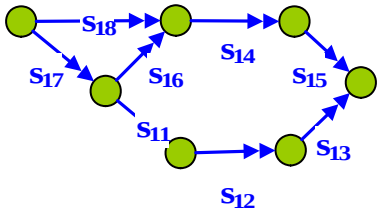

Then, the rest of the elementary steps are added on to compose the full routes for the 4 different overall reactions shown in Figure 14. From these figure you may notice the arrows being doubled to balance the mass balance. Step IR_2 is the reason for doubling rest of the steps.

.

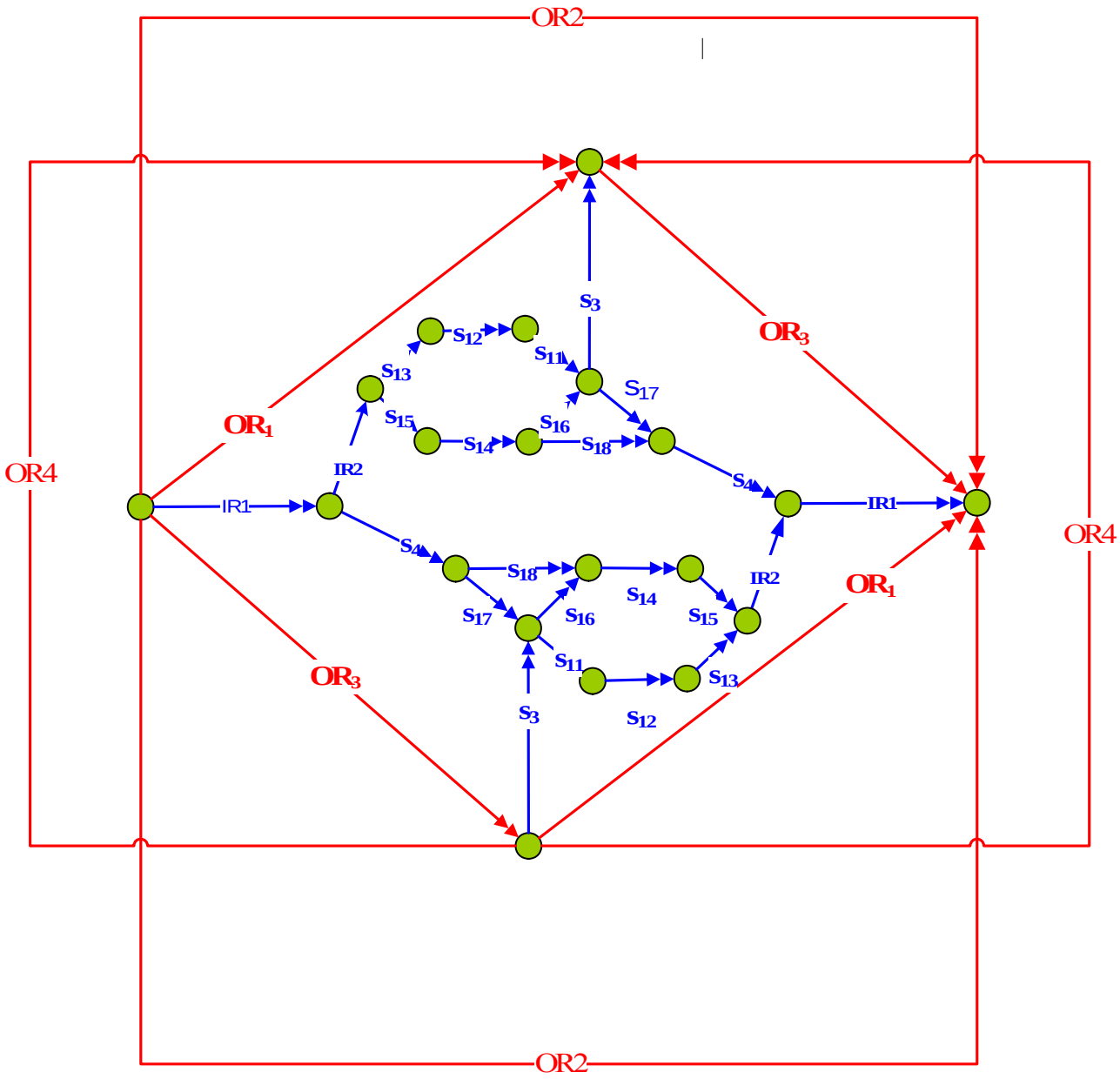

Figure 14 Reaction Route Network for Methane Steam Reforming

With overall reactions:

OR_1: $CH_4 + H_2O = CO + 3H_2$

OR_2: $CH_4 + 2H_2O = CO_2 + 4H_2$

OR_3: $H_2O + CO = CO_2 + H_2$

OR_4: $CH_4 + CO_2 = 2CO + 2H_2$

and $IR_2 = s_1 + 2s_5 + 2s_6 + s_7 + s_8$, i.e.,

s_1: $CH_4 + S = CH_4{\cdot}S$

$2s_5$: $2H{\cdot}S + 2H{\cdot}S = 2H_2{\cdot}S + 2S$

$2s_6$: $2H_2{\cdot}S = 2H_2 + 2S$
s_7: $CH_4{\cdot}S + S = CH_3{\cdot}S + H.S$
s_8: $CH_3{\cdot}S + S = CH_2{\cdot}S + H.S$
$IR_2 = CH_4 + 2HS - 2H_2 - S - CH_2S$

A program written by Callaghan [44] may be used to enumerate the full routes, empty routes, intermediate nodes, and terminal nodes. However, this program had some limitations with the amount of computational memory. Therefore a program in Maple was written that better assists in the repetitive work of copying and pasting and is therefore more efficient. The full program is attached in Appendix
Appendix A.

Finally, while four Ors result in our enumeration of the full routes, it is clear that only two of these Ors are independent, i.e., the remaining two can be obtained by their linear combination. For instance,

$OR_1 + OR_3 = OR_2$, methane steam reforming

and

$OR - OR_3 = OR4$, the carbon dioxide reforming.

These cycles among the ORs are also evident in Figure 14. For the kinetic analysis, only the independent ORs are needed, chosen here to be OR_1 and OR_3. The details of the microkinetic analysis are discussed next.

Chapter 6 Microkinetics of Methane Steam Reforming

6.1 Mechanism and Kinetics

The 3 additional steps added to the 13 step Xu and Froment mechanism are composed of the steps for carbon formation, which is crucial in understanding the effect of carbon deposition on the performance of the catalyst. Xu and Froment's mechanism thus becomes a 16 step mechanism, for which reaction route analysis was performed and presented above.

s_1: $CH_4 + S = CH_4{\cdot}S$
IR_1: $H_2O + S = O{\cdot}S + H_2$
s_3: $CO{\cdot}S = CO + S$
s_4: $CO_2{\cdot}S = CO_2 + S$
s_5: $H{\cdot}S + H{\cdot}S = H_2{\cdot}S + S$
s_6: $H_2{\cdot}S = H_2 + S$
s_9: $CH_4{\cdot}S + S = CH_3{\cdot}S + H.S$
s_{10}: $CH_3{\cdot}S + S = CH_2{\cdot}S + H.S$
s_{11}: $CH_2{\cdot}S + S = CH{\cdot}S + H{\cdot}S$
s_{12}: $CH{\cdot}S + S = C{\cdot}S + H{\cdot}S$
s_{13}: $C{\cdot}S + OS = CO{\cdot}S + S$
s_{14}: $CH_2{\cdot}S + O{\cdot}S = CH_2O{\cdot}S + S$
s_{15}: $CH_2O{\cdot}S + S = CHO{\cdot}S + H.S$
s_{16}: $CHO{\cdot}S + S = CO{\cdot}S + H.S$
s_{17}: $CO{\cdot}S + O{\cdot}S = CO_2{\cdot}S + S$
s_{18}: $CHO{\cdot}S + O{\cdot}S = CO_2{\cdot}S + H{\cdot}S$

In order to perform a microkinetic study of methane steam reforming, it is seen in Froment and Xu's mechanism that IR_1 is not an elementary reaction and UBI-QEP not be used for predictin its kinetics. Rather, IR_1 is composed of 5 elementary reactions, 3 of which are not listed in the 13 step mechanism. These 3 elementary steps are in red text as shown below:

$H_2O + S = H_2O{\cdot}S$
s_5: $H{\cdot}S + H{\cdot}S = H_2{\cdot}S + S$
s_6: $H_2{\cdot}S = H_2 + S$
$OH{\cdot}S + S = O{\cdot}S + H{\cdot}S$
$H_2O{\cdot}S + S = OH{\cdot}S + H{\cdot}S$
IR_1: $H_2O + S = O{\cdot}S + H_2$

By replacing IR_1 with the three additional elementary steps in red, we end up with a total of 18 steps for methane steam reforming. Enumerating the FRs and ERs for these 18 step mechanism resulted in 5 overall reactions rather than 4. To avoid the additional complexities, it was decided to stick with the 16 step mechanism to draw the reaction route graph, while 18 step mechanism was used to perform the microkinetic study. The 18 step mechanism used in kinetic analysis is shown below:

s_1: $CH_4 + S = CH_4{\cdot}S$
s_2: $H_2O + S = H_2OS$
s_3: $CO{\cdot}S = CO + S$
s_4: $CO_2{\cdot}S = CO_2 + S$
s_5: $H{\cdot}S + H{\cdot}S = H_2{\cdot}S + S$
s_6: $H_2{\cdot}S = H_2 + S$
s_7: $H_2O{\cdot}S + S = OH{\cdot}S + H{\cdot}S$
s_8: $OH{\cdot}S + S = O{\cdot}S + H{\cdot}S$
s_9: $CH_4{\cdot}S + S = CH_3{\cdot}S + H{\cdot}S$
s_{10}: $CH_3{\cdot}S + S = CH_2{\cdot}S + H{\cdot}S$
s_{11}: $CH_2{\cdot}S + S = CH{\cdot}S + H{\cdot}S$
s_{12}: $CH{\cdot}S + S = C{\cdot}S + H{\cdot}S$
s_{13}: $C{\cdot}S + O{\cdot}S = CO{\cdot}S + S$
s_{14}: $CH_2{\cdot}S + OS = CH_2O{\cdot}S + S$
s_{15}: $CH_2O{\cdot}S + S = CHO{\cdot}S + H{\cdot}S$
s_{16}: $CHO{\cdot}S + S = CO{\cdot}S + H.S$
s_{17}: $CO{\cdot}S + O{\cdot}S = CO_2{\cdot}S + S$
s_{18}: $CHO{\cdot}S + O{\cdot}S = CO_2{\cdot}S + H{\cdot}S$

Following Dumesic, as described in the last chapter, we assume an immobile transition state without rotation for all of the species, which results in pre-exponential factors of 10^1 $Pa^{-1}s^{-1}$ for adsorption/desorption reactions, and 10^{13} s^{-1} for surface reactions. The associated forward or reverse pre-exponential factors were calculated to ensure consistency with the thermodynamics of the overall reaction. [44, 47]

The energetics of these elementary steps were calculated from the UBI-QEP method. The UBI-QEP predictions are restricted to only three types of reactions. These reactions were listed in Chapter 3 along with the necessary formulae.

The set of elementary reactions for the MSR reaction is presented in Table 3 along with their respective energetics on a Rh(111) and Ni(111) catalyst and the pre-exponential factors.

Table 3 Microkinetic model for steam reforming of methane on Rh(111) and Ni(111). *A*ctivation energies in kcal/mol ($\theta \to 0$ limit) estimated according to Shustorovich and Sellers [46], preexponential factors from Dumesic[49], pre-exponential factors adjusted so as to fit the thermodynamics of the overall reaction

			Pre-exponential Factor		Activation Energy			
					Rh (111)		Ni (111)	
	Reactant	Product	Forward	Reverse	Forward	Reverse	Forward	Reverse
s1	$CH_4 + S$	$CH_4{\cdot}S$	1.00E+06	5.00E+13	0	6	0.0	6.0
s2	$H_2O + S$	$H_2O{\cdot}S$	1.00E+06	1.00E+14	0	13.3	0.0	16.5
s3	$CO{\cdot}S$	$CO + S$	1.00E+14	1.00E+06	32	0	27.0	0.0
s4	$CO_2{\cdot}S$	$CO_2 + S$	3.10E+12	1.00E+06	5.2	0	6.5	0.0
s5	$H{\cdot}S + H{\cdot}S$	$H_2{\cdot}S + S$	1.00E+13	1.00E+13	21.2	9.5	23.4	8.2
s6	$H_2{\cdot}S$	$H_2 + S$	6.00E+12	1.00E+06	6.4	0	6.8	0.0
s7	$H_2O{\cdot}S + S$	$OH{\cdot}S + H{\cdot}S$	3.00E+13	1.00E+13	23.5	4.2	20.8	10.2
s8	$OH{\cdot}S + S$	$O{\cdot}S + H{\cdot}S$	1.00E+13	1.00E+13	14.1	24.1	12.8	27.9
s9	$CH_4{\cdot}S + S$	$CH_3{\cdot}S + H.S$	5.00E+12	1.00E+13	14.7	11.8	13.8	13.4
s10	$CH_3{\cdot}S + S$	$CH_2{\cdot}S + H.S$	4.00E+12	1.00E+13	24.5	10.4	23.9	11.9
s11	CH2S + S	CHS + HS	4.00E+12	1.00E+13	23.8	16.0	23.2	17.6
s12	CHS + S	CS + HS	4.00E+12	2.00E+13	5.0	39.9	4.5	41.5
s13	CS + OS	COS + S	5.00E+13	1.00E+13	23.4	40.4	35.4	33.4
s14	$CH_2{\cdot}S + O{\cdot}S$	$CH_2O{\cdot}S + S$	4.00E+12	1.00E+13	17.8	27.6	24.2	23.9
s15	$CH_2O{\cdot}S + S$	$CHO{\cdot}S + H.S$	4.00E+12	2.00E+13	9.8	17.5	10.6	17.2
s16	$CHO{\cdot}S + S$	$CO{\cdot}S + H.S$	5.00E+13	1.00E+13	0	26.6	0.0	23.1
s17	$CO{\cdot}S + O{\cdot}S$	$CO_2{\cdot}S + S$	1.00E+13	1.00E+13	13.1	11.3	15.2	6.7
s18	$CHO{\cdot}S + O{\cdot}S$	$CO_2{\cdot}S + H{\cdot}S$	5.00E+13	1.00E+13			10.1	24.7

To begin the microkinetic analysis using the RR network approach, the RR network is pre-converted into an equivalent electric circuit, where in the elementary steps are replaced by reaction resistances and the Ors are replaced by a power source. This is shown in Figure 15. As mentioned before, only OR_1 and OR_3 are shown in Figure 15 for the purpose of kinetic analysis.

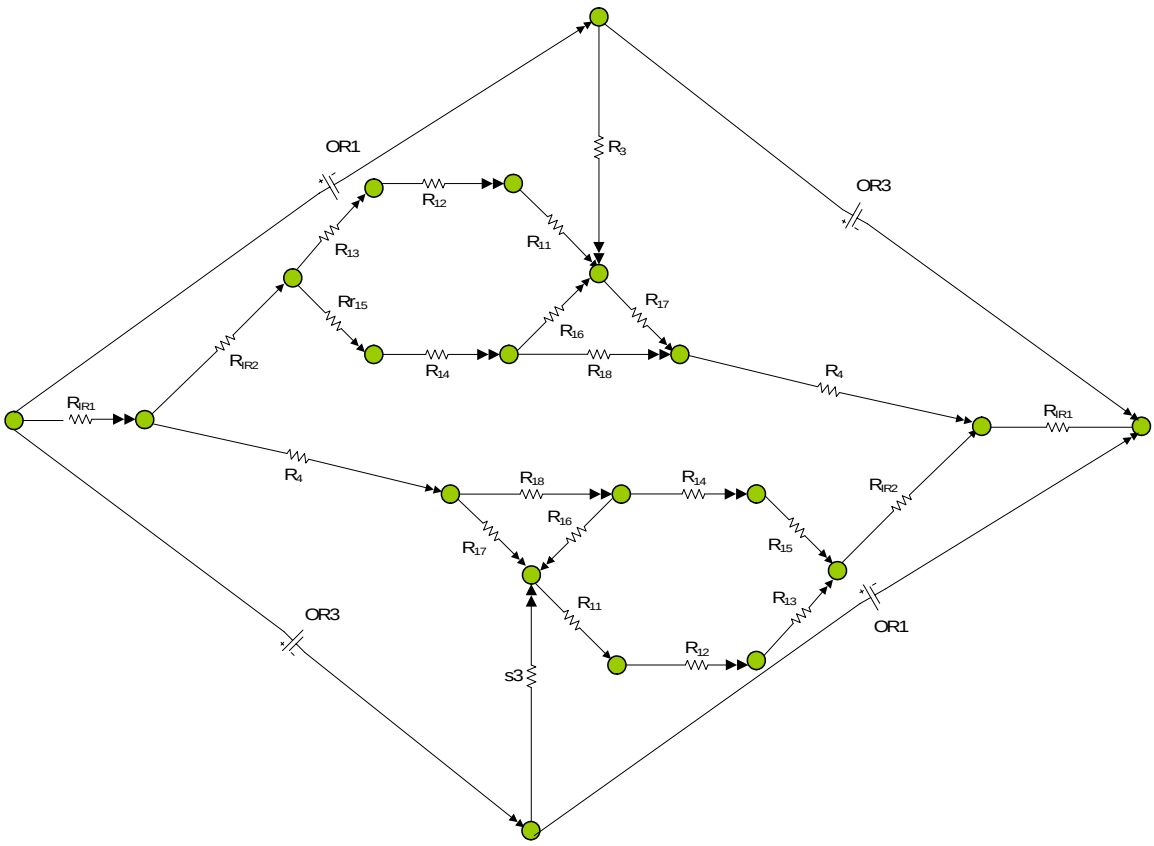

Figure 15 Electrical analog of RR Network

6.2 Network Reduction

The electrical diagram also allows a reduction of the network. The relative importance of links in parallel pathways between two given nodes, e.g., may be evaluated by comparing the resistances. After comparing the resistance, the path that has the highest resistance within a parallel pathway is eliminated and the kinetics of the removed pathway is compared with the overall kinetics of the mechanism.[44] For instance, if we compare the log resistance of step s_{18} to the sum of step s_{16}+s_{17}, corresponding to the *ER* $s_{16} + s_{17} - s_{18} = 0$, we find that, step s_{18} has a higher resistance than the summation of steps s_{16} and s_{17} shown in Figure 16.

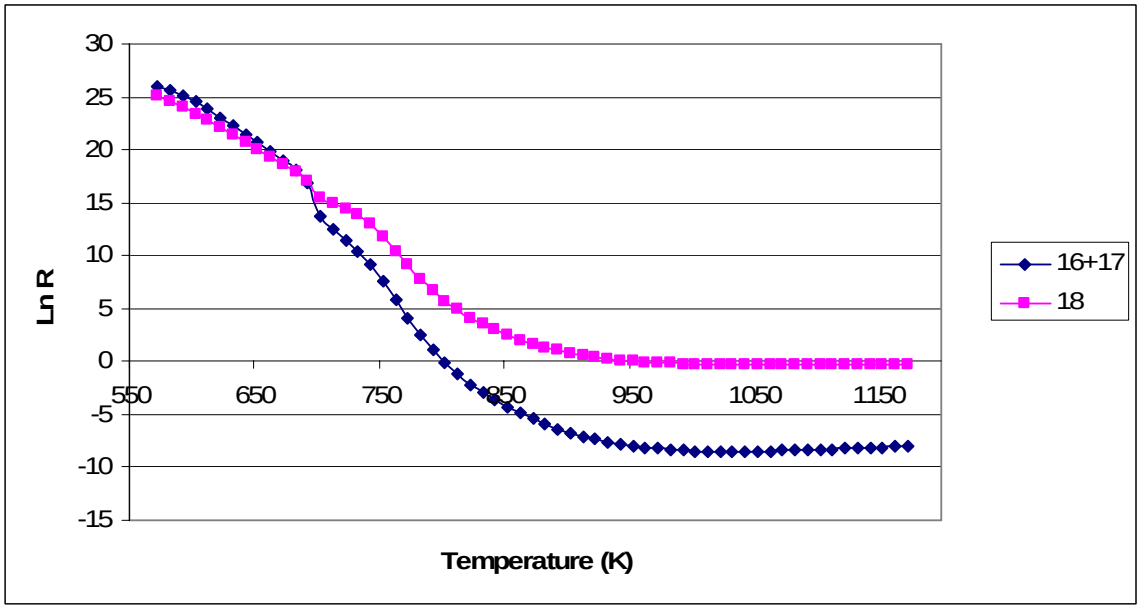

Figure 16 The resistance of s_{16}+s_{17} and s_{18} vs. temperature

This suggests that step s_{18} could be removed. To validate this elimination, we check the effect of removing s_{18} on the overall kinetics by comparing the simulated overall kinetics of the complete mechanism to the mechanism less s_{18}. In fact, we find that the elimination of steps s_{18} is not kinetically significant; therefore we should eliminate s_{18}.

For comparing the parallel pathways in the other ER, two options occur. The first option is to eliminate steps s_{18} and compare only the summation of step s_{14}, s_{15}, and s_{16} with the summation of steps s_{13}, s_{12}, s_{11}, because the empty route involving the summation of s_{13}, s_{12}, s_{11} and s_{17}, and the summation of steps s_{15}, s_4, and s_{18} have been eliminated. The second option is to compare the rest of the empty routes and eliminate the necessary steps at once. Both options provided the same result. Option two is thus presented next in Figure 17. So the log of the summation of steps s_{13}, s_{12}, and s_{11} is compared with the log of the summation of s_{15}, s_4, and s_{16} Figure 17.

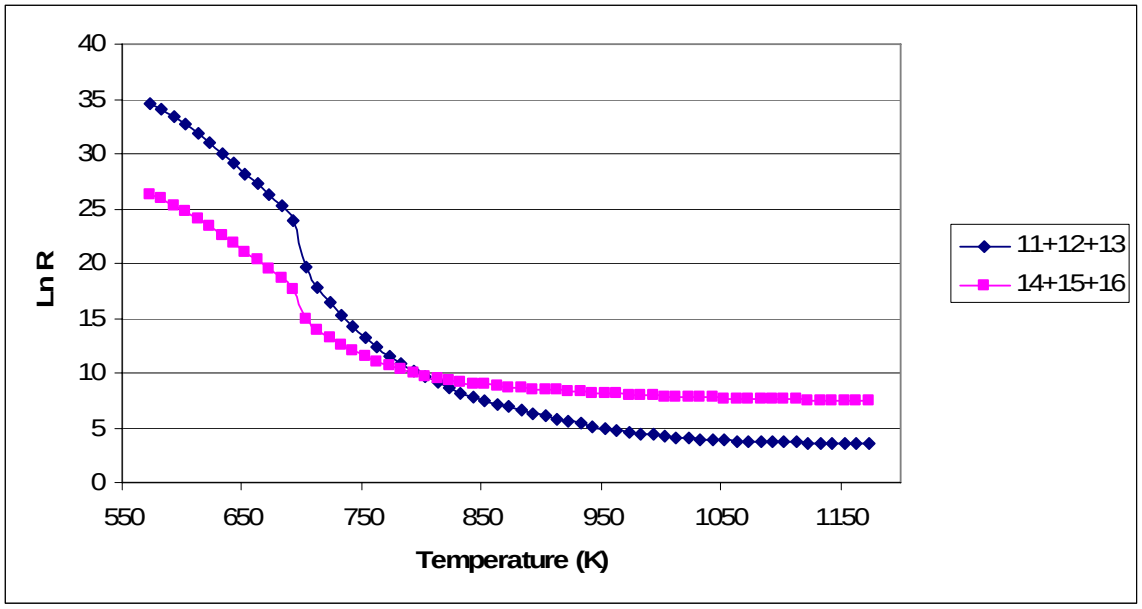

Figure 17 The resistance of $s_{14}+s_{15}+s_{16}$ and $s_{11}+s_{12}+s_{13}$ vs. temperature

In Figure 17, both curves intersect one another showing the summation of steps s_{11}, s_{12}, and s_{13} having higher resistance at temperatures below 760K and lower resistances at temperatures above 760K. Since, the conversion of methane doesn't occur substantially until around 760K, we may neglect the range of temperatures below 760K, and remove steps s_{14}, s_{15}, and s_{16}. Again comparing the overall kinetics to the mechanism less s_{14}, s_{15}, and s_{16} suggested that these steps are not kinetically significant.

The log of the summation of resistances s_{15}, s_{14}, and s_{18} is compared with the log of the summation of s_{13}, s_{12}, s_{11} and s_{17}, which provides similar curves as in Figure 17. Steps s_{15}, s_{14}, and s_{18} has higher resistance at temperatures above 675K range suggesting that steps s_{15}, s_{14}, and s_{18} should be removed. If the first option mentioned above was conducted. Thus steps s_{13}, s_{12}, s_{11} and s_{17} should be retained. Therefore, whether the results of Figure 17 are used or those of Figure 18 in the reduction of the network, the end result is the same.

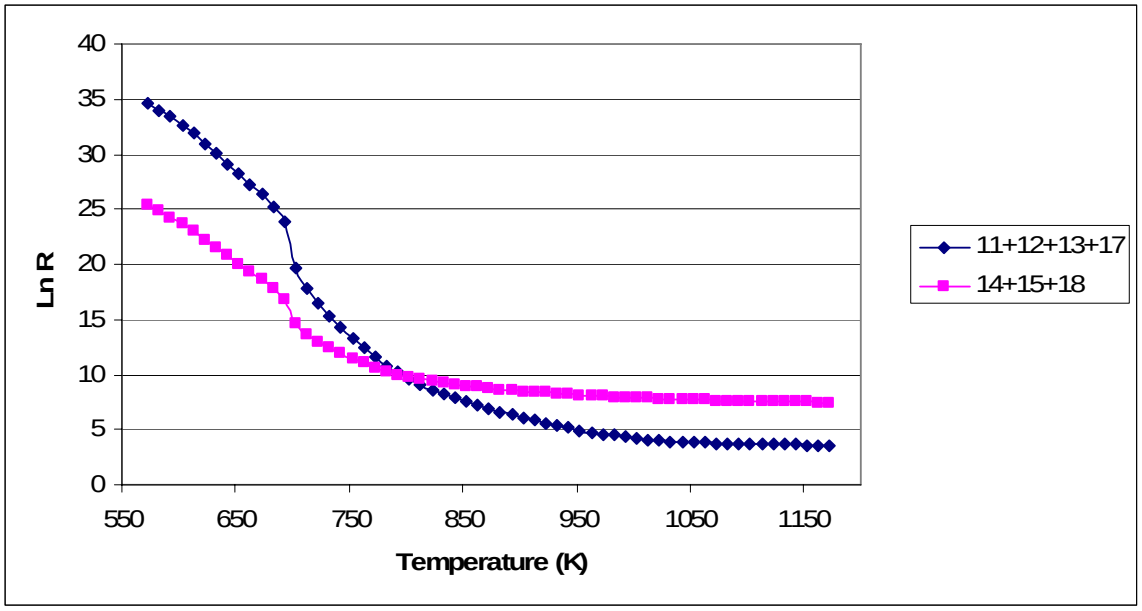

Figure 18 The resistance of $s_{11}+s_{12}+s_{13}+s_{17}$ and $s_{14}+s_{15}+s_{18}$ vs. temperature

After all these comparisons among the parallel pathways, steps s_4, s_{15}, s_{16}, and s_{18} are indicated to be removed. The final step is to compare the overall kinetics of the mechanism to the reduced mechanism, and it is found that these steps are not kinetically significant. The hence reduced version of electrical network of Figure 15 is presented in Figure 19.

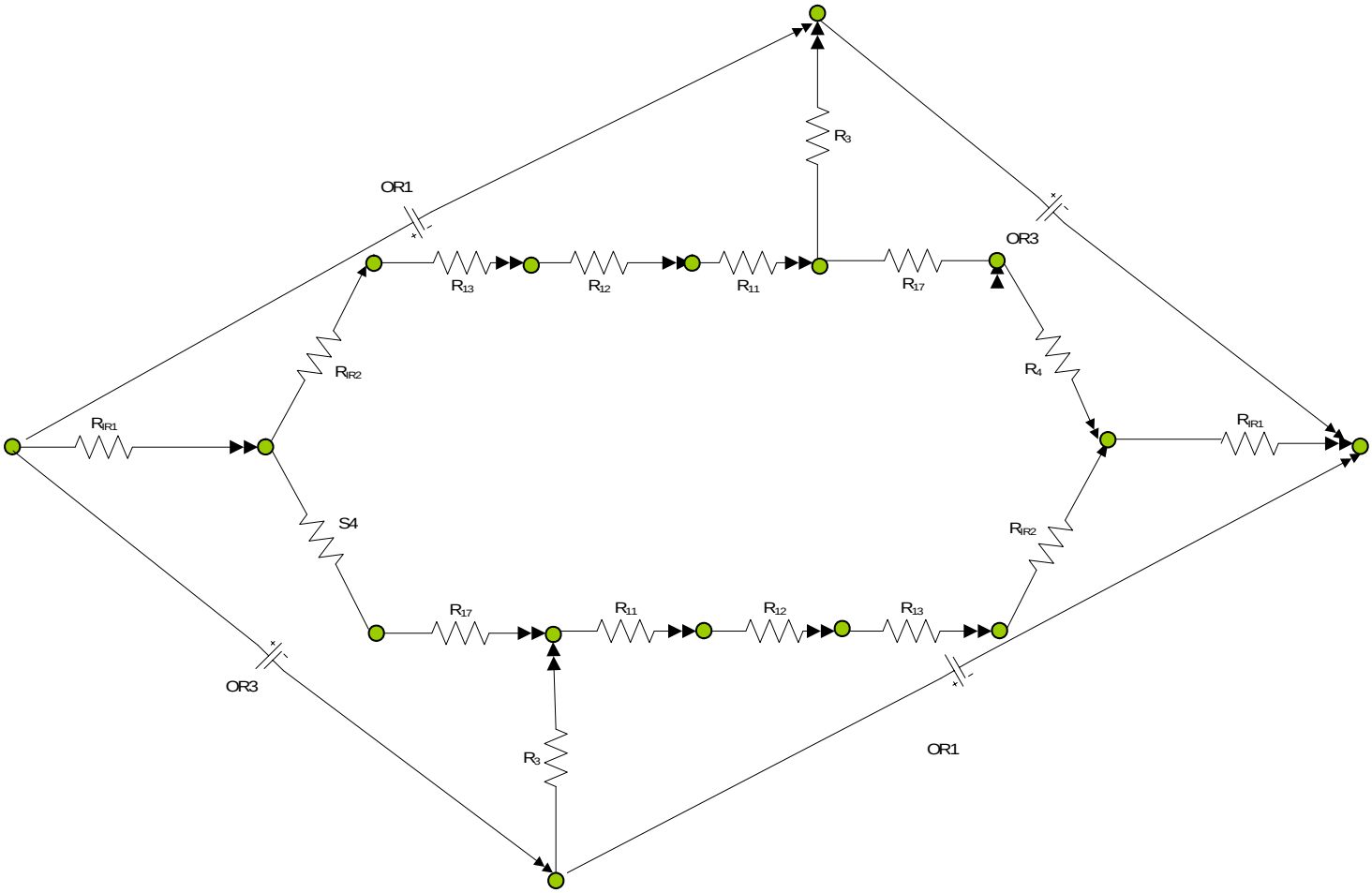

Figure 19 Reduced electrical analog of figure 11

Further reduction to determine the rate limiting step in a sequence is conducted by comparing the resistance in series. Steps IR_2, s_{13}, s_{12}, and s_{11} are compared to the summation of these resistances, showing s_{11} to be the dominant step, with a resistance closest to the summation as shown in Figure 20.

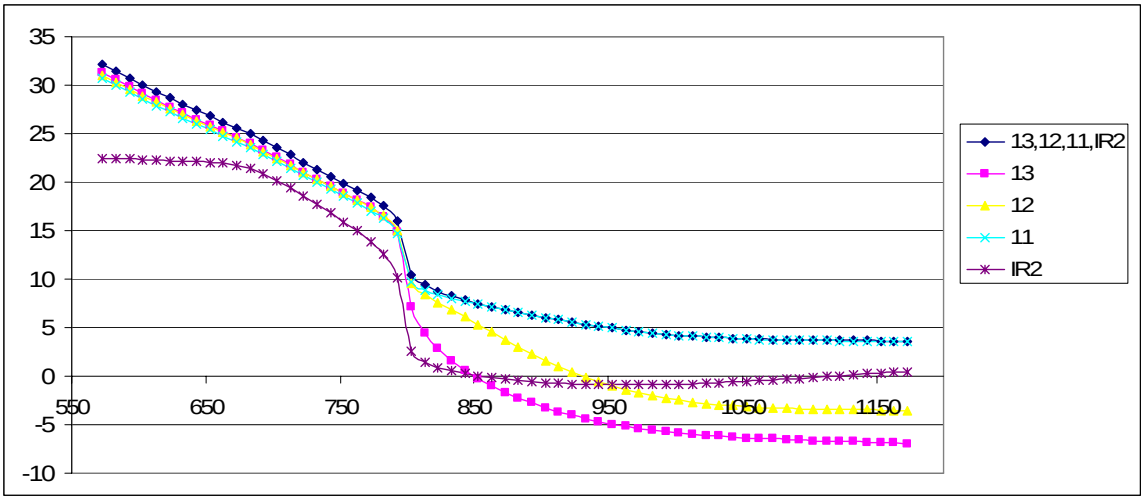

Figure 20 The resistance of $s_{11}+s_{12}+s_{13}+IR_2$, s_{11}, s_{12}, s_{13}, and IR_2, vs. temperature

The same types of comparison were made between steps s_{17} and s_4, and step s_4 was found to be the rate limiting step shown in Figure 21.

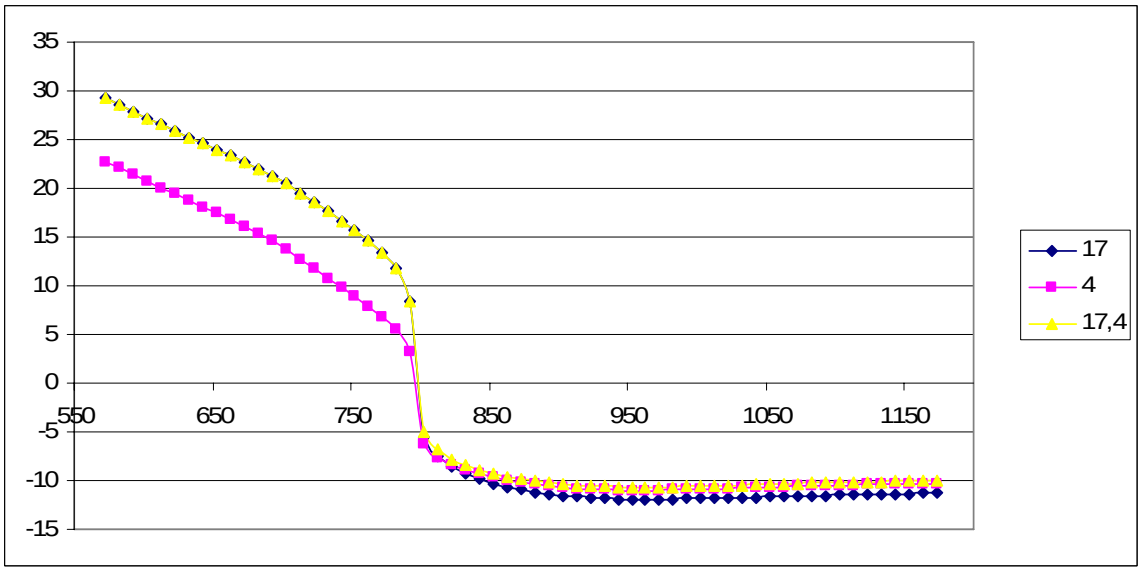

Figure 21 The resistance of $s_{17}+s_4$, s_{17}, s_4 vs. temperature

The hence reduced network is shown in Figure 22.

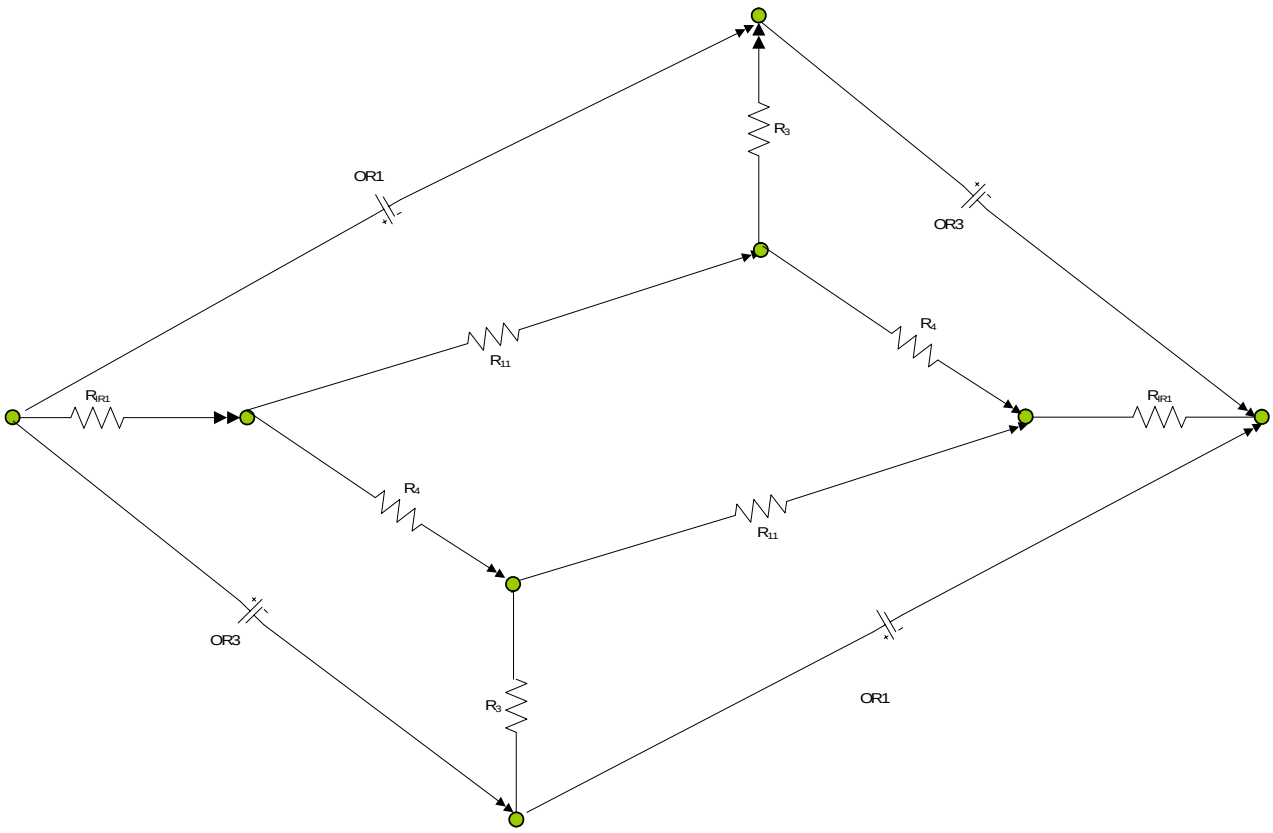

Figure 22 Reduced network without steps s_{17}, IR_2, s_{12}, and s_{13}

From the full route enumeration, it was seen that there are four overall reactions. One question that occurred was whether or not all four overall reactions are needed, since two of them are linearly dependent on the other two as discussed above. Multisim as discussed above assisted in determining this by showing that only two overall reactions are required to complete the circuit. When a third overall reaction was added, an error with a violation of nodal balance occurred. Hence only OR_1 and OR_3 are shown in the networks in this chapter. Of course choice of OR_1 and OR_3 is arbitrary. Any other two ORs could alternately be chosen for this purpose.

6.3 Multisim Analysis

A new methodology was implemented to assist in verifying the reaction route graph. This tool is known as Multisim. It is an interactive SPICE circuit simulator that allows you to design, create and then instantly simulate the circuit. This tool was used to provide a visual and instant simulation of the electrical circuit in Figure 15 and to provide

a confirmation of the results provided by the simulation to the results provided by Multisim. In addition, it also provided insight on the number of overall reactions needed for the system. Only 2 overall reactions are independent while the remaining 2 can be obtained by their linear combination. The electrical simulations of the overall electrical circuit at 2 different temperatures are provided in Figure 23 and Figure 24.

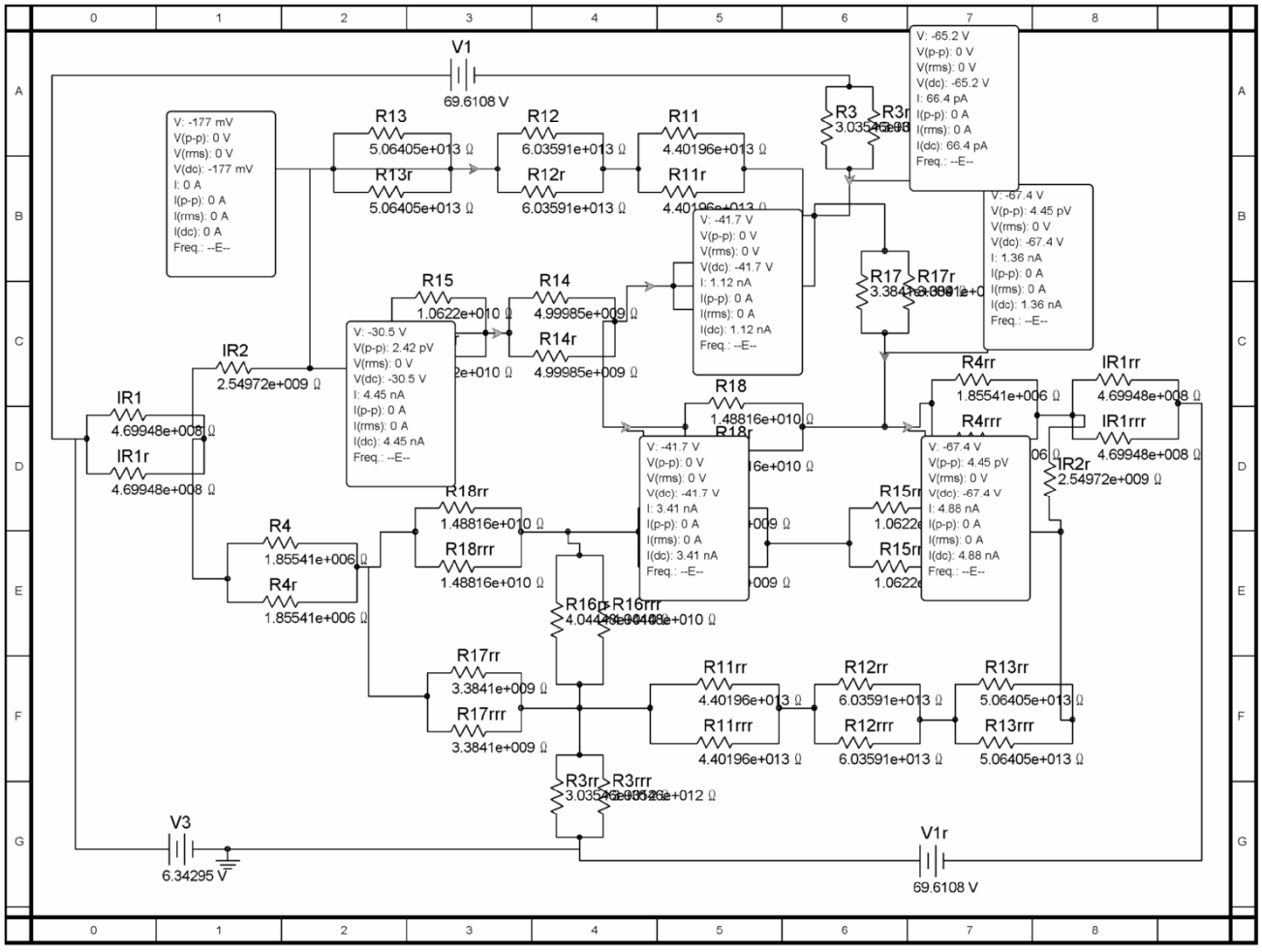

Figure 23 Complete overall reaction network at 603K with OR1 and OR3

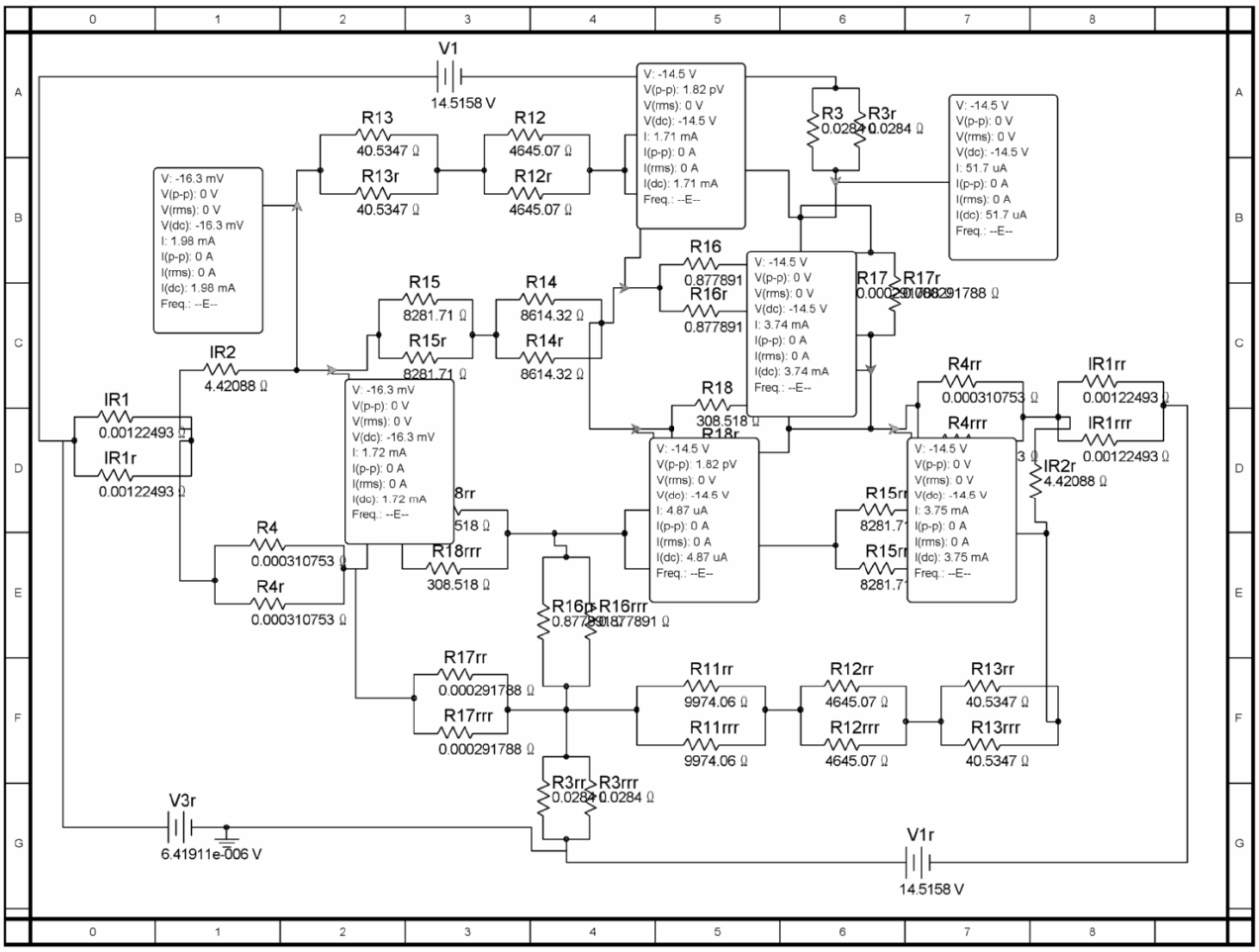

Figure 24 Complete overall reaction network at 903K with OR1 and OR3

6.4 Explicit rate expression

An explicit overall rate equation may be derived by solving the QSS condition for the surface intermediates. For OR_1, the rate limiting step is step s_{11} and for OR3 the rate limiting step is s_4. These rate expressions are derived from the 18 step mechanism, which includes the additional steps from the dissociated form of step IR_1 of the original 16 step mechanism. The derivation of the rate expression will be shown here.

From the reduced graph Figure 19, we see that the full route corresponds to OR*1* is IR_1, IR_2, s_{11}, s_{12}, s_{13}, and s_3. Using the 18 step mechanism, s_{11} (rate limiting step) and the rest of the steps at quasi-equilibrium, i.e., their rates are set equal to zero.

$$r_{11} = \vec{k}_{11}\theta_{CH_2S}\theta_S - \overleftarrow{k}_{11}\theta_{CHS}\theta_{HS}$$

$$0 = r_1 = \vec{k}_1 \theta_{CH_4S} - \overleftarrow{k}_1 P_{CH_4} \theta_S$$
$$0 = r_2 = \vec{k}_2 P_{H_2O} \theta_S - \overleftarrow{k}_2 \theta_{H_2OS}$$
$$0 = r_3 = \vec{k}_3 \theta_{COS} - \overleftarrow{k}_3 P_{CO} \theta_S$$
$$0 = r_5 = \vec{k}_5 \theta_{HS} \theta_{HS} - \overleftarrow{k}_5 \theta_{H_2S} \theta_S$$
$$0 = r_6 = \vec{k}_6 \theta_{H_2S} - \overleftarrow{k}_6 P_{H_2} \theta_S$$
$$0 = r_7 = \vec{k}_7 P_{H_2OS} \theta_S - \overleftarrow{k}_7 \theta_{OHS} \theta_{HS}$$
$$0 = r_8 = \vec{k}_8 \theta_{OHS} \theta_S - \overleftarrow{k}_8 \theta_{OS} \theta_{HS}$$
$$0 = r_9 = \vec{k}_9 \theta_{CH_4S} \theta_S - \overleftarrow{k}_9 \theta_{CH_3S} \theta_{HS}$$
$$0 = r_{10} = \vec{k}_{10} \theta_{CH_3S} \theta_S - \overleftarrow{k}_{10} \theta_{CH_2S} \theta_{HS}$$
$$0 = r_{12} = \vec{k}_{12} \theta_{CHS} \theta_S - \overleftarrow{k}_{12} \theta_{CS} \theta_{HS}$$
$$0 = r_{13} = \vec{k}_{13} \theta_{CS} \theta_{OS} - \overleftarrow{k}_{13} \theta_{COS} \theta_S$$

Solving these QSS conditions give:

$$\theta_{CH_4S} = K_1 P_{CH_4} \theta_S ; \qquad \theta_{H_2OS} = K_2 P_{H_2O} \theta_S ; \qquad \theta_{COS} = \frac{P_{CO} \theta_S}{K_3} ;$$

$$\theta_{H_2S} = \frac{P_{H_2} \theta_S}{K_6} \quad ; \qquad \theta_{HS} = \theta_S \left(\frac{P_{H_2}}{K_5 K_6} \right)^{\frac{1}{2}} ; \qquad \theta_{OHS} = \frac{K_2 K_7 P_{H_2O} \theta_S}{\left(\frac{P_{H_2}}{K_5 K_6} \right)^{\frac{1}{2}}} ;$$

$$\theta_{OS} = \frac{K_2 K_5 K_6 K_7 K_8 P_{H_2O} \theta_S}{P_{H_2}} ; \qquad \theta_{CH_3S} = \frac{K_1 K_9 P_{CH_4} \theta_S}{\left(\frac{P_{H_2}}{K_5 K_6} \right)^{\frac{1}{2}}} ; \qquad \theta_{CH_2S} = \frac{K_1 K_5 K_6 K_9 K_{10} P_{CH_4} \theta_S}{P_{H_2}} ;$$

$$\theta_{CHS} = \frac{P_{CO} \left(\frac{P_{H_2}}{K_5 K_6} \right)^{\frac{3}{2}} \theta_S}{K_2 K_3 K_7 K_8 K_{12} K_{13} P_{H_2O}} ; \qquad \theta_{CS} = \frac{P_{CO} P_{H_2} \theta_S}{K_2 K_3 K_5 K_6 K_7 K_8 K_{13} P_{H_2O}}$$

Substituting the solved intermediate species into the rate limiting step provides

$$r_{11} = \vec{k}_{11} \frac{K_1 K_5 K_6 K_9 K_{10} P_{CH_4} \theta_S^2}{P_{H_2}} - \overleftarrow{k}_{11} \frac{P_{CO} \left(\frac{P_{H_2}}{K_5 K_6} \right)^{\frac{3}{2}} \theta_S}{K_2 K_3 K_7 K_8 K_{12} K_{13} P_{H_2O}} \theta_S \left(\frac{P_{H_2}}{K_5 K_6} \right)^{\frac{1}{2}}$$

Factoring the rate by $\vec{k}_{11}$ and rearranging the equation gives the rate expression for OR1 as

$$R_{OR1} = r_{11} = \frac{\overrightarrow{k_{11}} K_1 K_5 K_6 K_9 K_{10} P_{CH_4} \theta_s^2}{P_{H_2}} \left(1 - \frac{1}{K_{OR_1}} \frac{P_{CO} P_{H_2}^3}{P_{CH_4} P_{H_2O}} \right) \tag{41}$$

where K_{OR_1} and θ_S are

$$K_{OR_1} = K_1 K_2 K_3 K_5^3 K_6^3 K_7 K_8 K_9 K_{10} K_{11} K_{12} K_{13} \tag{42}$$

$$\theta_s = \frac{1}{1 + K_1 P_{CH_4} + K_2 P_{H_2O} + \frac{P_{CO}}{K_3} + \frac{P_{H_2}}{K_6} + \left(\frac{P_{H_2}}{K_5 K_6}\right)^{\frac{1}{2}} + \frac{K_2 K_7 P_{H_2O}}{\left(\frac{P_{H_2}}{K_5 K_6}\right)^{\frac{1}{2}}} + \frac{K_2 K_7 K_8 P_{H_2O}}{\left(\frac{P_{H_2}}{K_5 K_6}\right)} + \frac{K_1 K_9 P_{CH_4}}{\left(\frac{P_{H_2}}{K_5 K_6}\right)^{\frac{1}{2}}} + \frac{K_1 K_9 K_{10} P_{CH_4}}{\left(\frac{P_{H_2}}{K_5 K_6}\right)} + \frac{P_{CO}\left(\frac{P_{H_2}}{K_5 K_6}\right)^{\frac{3}{2}}}{K_2 K_3 K_7 K_8 K_{12} K_{13} P_{H_2O}} + \frac{P_{CO} P_{H_2}}{K_2 K_3 K_5 K_6 K_7 K_8 K_{13} P_{H_2O}} + \frac{P_{CO} P_{H_2}}{K_5 K_6 K_{15} K_{16}} + \frac{P_{CO}\left(\frac{P_{H_2}}{K_5 K_6}\right)^{\frac{1}{2}}}{K_{16}} \frac{K_2 K_5 K_6 K_7 K_8 K_{17} P_{CO} P_{H_2O}}{K_3 P_{H_2}}}$$

θ_s is determined from substituting all the θ's in site balance and solving for θ_S.

$$1 = \theta_S + \theta_{CH_4S} + \theta_{H_2OS} + \theta_{COS} + \theta_{H_2S} + \theta_{HS} + \theta_{OHS} + \theta_{OS} + \theta_{CH_3S} + \theta_{CH_2S} + \theta_{CHS} + \theta_{CS} + \theta_{CO_2S} + \theta_{CHOS} + \theta_{CH_2OS}$$

Both θ_{CHOS} and θ_{CH_2OS} are obtained from the QSS conditions of steps s_9 and s_{12} of the 18 step mechanism.

$$\theta_{CH_2OS} = \frac{P_{CO} P_{H_2} \theta_S}{K_5 K_6 K_{15} K_{16}} \qquad \theta_{CHOS} = \frac{P_{CO} \theta_S \left(\frac{P_{H_2}}{K_5 K_6}\right)^{\frac{1}{2}}}{K_{16}} \qquad \theta_{CO_2S} = \frac{K_2 K_5 K_6 K_7 K_8 K_{17} P_{CO} P_{H_2O} \theta_S}{K_3 P_{H_2}}$$

$$\theta_{CHS} = \frac{P_{CO}\left(\frac{P_{H_2}}{K_5 K_6}\right)^{\frac{3}{2}} \theta_S}{K_2 K_3 K_7 K_8 K_{12} K_{13} P_{H_2O}} \qquad \theta_{CS} = \frac{P_{CO} P_{H_2} \theta_S}{K_2 K_3 K_5 K_6 K_7 K_8 K_{13} P_{H_2O}}$$

Performing the same calculations for OR_3:

$$r_4 = \vec{k}_4\theta_{CO_2S} - \overleftarrow{k}_4 P_{CO_2}\theta_S$$
$$0 = r_2 = \vec{k}_2 P_{H_2O}\theta_S - \overleftarrow{k}_2\theta_{H_2OS}$$
$$0 = r_3 = \vec{k}_3\theta_{COS} - \overleftarrow{k}_3 P_{CO}\theta_S$$
$$0 = r_4 = \vec{k}_4\theta_{CO_2S} - \overleftarrow{k}_4 P_{CO_2}\theta_S$$
$$0 = r_5 = \vec{k}_5\theta_{HS}\theta_{HS} - \overleftarrow{k}_5\theta_{H_2S}\theta_S$$
$$0 = r_6 = \vec{k}_6\theta_{H_2S} - \overleftarrow{k}_6 P_{H_2}\theta_S$$
$$0 = r_7 = \vec{k}_7 P_{H_2OS}\theta_S - \overleftarrow{k}_7\theta_{OHS}\theta_{HS}$$
$$0 = r_8 = \vec{k}_8\theta_{OHS}\theta_S - \overleftarrow{k}_8\theta_{OS}\theta_{HS}$$
$$0 = r_{17} = \vec{k}_{17}\theta_{COS}\theta_{OS} - \overleftarrow{k}_3\theta_{CO_2S}\theta_S$$

$$\theta_{H_2OS} = K_2 P_{H_2O}\theta_S; \qquad \theta_{COS} = \frac{P_{CO}\theta_S}{K_3}; \qquad \theta_{CO_2S} = \frac{K_2K_5K_6K_7K_8K_{17}P_{CO}P_{H_2O}\theta_S}{K_3 P_{H_2}};$$

$$\theta_{H_2S} = \frac{P_{H_2}\theta_S}{K_6}; \qquad \theta_{HS} = \theta_S\left(\frac{P_{H_2}}{K_5K_6}\right)^{\frac{1}{2}}; \qquad \theta_{OHS} = \frac{K_2K_7P_{H_2O}\theta_S}{\left(\frac{P_{H_2}}{K_5K_6}\right)^{\frac{1}{2}}};$$

$$\theta_{OS} = \frac{K_2K_7K_8P_{H_2O}\theta_S}{\left(\frac{P_{H_2}}{K_5K_6}\right)}$$

Doing the same type of calculations above give a rate expression for OR3

$$R_{OR3} = r_4 = \frac{\overrightarrow{k_4}K_2K_5K_6K_7K_8K_{17}P_{CO}P_{H_2O}\theta_S}{K_3P_{H_2}}\left(1 - \frac{1}{K_{OR_1}}\frac{P_{CO_2}P_{H_2}}{P_{CO}P_{H_2O}}\right) \qquad (43)$$

where K_{OR3} and θ_s are

$$K_{OR_3} = \frac{K_2K_4K_5K_6K_7K_8K_{17}}{K_3} \qquad (44)$$

Another method to obtain the rate expression may be from using the interrelations of the affinities and appropriate expressions for the rates of the elementary reaction steps,

according to $\vec{r}_\rho = \vec{A}_\rho e^{\frac{-\vec{E}_\rho}{RT}} \theta_o^{\vec{\alpha}_{\rho o}} \prod_{k=1}^{q} \theta_k^{\vec{\alpha}_{\rho k}} \prod_{i=1}^{n} P_i^{\vec{\beta}_{\rho k}}$, or without the intermediate derivation of the rate expression according to $r_{OR} = \mathscr{H}_{OR}/R_{OR.}$

The error in the conversion of CH_4 provided by this overall rate expression is pretty significant, as can be seen in Figure 25. The reasons for this are not yet clear.

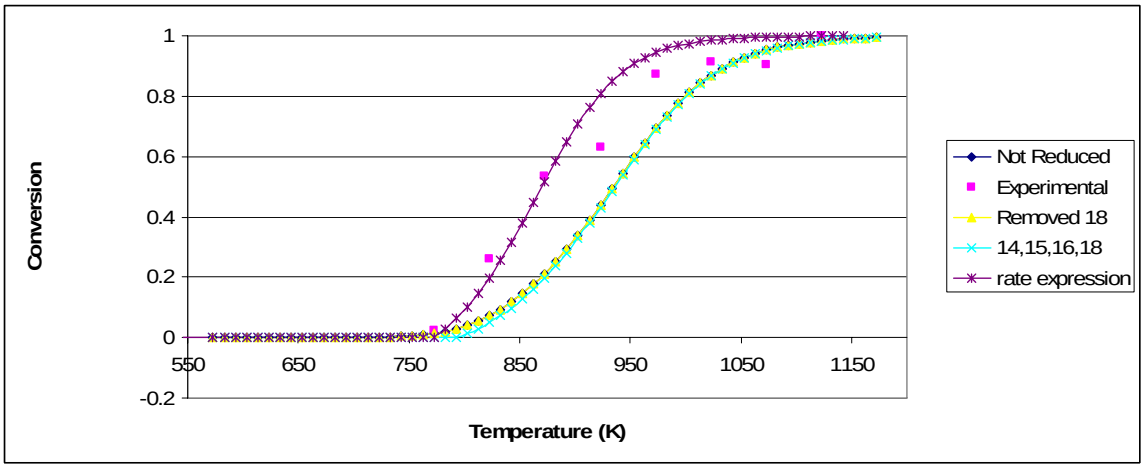

Figure 25 Rate expression conversion plotted against removal of s_{18}, s_{16}, s_{15}, s_{14} and experimental data point for Ni (111)

The mole fractions of the terminal species corresponding to the range of temperature used in the calculation of the micro-kinetic model were used to calculate the surface coverage of the intermediate species. These were than compared with the micro-kinetic model surface coverage of the intermediate species. This procedure is to confirm that the values calculated for the surface coverage of the intermediate species from the QSS equations would be the same for the micro-kinetic model calculation of the surface coverage of the intermediate species; however, the results showed that they are different, meaning that the assumption made to obtain the rate expression may be invalid. This may mean that the rate limiting steps s_{11} and s_4 that were assumed may have been insufficient to deduce the overall rate expression.

6.5 Nickel-based catalyst

$Ni/Al_2O_3/CaO$ from Süd-Chemie was used to perform experimental work. The reaction energetics for Ni(111), given in Table 3, as calculated from UBI-QEP method

and the transition state theory, were used in microkinetic analysis. As can be seen from Figure 26, the microkinetic model predicts a similar shape as the experimental data for the Ni catalyst and fits rather well. The active surface area, number of active sites, and catalyst density values used for Ni were: 3.43 x 10^4 cm^2/g, 1.41 x 10^{15} sites/cm^2, and 0.5 g/cm^3, respectivly. Xu and Froment [14]used a catalyst containing 15.2% nickel, supported on magnesium spinel with a BET-surface area of 58m^2, and nickel surface area of 9.8 m^2/g. Aparicio [51] used a catalyst with 25%Ni with a Ni surface area of 5.7 m^2/g and a BET surface area of 50 m^2/g. The active surface are used in accordance to the range of values provided by Callaghan [44], and they were 3 x 10^4 cm^2/g – 1.5 x 10^5 cm^2/g surface area.

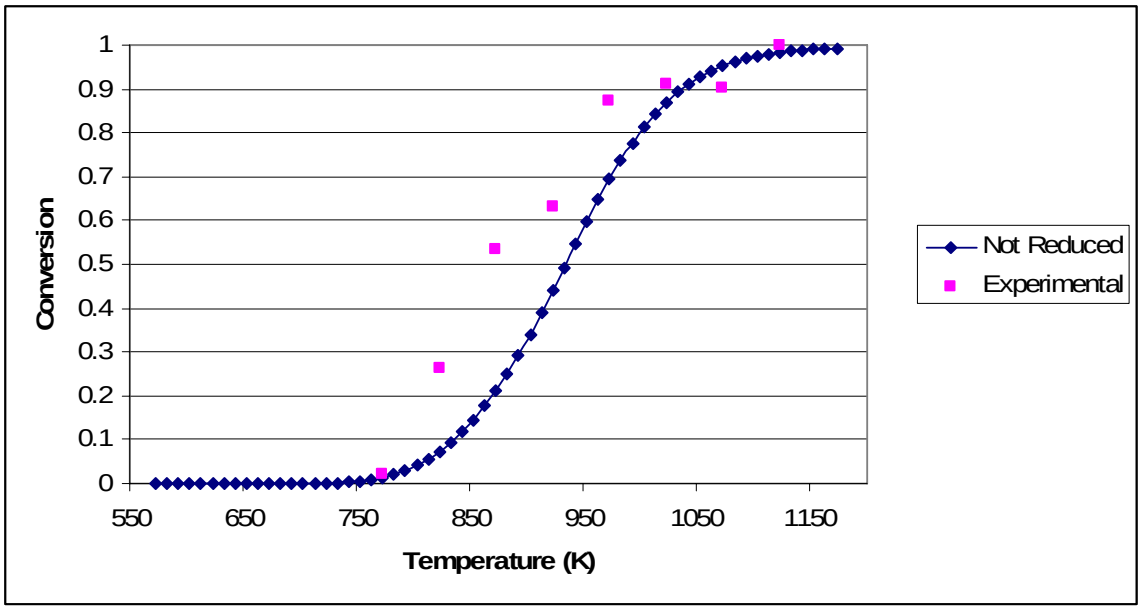

Figure 26 Feed composition: CH_4 (20%), H_2O (40%), and N_2 balance. Pressure of 1 atm, residence time τ =1.8 for Nickel (111)

6.6 Rhodium-based catalyst

The reaction energetics for Rh(111) on Al_2O_3, given in Table 3, are also calculated from UBI-QEP method and the transition state theory. The microkinetic model predicted the experimental data for the Rh catalyst with values that fitted well with the experimental results. The Rh catalysts used the same values for the active surface area, number of active sites, and catalyst density as for Nickel. These values are in within the ballpark of literature values. Rostrup-Nielsen [31] proposed a Rh catalyst on MgO with

1.1wt% having a metal surface area of 2.2 m^2/g. Johnson [52] has used a Rh wt% of 10 giving a surface area of 2.2 m^2/g. In addition, he also has used a 3.7 wt% Rh catalyst with a surface area of 0.58 m^2/g.

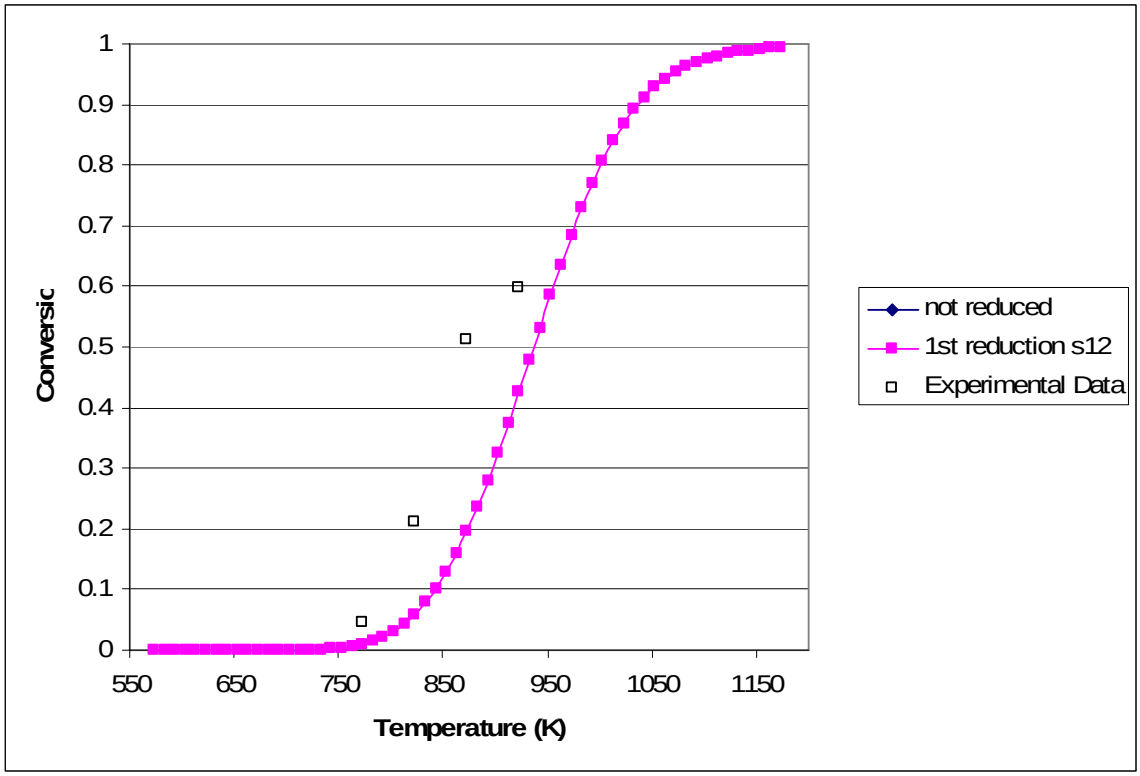

Figure 27 Feed composition: CH_4 (20%), H_2O (40%), and N_2 balance. Pressure of 1 atm, residence time τ =1.8 for Rhodium (111)

Chapter 7 Conclusions and Future Work

An interest in fuel cell has risen due to their high efficiency and ideally emission-free use. One fuel cell of interest is solid oxide fuel cell. It may operate at high temperatures in the range of 700-1000^{o}C, making it possible to use CO and even low hydrocarbons such as CH_4 directly as a fuel, unlike lower temperature fuel cells that require H_2.

To advance the fuel cell technology, one study of interest has been in catalysts. In the past, much attention has been paid to the preparation of catalysts and the evaluation of the process and equipment with little work being done on the kinetics and mechanism of the reaction. Further, developing reformers for hydrocarbon fuels requires good understanding of the fundamental mechanisms and kinetics studies. Kinetics of steam reforming have been previously studied by many groups such as Temkin et al, and Xu and Froment.

This study provides a theoretical and experimental approach in unraveling the mechanism and kinetics of logistic fuel external and internal reforming for solid oxide fuel cell. The building block to this began with studying the methane steam reforming process. The overall MSR reaction $CH_4 + 2H_2O = CO_2 + 4H_2$ is in fact composed of two reactions, the water gas shift reaction, $CO + H_2O = CO_2 + H_2$ and the first reaction $CH_4 + H_2O = CO + 3H_2$. A novel theoretical methodology known as the reaction route network approach developed by this group provides a detailed technique in analyzing the kinetics and thermodynamics of the reaction. The Unity Bond Index-Quadratic Exponential Potential (UBI-QEP) method of Shustorovich coupled with transition-state theory was combined with the reaction route to provide prediction to elementary step kinetics resulting a detailed microkinetic model of steam and dry reforming of methane has been developed for Rh(111) and Ni(111) in this thesis

Previous work, performed by Caitlin Callaghan, used an 18-step mechanism with predicted kinetics for the water-gas shift reaction, and used the reaction route graph theory to provide a depiction of the reaction pathways with branches representing elementary reaction steps and the nodes symbolize their connectivity within reaction routes. Basic concepts of graph theory and Kirchhoff's Laws have been employed to determine the connectivity of the elementary reaction steps in a mechanism and its

kinetics. Then using these concepts, an analogy can be made between the developed reaction route graph and the electrical circuit theory to analyze and reduce the reaction route graph to a simpler form where, the rate limiting steps, quasi-equilibrium steps, and dominant pathways are easily identified.

A 16-step mechanism composed of the standard 13 step mechanism of MSR from Xu and Froment with 3 additional elementary steps crucial to carbon formation, with predicted kinetics for methane steam reforming reaction was used to demonstrate the usefulness of the reaction route graph theory. A reaction route graph was constructed and converted into a reaction route network, where Kirchhoff's Laws were applied to reduce the diagram by examining comparable path resistances and eliminating the more resistant pathway.

Using reaction route theory, a total of 4 overall reactions were determined, of which any 2 of them are linearly independent. This means that only 2 overall reactions are needed and are characterized by the reaction route graph. While performing the reduction of the electrical graph, an 18 step mechanism was applied to perform the kinetics study. The reason for this is due to a step from Xu and Froment that is not an elementary step. That step was broken into 5 steps of which 2 of them were added to the 16 step mechanism. Enumerating the FRs and ERs for these 18 step mechanism resulted in 5 overall reactions rather than 4. To avoid the additional complexities, it was decided to stick with the 16 step mechanism to draw the reaction route graph, while the 18 step mechanism was used to perform the microkinetic study.

In enumerating the mechanisms to obtain the full routes, empty routes and intermediate nodes, a program created in Maple was utilized. This program was improved from an earlier based program from Matlab. The program created in Matlab had limitations with the size of the matrix and required excessive amounts of repetitive work. The Maple program improved the repetitive work by allowing the computer to do the work. Yet, there is still limitation with the size of the matrix as it requires a larger capacity of RAM to run larger sized matrix.

The reduced graph provided the dominant pathways and steps to be steps s_4 and s_{11}. While reducing the graph, an interactive electric circuit software known as Multisim was utilized to verify the reaction route graph and provide further insight about the graph

that we were unable to obtain from the normal reduction method. Multisim informed us that only 2 overall reactions are needed to define the system rather than 4 overall reactions. The assumed rate determining steps with remaining steps at pseudo-equilibrium along with the quasi steady state approximation was used to obtain an explicit rate expression. The resulting rate expression of methane steam reforming based on simple catalyst parameters as well as the experimental feed condition does not; however, predict the kinetics well. The experimental data were obtained from running a steam to carbon ratio of 2:1 while using wither Ni (111) from Süd-Chemie and Rh (111) from wet incipient technique as the packed catalyst within the reactor. Data were collected for a temperature range of 200-900^{o}C.

For future work, the rate expression will be looked into in more detail, to determine if the assumptions made to derive the rate expression is correct. This would be done by using Multisim to assist in confirming whether or not the assumed removed steps are correct. Further, after confirming the rate expression, it is necessary to perform more experimental work. The only experimental data that were obtained were only for the forward reaction. In addition, reverse and an intermediate feed condition. In addition, intermediate feed conditions will allow the comparison of the experimentally determined reaction order to those predicted by the model.

Supplementary feed condition and reaction order experiments will be conducted. We would also like to use other methods of calculating the surface energetics to see if changes with the catalyst parameters will change the result of the reaction route graph. Reliability of the reaction energetics is of importance to the approach used and described here. In this case, there are other methods in obtaining surface energetics, such as *ab initio* and semi-empirical methods. In our case, we used the UBI-QEP method, where it uses heats of adsorption and reaction activation barriers with a typical accuracy of 1-3 kcal.

References

1. Jack. *The Coming World Oil Crisis*. 2006 12 September [cited 2006 September 12]; Available from: http://www.planetforlife.com/index.html.

2. Ahmed, S. and M. Krumpelt, "Hydrogen from Hydrocarbon fuels for fuel cells." *International Journal of Hydrogen Energy, 2001*. **26**(4): p. 291-301.

3. Energy, U.D.o. *The Environment*. 2006 [cited 2006 August 12]; Available from: http://www.energy.gov/.

4. O'Hayre, R., Cha, S.W., Colella, W., and Prinz, F.B., *Fuel Cell Fundamentals*. 2006, Hoboken, New Jersey: John Wiley & Sons, Inc.

5. Larminie, J. and A. Dicks, *Fuel cell systems explained* 2000, New York John Wiley & Sons. 308

6. Wikipedia. *Fuel Cell*. 2006 12 September [cited 2006 September 12]; Available from: http://en.wikipedia.org/wiki/Fuel_cell.

7. Douvartzides, S.L., Coutelieries, F.A. , Demin, A.K., and P.E. Tsiakaras "Fuel Options for Solid Oxide Fuel cells: a Thermodynamic Analysis." *AIChE Journal*, 2003. **49**(1): p. 248-257.

8. Rostrup-Nielsen, J.R., "Conversion of hydrocarbons and alcohols for fuel cells." *Physical Chemistry Chemical Physics*, 2001. **3**(3): p. 283-288.

9. Rostrup-Nielsen, J.R., *Catalytic Steam Reforming*. 1984, Berlin: Springer-Verlag.

10. Huang, T.-J., T.-C. Yu, and S.-Y. Jhao, "Weighing Variation of Water-Gas Shift in Steam Reforming of Methane over Supported Ni and Ni-Cu Catalysts." *Industrial and Engineering Chemistry*, 2006. **45**(1).

11. Joensen, F. and J.R. Rostrup-Nielsen, "Conversion of hydrocarbons and alcohols for fuel cells." *Journal of Power Sources*, 2002. **105**(2): p. 195-201

12. Ming, Q., Healey, T., Allen L., and P. Irving, "Steam reforming of hydrocarbon fuels" *Catalysis Today*, 2002. **77**(1-2): p. 51-64

13. Temkin, M.I., "Industrial Heterogeneous Catalytic Reactions." *Adv. Catal.,* 1979. **28**: p. 175–292.

14. Xu, J. and G.F. Froment, "Methane steam reforming, methanation and water-gas shift: I. Intrinsic kinetics." *AIChE Journal*, 1989. **35**(1): p. 88-96.

15. Wei, J. and E. Iglesia, "Mechanism and Site Requirements for Activation and Chemical COnversion of Methane on Supported Pt Clusters and Turnover Rate Comparisons among Noble Metals." *J. Phys. Chem. B*, 2004. **108**: p. 4094-4103.

16. Dreyer, B.J., Lee, I.C., Krummenacher, J.J, and L.D Schmidt, "Autothermal steam reforming of higher hydrocarbons: n-Decane, n-hexadecane, and JP-8." *Applied Catalysis A: General*, 2006. **307**(2): p. 184-194

17. Horn, R., Williams, K.A., Degenstein, N.J., and L.D. Schmidt, "Syngas by catalytic partial oxidation of methane on rhodium: Mechanistic conclusions from spatially resolved measurements and numerical simulations." *Journal of Catalysis*, 2006. **242**(1): p. 92-102

18. Kusakabe, K., Sotowa, K.I., Eda, T. and Y. Iwamoto "Methane steam reforming over Ce–ZrO2-supported noble metal catalysts at low temperature." *Fuel Processing Technology*, 2004. **86**(3): p. 319-326

19. Wanat, E.C., K. Venkataraman, and L.D. Schmidt, "Steam reforming and water-gas shift of ethanol on Rh and Rh-Ce catalysts in a catalytic wall reactor." *Applied Catalysis A: General*, 2004. **276**(1-2): p. 155-162

20. Liguras, D.K., D.I. Kondarides, and X.E. Verykios, "Production of hydrogen for fuel cells by steam reforming of ethanol over supported noble metal catalysts" *Applied Catalysis B: Environmental*, 2003. **43**(4): p. 345-354

21. Venkataraman, K., E.C. Wanat, and L.D. Schmidt, "Steam reforming of methane and water-gas shift in catalytic wall reactors." *AIChE Journal*, 2003. **49**(5): p. 1277-1284.

22. Rakass, S., Oudghiri-Hassani, H., Rowntree, P. and N. Abatzoglou, "Steam reforming of methane over unsupported nickel catalysts," *Journal of Power Sources*, 2006. **158**(1): p. 485-496

23. Jeong, J.H., Lee, J.W., Seo, D.J., Seo, Y., Yoon, W.L., Lee, D.K., and D.H. Kim, "Ru-doped Ni catalysts effective for the steam reforming of methane without the pre-reduction treatment with H_2," *Applied Catalysis A: General*, 2006. **302**(2): p. 151-156

24. Berman, A., R.K. Karn, and M. Epstein, "Kinetics of steam reforming of methane on Ru/Al2O3 catalyst promoted with Mn oxides," *Applied Catalysis A: General*, 2005. **282**(1-2): p. 73-83

25. Ishihara, A., Qian, E.W., Finahari, I.N., Sutrisna, I.P., and T. Kabe, "Addition effect of ruthenium on nickel steam reforming catalysts," *Fuel,* 2005. **84**(12-13): p. 1462-1468

26. Souza, M.M.V.M., O.R.M. Neto, and M. Schmal, "Synthesis Gas Production from Natural Gas on Supported Pt Catalysts," *Journal of Natural Gas Chemistry*, 2006. **15**(1): p. 21-27

27. McMinn, T.E., F.C. Moates, and J.T. Richardson, "Catalytic steam reforming of chlorocarbons: catalyst deactivation," *Applied Catalysis B: Environmental*, 2001. **31**(2): p. 93-105

28. Johns, M., Collier, P., Spencer, M.S., Alderson, T., and G.J. Hutchings, "Combined Steam Reforming of Methane and Fischer–Tropsch Synthesis for the Formation of Hydrocarbons: A Proof of Concept Study," *Catalysis Letters*, 2003. **90**(3-4): p. 187-194.

29. Agrell, J, "Production of hydrogen by partial oxidation of methanol over ZnO-supported palladium catalysts prepared by microemulsion technique," *Applied Catalysis A: General*, 2003. **242**(2): p. 233-245

30. Goula, M.A., S.K. Kontou, and P.E. Tsiakaras, "Hydrogen production by ethanol steam reforming over a commercial Pd/γ-Al2O3 catalyst," *Applied Catalysis B: Environmental*, 2004. **49**(2): p. 135-144

31. Rostrup-Nielsen, J. and H.J.H. B., "CO2-Reforming of Methane over Transition Metals," *Journal of Catalysis*, 1993. **144**(1): p. 38-49

32. Smith, D.J. and L.D. Marks, "Direct Lattice Imaging of Small Metal Particles," *Philosophical Magazine A*., 1981 **44**(3): p. 735-740.

33. Wei, J. and E. Iglesia, "Structural requirements and reaction pathways in methane activation and chemical conversion catalyzed by rhodium," *Journal of Catalysis*, 2004. **225**(1): p. 116-127

34. Yokota, S., K. Okumura, and M. Niwa, "Support Effect of Metal Oxide on Rh Catalysts in the CH4-CO2 Reforming Reaction," *Catalysis Letters*, 2002. **84**: p. 131-134.

35. Wang, S. and G.Q.M. Lu, "CO2 reforming of methane on Ni catalysts: Effects of the support phase and preparation technique," *Applied Catalysis B: Environmental* 1998. **16**(3): p. 269-277

36. Bradford, M.C.J. and M.A. Vannice, "Catalytic reforming of methane with carbon dioxide over nickel catalysts I. Catalyst characterization and activity," *Applied Catalysis A: General* 1996. **142**(1): p. 73-96

37. Dong, W.-S., Roh, H.-S., Jun K.-W., Park S.-E., and Y.-S. Oh "Methane reforming over Ni/Ce-ZrO2 catalysts: effect of nickel content," *Applied Catalysis A: General*, 2002. **226**(1-2): p. 63-72.

38. Khomenko, A.A., L.O. Apel'baum, and Temkin, *Kinetics and Catalysis*, 1971. **12**: p. 367.

39. Rostrup-Nielsen, J.R., J. Sehested, and J.K. Norskov, "Hydrogen and synthesis gas by steam-and CO_2 reforming." *Advances in Catalysis*, 2002. **47**: p. 65-139.

40. Compton, R.G., *Kinetic models of catalytic reactions* 1991, New York Elsevier. 392

41. Fishtik, I., C.A. Callaghan, and R. Datta, "Reaction Route Graphs. I. Theory and Algorithm," *J. Phys. Chem. B*, 2004. **108**(18): p. 5671-5682.

42. Fishtik, I., C.A. Callaghan, and R. Datta, "Reaction Route Graphs. II. Examples of Enzyme- and Surface-Catalyzed Single Overall Reactions," *J. Phys. Chem. B*, 2004. **108**(18): p. 5683-5697.

43. Fishtik, I., C.A. Callaghan, and R. Datta, "Reaction Route Graphs. III. Non-Minimal Kinetic Mechanisms." *J. Phys. Chem. B*, 2005. **109**(7): p. 2710-2722.

44. Callaghan, C., *Kinetics and Catalysis of the Water-Gas-Shift Reaction: A Microkinetic and Graph Theoretic Approach* 2006, Worcester Polytechnic Institute: Chemical Engineering. p. 401.

45. Fishtik, I. and R. Datta, "A UBI–QEP microkinetic model for the water–gas shift reaction on Cu(1 1 1)." *Surface Science*, 2002. **512**(3): p. 229-254

46. Shustorovich, E. and H. Sellers, "The UBI-QEP method: A practical theoretical approach to understanding chemistry on transition metal surfaces Surface Science," *Reports*, 1998. **31**(1-3): p. 1-119

47. Fishtik, I., et al., "A reaction route graph analysis of the electrochemical hydrogen oxidation and evolution reactions," *Journal of Electroanalytical Chemistry*, 2005. **576**(1): p. 57-63

48. Lund, C.R.F., "Microkinetics of Water-Gas Shift over Sulfided Mo/Al2O3 Catalysts" Ind., *Eng. Chem. Res*., 1996. **35**: p. 2531-2538.

49. Dumesic, J.A., Rudd, D.F., Aparicio, L.M., Rekoske, J.E., and A.A. Trevino, *The Microkinetics of Heterogeneous Catalysis*. 1993, Washington, DC: American Chemical Society.

50. Rostrup-Nielsen, J.R., *Steam Reforming Catalysts: An Investigation of Catalysts for Tubular Steam Reforming of Hydrocarbons*. 1975, Copenhagen : Teknisk Forlag.

51. Aparicio, L.M., "Transient Isotopic Studies and Microkinetic Modeling of Methane Reforming over Nickel Catalysts." *Journal of Catalysis*, 1997. **165**(2): p. 262-274
52. Johnson, B.R., Canfield, N.L., Tran, D.N., Dagle, R.A., Li, X.S., Holladay, J.D., Wang, Y., "Engineered SMR catalysts based on hydrothermally stable, porous, ceramic supports for microchannel reactors," *Catalysis Today*, 2007. **120**: p. 54–62.

Appendix

Appendix A: Maple Program

```
> restart;
> with(Student[LinearAlgebra]):
> with(combinat):
> ########Input stoichiometric matrix: Double click on the
matrix to edit
```

Replace with the filename of your stoichimetric matrix. You need a "csv" file, accessible in Excel.

```
>
> stoich := ImportMatrix("c:/ReactionRoute/16MSR.csv",
source = csv);
```

$$stoich := \begin{bmatrix} 17 \text{ x } 19 \text{ Matrix} \\ \text{Data Type: anything} \\ \text{Storage: rectangular} \\ \text{Order: Fortran\_order} \end{bmatrix}$$

nINTS: Number of intermediates. Needs to be changed by user.

```
> nINTS:=12;
```

$$nINTS := 12$$

Input filename. Warning: The files will be overwritten without notice

```
> filename:="16MSR":
>
AllFR_file:=cat("c:/ReactionRoute/AllFR_",filename,".csv"):
>
AllER_file:=cat("c:/ReactionRoute/AllER_",filename,".csv"):
>
>
UniqueFR_file:=cat("c:/ReactionRoute/UniqueFR_",filename,".
csv"):
>
UniqueER_file:=cat("c:/ReactionRoute/UniqueER_",filename,".
csv"):
```

```
>
AllIN_file:=cat("c:/ReactionRoute/AllIN_",filename,".csv"):
>
UniqueIN_file:=cat("c:/ReactionRoute/UniqueIN_",filename,".
csv"):
>  nES := RowDimension(stoich)-1:
 nSPECIES := ColumnDimension(stoich)-1:
> for i from 2 to nES+1
do
   rxnR[i] := 0;
   rxnP[i] := 0;
   for j from 2 to nSPECIES+1
   do
     if stoich[i, j] < 0
        then rxnR[i] := evalf(rxnR[i])-stoich[i,
j]*convert(stoich[1, j], symbol);
        else rxnP[i] := evalf(rxnP[i])+stoich[i,
j]*convert(stoich[1, j], symbol);
     end if:
   od:
od:
>
> for i to nES
do
   ESlist[i] := cat(stoich[i+1, 1], ":     ",
convert(rxnR[i+1], string), "  <->  ", convert(rxnP[i+1],
string));   print(ESlist[i]);
od:
```

"S1: SC CH4 ! -O CH4S"

"S2: SC H20 ! -O OSC H2"

"S3: COS ! -O SC CO"

"S4: CO2S ! -O SC CO2"

"S5: 2*HS ! -O H2SC S"

"S6: H2S ! -O SC H2"

"S7: CH4SC S ! -O CH3SC HS"

"S8: CH3SC S ! -O CH2SC HS"

"S9: CH2SC OS ! -O CH2OSC S"

"S10: CH2OSC S ! -O HSC CHOS"

"S11: CHOSC S ! -O COSC HS"

"S12: OSC CHOS ! -O CO2SC HS"

"S13: OSC COS ! -O CO2SC S"

"S14: CH2SC S ! -O CHSC HS"

"S15: CHSC S ! -O HSC CS"

"S16: OSC CS ! -O COSC S"

```
> for i from 1 to nINTS
do
  Q[i]:=0:
  for k from 1 to nES
    do

Q[i]:=Q[i]+stoich[k+1,i+1]*convert(stoich[k+1,1],symbol);
    od:
  print(cat("Q",i,"=",convert(Q[i],string))):
od:
>
```

"Q1=S1-S7"

"Q2=S7-S8"

"Q3=S8-S9-S14"

"Q4=S14-S15"

"Q5=S2-S9-S12-S13-S16"

"Q6=-S3C S11-S13C S16"

"Q7=-S4C S12C S13"

"Q8=-2*S5C S7C S8C S10C S11C S12C S14C S15"

"Q9=S5-S6"

"Q10=S9-S10"

"Q11=S10-S11-S12"

"Q12=S15-S16"

```
> intM := Matrix(nES, nINTS): #Intermediate submatrix
> for i to nINTS
do
  for j to nES
  do intM[j, i] := stoich[j+1, i+1]
  od:
od:
> print("intM:=",intM);
```

"intM:=", *16 x 12 Matrix*
Data Type: anything
Storage: rectangular
Order: Fortran_order

```
> ES:=Rank(intM)+1;
```

$$ES := 13$$

```
>
##############################################################
##############################################################
########
##############################################################
##############################################################
########
##############################################################
##############################################################
########
##############################################################
##############################################################
########
```

Full Routes enumeration:

```
> FRmax := factorial(nES)/(factorial(nES-
ES)*factorial(ES));
```

$$FRmax := 560$$

```
> RRsubmatrix := Matrix(ES-1, nINTS): #Submatrix used to
determine the Si coefficient in the reaction route
> Enumerated:=choose(nES,ES):
> ORcounter:=0:
unique:=1:
AllFR := fopen(AllFR_file, WRITE):
UniqueFR:= fopen(UniqueFR_file,WRITE):
fprintf(UniqueFR,cat(", , Number of steps, Associated OR
\n")):
for k  from 1 to FRmax
do
 counter:=0:
 Steps[k]:="";
 for i from 1 to ES
 do
   for l from 1 to ES-1
   do
     for m from 1 to nINTS
     do
       if (l=i)
          then jump:=1;
       end if;
       RRsubmatrix[l,m]:=intM[Enumerated[k,l+jump],m];

#print(jump,k,l,m,RRsubmatrix[l,m],Enumerated[k,l+jump]);
     od:
   od:
   Scoeff[i]:= (-1)^((i+1))*Determinant(RRsubmatrix);
   jump:= 0;
   #print(Enumerated[k],RRsubmatrix,jump,k,l,m, Scoeff[i]);
  od:
  #Determine gcd of Scoeff
  g:=0;
  for i from 1 to ES
  do
    g:= gcd(g,Scoeff[i]);
    if (g=1) then break end if:
```

```
  od:
  #Check sign of the first non-zero Si coefficient
  neg:=1:
  for i from 1 to ES
  do
    if (Scoeff[i]<>0)
    then
      if (Scoeff[i]<0)
      then
        neg:=-1;
        break;
      else
        neg:=1;
        break;
      end if;
    else
      neg:=0;
    end if;
  od:
  #Puts possible FR into "canonical" form
  for i from 1 to ES
  do
    if (neg<>0) and (g<>0)
    then
      Scoeff[i]:=(Scoeff[i])/(neg*g);
    end if;
  od:
  FR[k]:=0;
  for i from 1 to ES
  do

FR[k]:=FR[k]+convert(stoich[Enumerated[k,i]+1,1],symbol)*Sc
oeff[i];
    if (i<>ES)
    then

Steps[k]:=cat(Steps[k],stoich[Enumerated[k,i]+1,1],";")
    else
Steps[k]:=cat(Steps[k],stoich[Enumerated[k,i]+1,1])
    end if:
  od:
  ###Check if the reaction obtained is "zero"
  OR[k]:=0;
  for i from 1 to ES
  do
    for j from 2 to nSPECIES+1
    do
```

```
OR[k]:=OR[k]+Scoeff[i]*stoich[Enumerated[k,i]+1,j]*convert(
stoich[1,j],symbol);
    od:
  od:
  OR[k]:=simplify(OR[k]);
  ER[k]:=0:
  if (OR[k]=0)
  then
    ER[k]:=1
  end if:
  fprintf(AllFR,cat("FR(",Steps[k],")=", convert(FR[k],
string),"\n")):
  #print(cat("FR(",Steps[k],")=", convert(FR[k], string)));
  if (ER[k]=1)
  then
    Buffer[k]:=0;
  else
    unique:=1:
    for i from 1 to k-1
      do
        if (Buffer[i]=FR[k])
        then
          #print(Buffer[i],FR[k]);
          unique:=0:
          break:
        end if:
      od:
    if (unique=1)
    then
      #uniqueOR:=1:
      for i from 1 to ES
      do
        if (Scoeff[i]<>0) then counter:=counter+1 end if:
      od:
      uniqueORtrue:=1:
      #print(ORcounter):
      for i from 1 to ORcounter
      do
        if (OR[k]<>0)
        then
          #print(OR[k],uniqueOR[i]);
          if (abs(uniqueOR[i])=abs(OR[k]))
          then
            uniqueORtrue:=0:
            ORnumber:=i:
            #print("break",OR[k],OR[i],k,i);
```

```
            break:
          else
            uniqueORtrue:=1:
          end if:
        else
          #print("zero",k,i);
        end if:
      od:
      if (uniqueORtrue=1)
      then
        ORcounter:=ORcounter+1:
        ORnumber:=ORcounter:
        #print("no zero",OR[k],OR[i],ORcounter,i);
        uniqueOR[ORcounter]:=OR[k]:
      end if:
      fprintf(UniqueFR,cat("FR(",Steps[k],")=,",
convert(FR[k],
string),",",convert(counter,string),",OR",convert(ORnumber,
string),"\n"));
    end if:
    Buffer[k]:=FR[k]
  end if:
od:
fprintf(UniqueFR,"\n \n \n"):
for i from 1 to ORcounter
do

fprintf(UniqueFR,cat("OR",convert(i,string),"=",convert(uni
queOR[i],string),"\n"));
od:
fclose(AllFR):
fclose(UniqueFR):
> #uniqueOR;
> for i from 1 to ORcounter
do
 print(uniqueOR[i]);
 #fprintf(UniqueFR,cat("FR(",Steps[k],")=,", convert(FR[k],
string),",",convert(counter,string),"\n"));
od:
```

$$K\,CH4\,K\,H20\,C\,3\,H2\,C\,CO$$

$$K\,CH4\,K\,2\,H20\,C\,4\,H2\,C\,CO2$$

$$K\,H20\,C\,H2\,K\,CO\,C\,CO2$$

K *CH4* C 2 *CO* K *CO2* C 2 *H2*

```
>
##################################################################
##################################################################
########
##################################################################
##################################################################
########
##################################################################
##################################################################
########
##################################################################
##################################################################
########
>
```

Empty Routes Enumeration

```
> gammaM := Matrix(nES, nINTS+1): #reduced stoichiometric
submatrix
>
> for i to nINTS
do
  for j to nES
  do gammaM[j, i] := stoich[j+1, i+1]
  od:
od:
> for j from 1 to nES
do
   gammaM[j, nINTS+1] := stoich[j+1, nINTS+3]:
od:

> print("gammaM:=",gammaM);
```

"gammaM:=" *16 x 13 Matrix*
Data Type: anything
Storage: rectangular
Order: Fortran_order

```
> qp2:=Rank(gammaM)+1;
```

$$qp2 := 14$$

```
> ERmax := factorial(nES)/(factorial(nES-
qp2)*factorial(qp2));
```

$$ERmax := 120$$

```
> ERsubmatrix := Matrix(qp2-1, nINTS+1): #Submatrix used to
determine the Si coefficient in the reaction route
> Enumerated:=choose(nES,qp2):
>

AllER := fopen(AllER_file, WRITE):
UniqueER:= fopen(UniqueER_file,WRITE):
for k  from 1 to ERmax
do
 counter:=0:
 Steps[k]:="";
 for i from 1 to qp2
```

```
do
  for l from 1 to qp2-1
  do
    for m from 1 to nINTS+1
    do
      if (l=i)
         then jump:=1;
      end if;
      ERsubmatrix[l,m]:=gammaM[Enumerated[k,l+jump],m];
    od:
  od:
  Scoeff[i]:= (-1)^((i+1))*Determinant(ERsubmatrix);
  #print(Scoeff[i],i,k);
  jump:= 0;
 od:
 #Determine gcd of Scoeff
 g:=0;
 for i from 1 to qp2
 do
   g:= gcd(g,Scoeff[i]);
   if (g=1) then break end if:
 od:
 #Check sign of the first non-zero Si coefficient
 neg:=1:
 for i from 1 to qp2
 do
   if (Scoeff[i]<>0)
   then
     #print(Scoeff[i],i,k);
     if (Scoeff[i]<0)
     then
       neg:=-1;
       break;
     else
       neg:=1;
       break;
     end if;
   else
     neg:=0;
   end if;
 od:
 #Puts possible ER into "canonical" form
 for i from 1 to qp2
 do
   if (neg<>0) and (g<>0)
   then
     Scoeff[i]:=(Scoeff[i])/(neg*g);
```

```
    end if;
  od:
  ER[k]:=0;
  for i from 1 to qp2
  do

ER[k]:=ER[k]+convert(stoich[Enumerated[k,i]+1,1],symbol)*Sc
oeff[i];
    if (i<>qp2)
    then

Steps[k]:=cat(Steps[k],stoich[Enumerated[k,i]+1,1],";")
    else
Steps[k]:=cat(Steps[k],stoich[Enumerated[k,i]+1,1])
    end if:
  od:
  ###Check if the reaction obtained is "zero"
  OR[k]:=0;
  for i from 1 to qp2
  do
    for j from 2 to nSPECIES+1
    do

OR[k]:=OR[k]+Scoeff[i]*stoich[Enumerated[k,i]+1,j]*convert(
stoich[1,j],symbol);

##############################################################
###################
      #print("OR,Scoeff,stoich,stoich coeff,
i,j,k",OR[k],Scoeff[i],stoich[Enumerated[k,i]+1,j],stoich[1
,j],i,j,k);
    od:
    #print(" j loop end");
  od:
  #print("i loop end");
  #OR[k]:=simplify(OR[k]);
  #print("Final",OR[k],k);
  ERcheck[k]:=0:
  if (OR[k]=0)
  then
    ERcheck[k]:=1
  end if:
  fprintf(AllER,cat("ER(",Steps[k],")=", convert(ER[k],
string),"\n"));
  #print(cat("ER(",Steps[k],")=", convert(OR[k], string)));
  if (ERcheck[k]<>1)
  then
```

```
    Buffer[k]:=0;
  else
    unique:=1:
    for i from 1 to k-1
      do
        if (Buffer[i]=ER[k])
        then
          unique:=0:
          break:
        end if:
      od:
    if (unique=1)
    then
      for i from 1 to qp2
      do
        if (Scoeff[i]<>0) then counter:=counter+1 end if:
      od:
      fprintf(UniqueER,cat("ER(",Steps[k],")=,",
convert(ER[k], string),",",convert(counter,string),"\n"));
    end if:
  Buffer[k]:=ER[k]
  end if:
od:
fclose(AllER);
fclose(UniqueER);
>
#############################################################
#############################################################
########
#############################################################
#############################################################
########
#############################################################
#############################################################
########
#############################################################
#############################################################
########
>
```

Intermediate Nodes Enumeration

```
>
> intMT:=Transpose(intM);
```

$$intMT := \begin{bmatrix} 12 \text{ x } 16 \text{ Matrix} \\ \text{Data Type: anything} \\ \text{Storage: rectangular} \\ \text{Order: Fortran\_order} \end{bmatrix}$$

```
> nES;
> ES;
>
```

$$16$$

$$13$$

```
> q:=Rank(intMT);
```

$$q := 12$$

```
> INmax := factorial(nES)/(factorial(nES-(q-
1))*factorial(q-1));
```

$$INmax := 4368$$

```
> INsubmatrix := Matrix((q-1), (q-1) ): #Submatrix used to
determine the Si coefficient in the reaction route
> Enumerated:=choose(nES,q-1):
>
> AllIN := fopen(AllIN_file, WRITE):
UniqueIN:= fopen(UniqueIN_file,WRITE):
for k  from 1 to INmax
do
  counter:=0:
  jump:=0:
  Steps[k]:="";
  for l from 1 to nINTS
  do
    for i from 1 to q-1
    do
      for j from 1 to q-1
      do
        if (j=l) then jump:=1 end if:
```

```
          INsubmatrix[j,i]:=intMT[j+jump,Enumerated[k,i]];
          #print("something",i,j,k,l,jump);
        od:
        jump:=0:
      od:
      #jump:=0:
      #print(INsubmatrix);
      Qcoeff[l]:=(-1)^(l+1)*Determinant(INsubmatrix):
      #print("plus");
    od:
    #print("out");
    Steps:=cat("IN("):
    for i from 1 to nES
    do
      fait:=0:
      for j from 1 to q-1
      do
        if (i<>Enumerated[k,j]) and (fait=0)
        then
          Steps:=cat(Steps,stoich[i+1,1],";"):
          fait:=1:
        end if:
      od:
    od:
    Steps:=cat(Steps,")"):
    IN[k]:=0:
    for i from 1 to nINTS
    do
      IN[k]:=IN[k]+Qcoeff[i]*Q[i]:
      #print("do"):
    od:
    simplify(IN[k]):
    #fprintf(AllIN,cat(Steps,"=,
",convert(IN[k],string),"\n"));
    #Calculate individual Si coefficients
    for j from 1 to nES
    do
      Scoeff[j]:=0:
    od:
    #print("done");
    for i from 1 to nINTS
    do
      for j from 1 to nES
      do
        Scoeff[j]:=Scoeff[j]+Qcoeff[i]*stoich[j+1,i+1]:
        #print("OK");
      od:
```

```
  od:
  Scoeffprint:=0:
  for i from 1 to nES
  do
    Scoeffprint:=Scoeffprint+
Scoeff[i]*convert(stoich[i+1,1],symbol);
  od:
  #print(Scoeffprint);
  #Check sign of the first nonzero coeff
  neg:=1:
  for i from 1 to nES
  do
    if (Scoeff[i]<>0)
    then
      if (Scoeff[i]<0)
      then
        neg:=-1:
        break:
      else
        neg:=1:
        break:
      end if:
    else
      neg:=0:
    end:
  od:
  #Determine GCD of Scoeff
  g:=0:
  for i from 1 to nES
  do
    g:=gcd(g,Scoeff[i]):
    if (g=1) then break end if:
  od:
  #Puts IN into canonical form
  for i from 1 to nES
  do
    if (neg<>0) and (g<>0)
    then
      Scoeff[i]:=Scoeff[i]/(neg*g);
    end if:
  od:
    Scoeffprint:=0:
  for i from 1 to nES
  do
    Scoeffprint:=Scoeffprint+
Scoeff[i]*convert(stoich[i+1,1],symbol);
  od:
```

```
  fprintf(AllIN,cat(Steps,"=,
",convert(Scoeffprint,string),"\n"));
  #Determine Unique INs
  unique:=1:
  for i from 1 to k-1
  do
    if (Buffer[i]=Scoeffprint)
    then
      unique:=0:
      break:
    end if:
  od:
  if (unique=1)
  then
    Buffer[k]:=Scoeffprint:
    fprintf(UniqueIN,cat(Steps,"=,
",convert(Scoeffprint,string),"\n"));
  end if:
od:


> fclose(AllIN);
fclose(UniqueIN);
>
>
>
>
>
```

1

```
>

>
################################################################
################################################################
########
################################################################
################################################################
########
################################################################
################################################################
########
################################################################
################################################################
########
>
```

Appendix B: Reaction Mechanism Enumeration

Reaction Mechanism Enumeration

s_1: $CH_4 + S = CH_4{\cdot}S$
s_2: $H_2O + S = O{\cdot}S + H_2$
s_3: $CO{\cdot}S = CO + S$
s_4: $CO_2{\cdot}S = CO_2 + S$
s_5: $H{\cdot}S + H{\cdot}S = H_2{\cdot}S + S$
s_6: $H_2{\cdot}S = H_2 + S$
s_9: $CH_4{\cdot}S + S = CH_3{\cdot}S + H.S$
s_{10}: $CH_3{\cdot}S + S = CH_2{\cdot}S + H.S$
s_{14}: $CH_2{\cdot}S + O{\cdot}S = CH_2O{\cdot}S + S$
s_{15}: $CH_2O{\cdot}S + S = CHO{\cdot}S + H.S$
s_{16}: $CHO{\cdot}S + S = CO{\cdot}S + H.S$
s_{18}: $CHO{\cdot}S + O{\cdot}S = CO_2{\cdot}S + H{\cdot}S$
s_{17}: $CO{\cdot}S + O{\cdot}S = CO_2{\cdot}S + S$
s_{11}: CH2S + S = CHS + HS
s_{12}: CHS + S = CS + HS
s_{13}: CS + OS = COS + S

$OR_1 = -CH_4 - H_2O + CO + 3H_2 = 0$
$FR_1 = s_1+s_2+s_3+2*s_5+2*s_6+s_9+s_{10}+s_{14}+s_{15}+s_{16}$
$FR_2 = s_1+s_2+s_3+2*s_5+2*s_6+s_9+s_{10}+s_{11}+s_{12}+s_{13}$
$FR_3 = s_1+s_2+s_3+2*s_5+2*s_6+s_9+s_{10}+s_{14}+s_{15}+s_{18}-s_{17}$

$OR_2 = -CH_4 - {}_2H_2O + CO_2 + 4H_2 = 0$
$FR_4 = s_1+2*s_2+s_4+2*s_5+2*s_6+s_9+s_{10}+s_{17}+s_{11}+s_{12}+s_{13}$
$FR_5 = s_1+2*s_2+s_4+2*s_5+2*s_6+s_9+s_{10}-s_{16}+s_{18}+s_{11}+s_{12}+s_{13}$

$OR_3 = -H_2O - CO + CO_2 + H_2 = 0$
$FR_6 = s_2-s_3+s_4+s_{17}$
$FR_7 = s_2-s_3+s_4-s_{16}+s_{18}$
$FR_8 = s_2-s_3+s_4+s_{14}+s_{15}+s_{18}-s_{11}-s_{12}-s_{13}$

$OR_4 = -CH_4 - CO_2 + {}_2CO + {}_2H_2 = 0$
$FR_9 = s_1+2*s_3-s_4+2*s_5+2*s_6+s_9+s_{10}-s_{17}+s_{11}+s_{12}+s_{13}$
$FR_{10} = s_1+2*s_3-s_4+2*s_5+2*s_6+s_9+s_{10}+s_{14}+s_{15}+s_{16}-s_{17}$
$FR_{11} = s_1+2*s_3-s_4+2*s_5+2*s_6+s_9+s_{10}+s_{16}-s_{18}+s_{11}+s_{12}+s_{13}$
$FR_{12} = s_1+2*s_3-s_4+2*s_5+2*s_6+s_9+s_{10}+s_{14}+s_{15}+2*s_{16}-s_{18}$
$FR_{13} = s_1+2*s_3-s_4+2*s_5+2*s_6+s_9+s_{10}+s_{14}+s_{15}+s_{18}-2*s_{17}$
$FR_{14} = s_1+2*s_3-s_4+2*s_5+2*s_6+s_9+s_{10}-s_{14}-s_{15}-s_{18}+2*s_{11}+2*s_{12}+2*s_{13}$
$FR_{15} = s_1+2*s_3-s_4+2*s_5+2*s_6+s_9+s_{10}-s_{14}-s_{15}-s_{18}+2*s_{11}+2*s_{12}+2*s_{13}$

Empty Route Enumeration

$ER_1 = s_{16}-s_{18}+s_{17}$

$ER_2 = s_{14}+s_{15}+s_{16}-s_{11}-s_{12}-s_{13}$

$ER_3 = s_{14}+s_{15}+s_{18}-s_{17}-s_{11}-s_{12}-s_{13}$

Intermediate Node

$IN_1 = 2*s_1-s_5$

$IN_2 = 2*s_1-s_6$

$IN_3 = s_{11}-s_{12}$

$IN_4 = s_{11}-s_{13}$

$IN_5 = s_{12}-s_{13}$

$IN_6 = s_1-s_9$

$IN_7 = s_1-s_{10}$

$IN_8 = s_5-2*s_9$

$IN_9 = s_5-2*s_{10}$

$IN_{10} = s_5-s_6$

$IN_{11} = s_6-2*s_9$

$IN_{12} = s_6-2*s_{10}$

$IN_{13} = s_9-s_{10}$

$IN_{14} = s_{14}-s_{15}$

$IN_{15} = 2*s_1-s_2-s_3$

$IN_{16} = 2*s_2-2*s_4-s_5$

$IN_{17} = 2*s_2-2*s_4-s_6$

$IN_{18} = 2*s_3+2*s_4-s_5$

$IN_{19} = 2*s_3+2*s_4-s_6$

$IN_{20} = s_{15}-s_{16}-s_{18}$

$IN_{21} = s_1-s_{15}-s_{11}$

$IN_{22} = s_1-s_{15}-s_{12}$

$IN_{23} = s_1-s_{15}-s_{13}$

$IN_{24} = s_1-s_2+s_4$

$IN_{25} = s_1-s_3-s_4$

$IN_{26} = s_1-s_{14}-s_{11}$

$IN_{27} = s_1-s_{14}-s_{12}$

$IN_{28} = s_1-s_{14}-s_{13}$

$IN_{29} = s_2+s_3-2*s_9$

$IN_{30} = s_2+s_3-2*s_{10}$

$IN_{31} = s_2+s_3-s_5$

$IN_{32} = s_2+s_3-s_6$

$IN_{33} = s_2-s_3-2*s_4$

$IN_{34} = s_2-s_4-s_9$

$IN_{35} = s_2-s_4-s_{10}$

$IN_{36} = s_3+s_4-s_9$

$IN_{37} = s_3+s_4-s_{10}$

$IN_{38} = s_4-s_{18}-s_{17}$

$IN_{39} = s_6-2*s_{15}-2*s_{11}$

$IN_{40} = s_6-2*s_{15}-2*s_{12}$
$IN_{41} = s_6-2*s_{15}-2*s_{13}$
$IN_{42} = s_6-2*s_{14}-2*s_{11}$
$IN_{43} = s_6-2*s_{14}-2*s_{12}$
$IN_{44} = s_6-2*s_{14}-2*s_{13}$
$IN_{45} = s_9-s_{15}-s_{11}$
$IN_{46} = s_9-s_{15}-s_{12}$
$IN_{47} = s_9-s_{15}-s_{13}$
$IN_{48} = s_9-s_{14}-s_{11}$
$IN_{49} = s_9-s_{14}-s_{12}$
$IN_{50} = s_9-s_{14}-s_{13}$
$IN_{51} = s_{10}-s_{15}-s_{11}$
$IN_{52} = s_{10}-s_{15}-s_{12}$
$IN_{53} = s_{10}-s_{15}-s_{13}$
$IN_{54} = s_{10}-s_{14}-s_{11}$
$IN_{55} = s_{10}-s_{14}-s_{12}$
$IN_{56} = s_{10}-s_{14}-s_{13}$
$IN_{57} = s_{14}-s_{16}-s_{18}$
$IN_{58} = 2*s_2-s_5-2*s_{18}-2*s_{17}$
$IN_{59} = 2*s_2-s_6-2*s_{18}-2*s_{17}$
$IN_{60} = 2*s_3-s_5+2*s_{18}+2*s_{17}$
$IN_{61} = 2*s_3-s_6+2*s_{18}+2*s_{17}$
$IN_{62} = s_1-s_{16}-s_{18}-s_{11}$
$IN_{63} = s_1-s_{16}-s_{18}-s_{12}$
$IN_{64} = s_1-s_{16}-s_{18}-s_{13}$
$IN_{65} = s_1-s_2+s_{18}+s_{17}$
$IN_{66} = s_1-s_3-s_{18}-s_{17}$
$IN_{67} = s_2+s_3-2*s_{15}-2*s_{11}$
$IN_{68} = s_2+s_3-2*s_{15}-2*s_{12}$
$IN_{69} = s_2+s_3-2*s_{15}-2*s_{13}$
$IN_{70} = s_2+s_3-2*s_{14}-2*s_{11}$
$IN_{71} = s_2+s_3-2*s_{14}-2*s_{12}$
$IN_{72} = s_2+s_3-2*s_{14}-2*s_{13}$
$IN_{73} = s_2-s_3-2*s_{18}-2*s_{17}$
$IN_{74} = s_2-s_4-s_{15}-s_{11}$
$IN_{75} = s_2-s_4-s_{15}-s_{12}$
$IN_{76} = s_2-s_4-s_{15}-s_{13}$
$IN_{77} = s_2-s_4-s_{14}-s_{11}$
$IN_{78} = s_2-s_4-s_{14}-s_{12}$
$IN_{79} = s_2-s_4-s_{14}-s_{13}$
$IN_{80} = s_2-s_9-s_{18}-s_{17}$
$IN_{81} = s_2-s_{10}-s_{18}-s_{17}$
$IN_{82} = s_3+s_4-s_{15}-s_{11}$
$IN_{83} = s_3+s_4-s_{15}-s_{12}$
$IN_{84} = s_3+s_4-s_{15}-s_{13}$
$IN_{85} = s_3+s_4-s_{14}-s_{11}$

$IN_{86} = s_3+s_4-s_{14}-s_{12}$
$IN_{87} = s_3+s_4-s_{14}-s_{13}$
$IN_{88} = s_3-s_{16}+s_{17}-s_{11}$
$IN_{89} = s_3-s_{16}+s_{17}-s_{12}$
$IN_{90} = s_3-s_{16}+s_{17}-s_{13}$
$IN_{91} = s_3-s_9+s_{18}+s_{17}$
$IN_{92} = s_3-s_{10}+s_{18}+s_{17}$
$IN_{93} = s_4-s_{15}+s_{16}-s_{17}$
$IN_{94} = s_4-s_{14}+s_{16}-s_{17}$
$IN_{95} = s_5-2*s_{15}-2*s_{11}$
$IN_{96} = s_5-2*s_{15}-2*s_{12}$
$IN_{97} = s_5-2*s_{15}-2*s_{13}$
$IN_{98} = s_5-2*s_{16}-2*s_{18}-2*s_{11}$
$IN_{99} = s_5-2*s_{16}-2*s_{18}-2*s_{12}$
$IN_{100} = s_5-2*s_{16}-2*s_{18}-2*s_{13}$
$IN_{101} = s_5-2*s_{14}-2*s_{11}$
$IN_{102} = s_5-2*s_{14}-2*s_{12}$
$IN_{103} = s_5-2*s_{14}-2*s_{13}$
$IN_{104} = s_6-2*s_{16}-2*s_{18}-2*s_{11}$
$IN_{105} = s_6-2*s_{16}-2*s_{18}-2*s_{12}$
$IN_{106} = s_6-2*s_{16}-2*s_{18}-2*s_{13}$
$IN_{107} = s_9-s_{16}-s_{18}-s_{11}$
$IN_{108} = s_9-s_{16}-s_{18}-s_{12}$
$IN_{109} = s_9-s_{16}-s_{18}-s_{13}$
$IN_{110} = s_{10}-s_{16}-s_{18}-s_{11}$
$IN_{111} = s_{10}-s_{16}-s_{18}-s_{12}$
$IN_{112} = s_{10}-s_{16}-s_{18}-s_{13}$
$IN_{113} = 2*s_1-s_2-s_{16}+s_{17}-s_{11}$
$IN_{114} = 2*s_1-s_2-s_{16}+s_{17}-s_{12}$
$IN_{115} = 2*s_1-s_2-s_{16}+s_{17}-s_{13}$
$IN_{116} = 2*s_2-s_5-2*s_{15}+2*s_{16}-2*s_{17}$
$IN_{117} = 2*s_2-s_5-2*s_{14}+2*s_{16}-2*s_{17}$
$IN_{118} = 2*s_2-s_6-2*s_{15}+2*s_{16}-2*s_{17}$
$IN_{119} = 2*s_2-s_6-2*s_{14}+2*s_{16}-2*s_{17}$
$IN_{120} = 2*s_3-s_5+2*s_{15}-2*s_{16}+2*s_{17}$
$IN_{121} = 2*s_3-s_5+2*s_{14}-2*s_{16}+2*s_{17}$
$IN_{122} = 2*s_3-s_6+2*s_{15}-2*s_{16}+2*s_{17}$
$IN_{123} = 2*s_3-s_6+2*s_{14}-2*s_{16}+2*s_{17}$
$IN_{124} = 2*s_4-s_5+2*s_{16}-2*s_{17}+2*s_{11}$
$IN_{125} = 2*s_4-s_5+2*s_{16}-2*s_{17}+2*s_{12}$
$IN_{126} = 2*s_4-s_5+2*s_{16}-2*s_{17}+2*s_{13}$
$IN_{127} = 2*s_4-s_6+2*s_{16}-2*s_{17}+2*s_{11}$
$IN_{128} = 2*s_4-s_6+2*s_{16}-2*s_{17}+2*s_{12}$
$IN_{129} = 2*s_4-s_6+2*s_{16}-2*s_{17}+2*s_{13}$
$IN_{130} = s_1-s_2+s_{15}-s_{16}+s_{17}$
$IN_{131} = s_1-s_2+s_{14}-s_{16}+s_{17}$

$IN_{132} = s_1-s_3-s_{15}+s_{16}-s_{17}$

$IN_{133} = s_1-s_3-s_{14}+s_{16}-s_{17}$

$IN_{134} = s_1-s_4-s_{16}+s_{17}-s_{11}$

$IN_{135} = s_1-s_4-s_{16}+s_{17}-s_{12}$

$IN_{136} = s_1-s_4-s_{16}+s_{17}-s_{13}$

$IN_{137} = s_2+s_3-2*s_{16}-2*s_{18}-2*s_{11}$

$IN_{138} = s_2+s_3-2*s_{16}-2*s_{18}-2*s_{12}$

$IN_{139} = s_2+s_3-2*s_{16}-2*s_{18}-2*s_{13}$

$IN_{140} = s_2-2*s_{15}+s_{16}-s_{17}-s_{11}$

$IN_{141} = s_2-2*s_{15}+s_{16}-s_{17}-s_{12}$

$IN_{142} = s_2-2*s_{15}+s_{16}-s_{17}-s_{13}$

$IN_{143} = s_2-2*s_4-s_{16}+s_{17}-s_{11}$

$IN_{144} = s_2-2*s_4-s_{16}+s_{17}-s_{12}$

$IN_{145} = s_2-2*s_4-s_{16}+s_{17}-s_{13}$

$IN_{146} = s_2-2*s_9+s_{16}-s_{17}+s_{11}$

$IN_{147} = s_2-2*s_9+s_{16}-s_{17}+s_{12}$

$IN_{148} = s_2-2*s_9+s_{16}-s_{17}+s_{13}$

$IN_{149} = s_2-2*s_{10}+s_{16}-s_{17}+s_{11}$

$IN_{150} = s_2-2*s_{10}+s_{16}-s_{17}+s_{12}$

$IN_{151} = s_2-2*s_{10}+s_{16}-s_{17}+s_{13}$

$IN_{152} = s_2-2*s_{14}+s_{16}-s_{17}-s_{11}$

$IN_{153} = s_2-2*s_{14}+s_{16}-s_{17}-s_{12}$

$IN_{154} = s_2-2*s_{14}+s_{16}-s_{17}-s_{13}$

$IN_{155} = s_2-s_{15}-s_{18}-s_{17}-s_{11}$

$IN_{156} = s_2-s_{15}-s_{18}-s_{17}-s_{12}$

$IN_{157} = s_2-s_{15}-s_{18}-s_{17}-s_{13}$

$IN_{158} = s_2-s_{16}-2*s_{18}-s_{17}-s_{11}$

$IN_{159} = s_2-s_{16}-2*s_{18}-s_{17}-s_{12}$

$IN_{160} = s_2-s_{16}-2*s_{18}-s_{17}-s_{13}$

$IN_{161} = s_2-s_3-2*s_{15}+2*s_{16}-2*s_{17}$

$IN_{162} = s_2-s_3-2*s_{14}+2*s_{16}-2*s_{17}$

$IN_{163} = s_2-s_4-s_{16}-s_{18}-s_{11}$

$IN_{164} = s_2-s_4-s_{16}-s_{18}-s_{12}$

$IN_{165} = s_2-s_4-s_{16}-s_{18}-s_{13}$

$IN_{166} = s_2-s_5+s_{16}-s_{17}+s_{11}$

$IN_{167} = s_2-s_5+s_{16}-s_{17}+s_{12}$

$IN_{168} = s_2-s_5+s_{16}-s_{17}+s_{13}$

$IN_{169} = s_2-s_6+s_{16}-s_{17}+s_{11}$

$IN_{170} = s_2-s_6+s_{16}-s_{17}+s_{12}$

$IN_{171} = s_2-s_6+s_{16}-s_{17}+s_{13}$

$IN_{172} = s_2-s_9-s_{15}+s_{16}-s_{17}$

$IN_{173} = s_2-s_9-s_{14}+s_{16}-s_{17}$

$IN_{174} = s_2-s_{10}-s_{15}+s_{16}-s_{17}$

$IN_{175} = s_2-s_{10}-s_{14}+s_{16}-s_{17}$

$IN_{176} = s_2-s_{14}-s_{18}-s_{17}-s_{11}$

$IN_{177} = s_2-s_{14}-s_{18}-s_{17}-s_{12}$

$IN_{178} = s_2\text{-}s_{14}\text{-}s_{18}\text{-}s_{17}\text{-}s_{13}$
$IN_{179} = s_3\text{+}s_4\text{-}s_{16}\text{-}s_{18}\text{-}s_{11}$
$IN_{180} = s_3\text{+}s_4\text{-}s_{16}\text{-}s_{18}\text{-}s_{12}$
$IN_{181} = s_3\text{+}s_4\text{-}s_{16}\text{-}s_{18}\text{-}s_{13}$
$IN_{182} = s_3\text{-}s_{15}\text{+}s_{18}\text{+}s_{17}\text{-}s_{11}$
$IN_{183} = s_3\text{-}s_{15}\text{+}s_{18}\text{+}s_{17}\text{-}s_{12}$
$IN_{184} = s_3\text{-}s_{15}\text{+}s_{18}\text{+}s_{17}\text{-}s_{13}$
$IN_{185} = s_3\text{-}s_9\text{+}s_{15}\text{-}s_{16}\text{+}s_{17}$
$IN_{186} = s_3\text{-}s_9\text{+}s_{14}\text{-}s_{16}\text{+}s_{17}$
$IN_{187} = s_3\text{-}s_{10}\text{+}s_{15}\text{-}s_{16}\text{+}s_{17}$
$IN_{188} = s_3\text{-}s_{10}\text{+}s_{14}\text{-}s_{16}\text{+}s_{17}$
$IN_{189} = s_3\text{-}s_{14}\text{+}s_{18}\text{+}s_{17}\text{-}s_{11}$
$IN_{190} = s_3\text{-}s_{14}\text{+}s_{18}\text{+}s_{17}\text{-}s_{12}$
$IN_{191} = s_3\text{-}s_{14}\text{+}s_{18}\text{+}s_{17}\text{-}s_{13}$
$IN_{192} = s_4\text{-}s_9\text{+}s_{16}\text{-}s_{17}\text{+}s_{11}$
$IN_{193} = s_4\text{-}s_9\text{+}s_{16}\text{-}s_{17}\text{+}s_{12}$
$IN_{194} = s_4\text{-}s_9\text{+}s_{16}\text{-}s_{17}\text{+}s_{13}$
$IN_{195} = s_4\text{-}s_{10}\text{+}s_{16}\text{-}s_{17}\text{+}s_{11}$
$IN_{196} = s_4\text{-}s_{10}\text{+}s_{16}\text{-}s_{17}\text{+}s_{12}$
$IN_{197} = s_4\text{-}s_{10}\text{+}s_{16}\text{-}s_{17}\text{+}s_{13}$

Appendix C: Calibration Plots

GC Calibration — Hydrogen

volume H_2/ volume N_2	area H_2/ area N_2
0.0526	0.6419
0.1111	1.3262
0.1765	2.0845
0.2500	2.8922
0.3333	3.8458
0.4286	4.9081
0.5385	6.0770
0.6667	7.4732
0.8182	8.9820
1.0000	10.8664

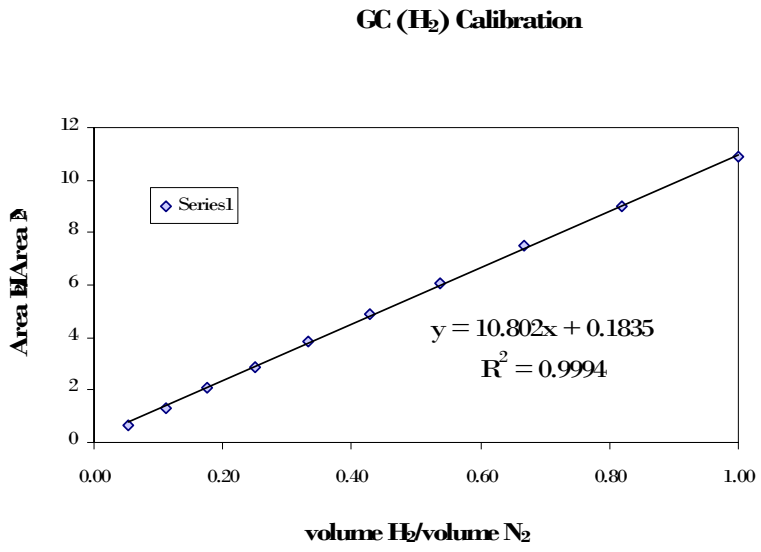

GC Calibration — Carbon Dioxide

volume CO/ volume N_2	area CO/ area N_2
0.0526	0.0626
0.1111	0.1194
0.1765	0.1903
0.2500	0.2590
0.3333	0.3457
0.4286	0.4389
0.5385	0.5429
0.6667	0.6846
0.8182	0.8271
1.0000	1.0135

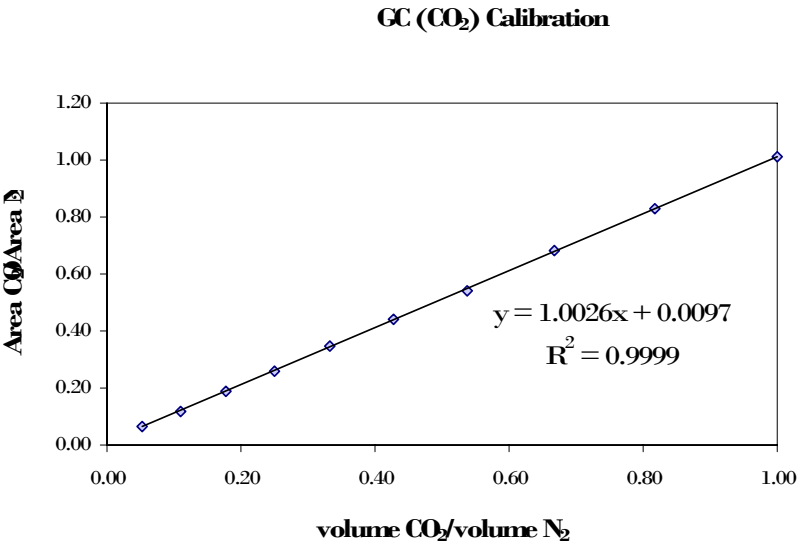

GC Calibration Carbon Monoxide

volume CO/ volume N_2	area CO/ area N_2
0.0526	0.0541
0.1111	0.1141
0.1765	0.1811
0.2500	0.2474
0.3333	0.3299
0.4286	0.4177
0.5385	0.5298
0.6667	0.6463
0.8182	0.7984
1.0000	0.9562

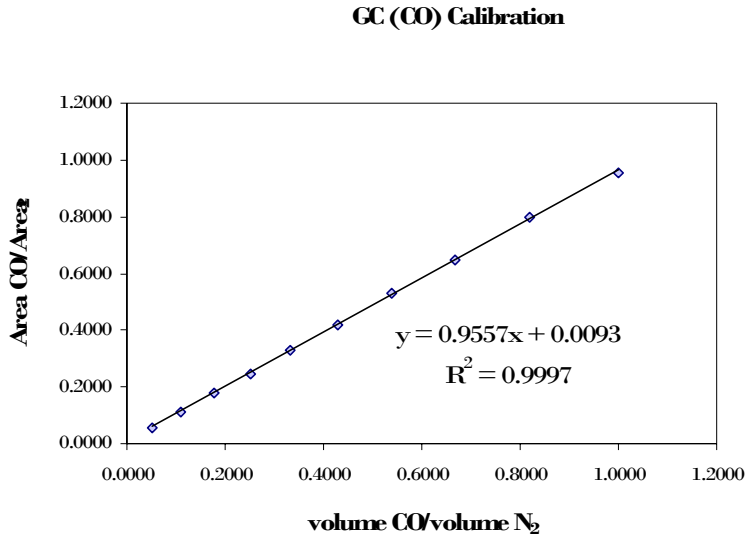

GC Calibration Methane

volume CO/ volume N_2	area CO/ area N_2
0.0526	0.0626
0.1111	0.1194
0.1765	0.1903
0.2500	0.2590
0.3333	0.3457
0.4286	0.4389
0.5385	0.5429
0.6667	0.6846
0.8182	0.8271
1.0000	1.0135

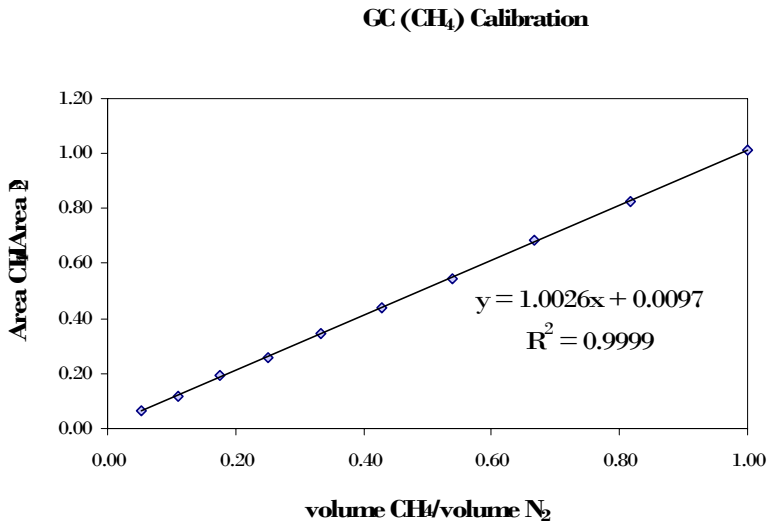

Mass Flow Controller

Carbon Monoxide

MFC Reading *mL/min*	Flow Meter Reading 1 *mL/min*	Flow Meter Reading 2 *mL/min*	Flow Meter Reading 3 *mL/min*	Flow Meter Reading 4 *mL/min*	Actual Flow Rate *mL/min*	Actual Flow Error	Set Point Value *mL/min*
0.0							
2.0							
5.0	4.43	4.43	4.45	4.41	4.43	0.02	5.2
7.0							
10.0	8.08	8.09	8.12	8.02	8.08	0.04	10.2
12.0							
15.0	11.8	11.8	11.8	11.8	11.80	0.00	
20.0	15.5	15.5	15.5	15.5	15.50	0.00	20.1
25.0	19.2	19.3	19.2	19.2	19.23	0.05	25.2
30.0	22.6	23.0	22.9	23.0	22.88	0.19	30.2
40.0	30.3	30.5	30.5	30.3	30.40	0.12	40.2

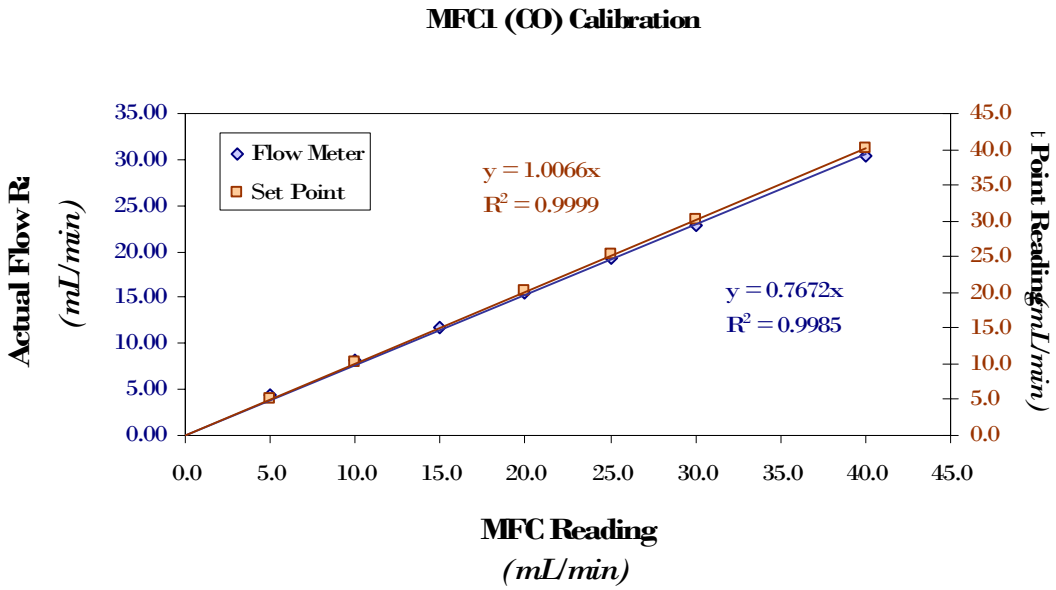

Hydrogen

MFC Reading *mL/min*	Flow Meter Reading 1 *mL/min*	Flow Meter Reading 2 *mL/min*	Flow Meter Reading 3 *mL/min*	Flow Meter Reading 4 *mL/min*	Actual Flow Rate *mL/min*	Actual Flow Error	Set Point Value *mL/min*
0.0	0.00	0.00	0.00	0.00	0.00	0.00	0.0
2.0	1.52	1.52	1.52	1.52	1.52	0.00	2.2
5.0	4.61	4.65	4.64	4.65	4.64	0.02	5.2
7.0	6.82	6.73	6.66	6.63	6.71	0.08	7.2
10.0	10.00	9.94	9.95	9.75	9.91	0.11	10.2
12.1	12.1	11.9	12.1	12.1	12.05	0.10	12.2
15.0	15.2	15.5	15.5	15.4	15.40	0.14	15.2
20.0	20.8	20.8	20.7	20.6	20.73	0.10	20.2
25.0	26.2	26.1	26.0	26.0	26.08	0.10	25.2
30.0	31.3	31.3	31.4	31.3	31.33	0.05	30.1
40.0	41.6	41.9	41.7	41.9	41.78	0.15	40.1

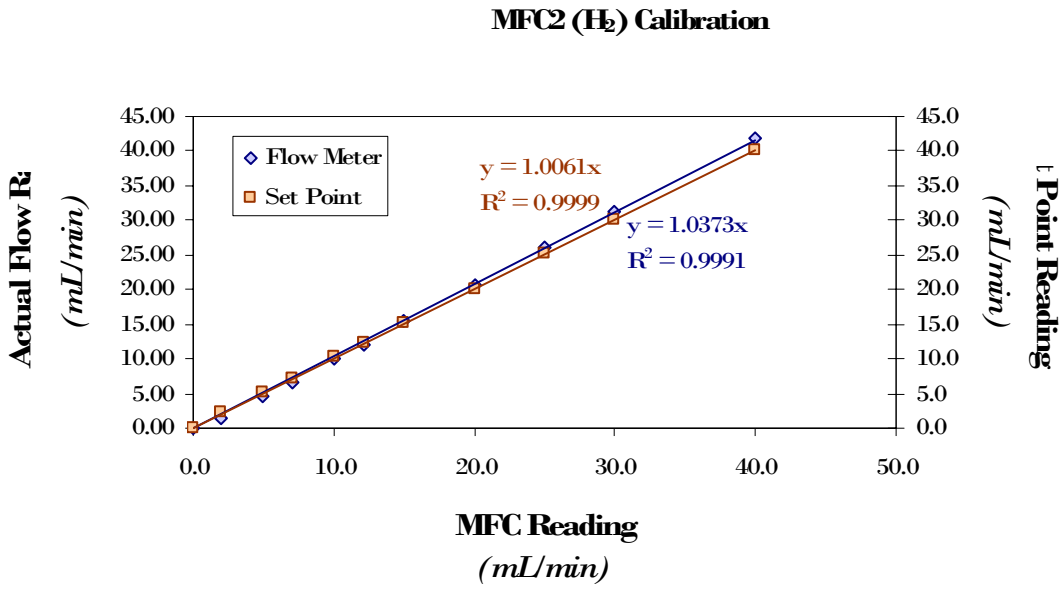

Carbon Dioxide

MFC Reading *mL/min*	Flow Meter Reading 1 *mL/min*	Flow Meter Reading 2 *mL/min*	Flow Meter Reading 3 *mL/min*	Flow Meter Reading 4 *mL/min*	Actual Flow Rate *mL/min*	Actual Flow Error	Set Point Value *mL/min*
0.0							
2.0							
5.0							
7.0							
10.0	8.03	8.02	8.00	7.99	8.01	0.02	10.0
12.0							12.0
15.0	12.0	11.9	12.0	12.0	11.98	0.05	15.0
20.0	15.8	15.7	15.9	16.0	15.85	0.13	20.0
25.0	19.8	19.9	19.9	20.1	19.93	0.13	25.0
30.0	23.2	23.8	23.1	23.0	23.28	0.36	30.0
40.0	31.4	31.5	31.6	31.6	31.53	0.10	40.0

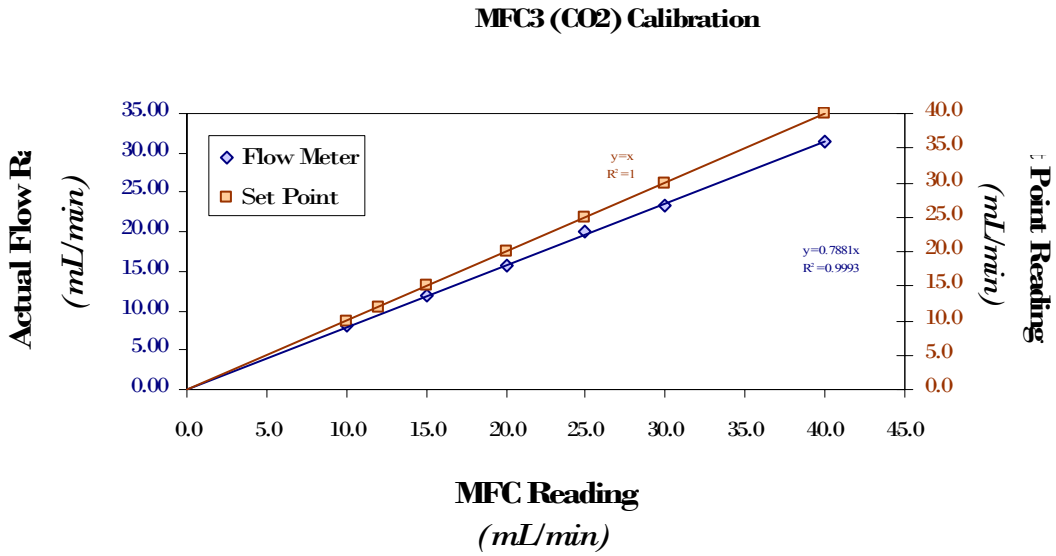

Nitrogen

MFC Reading *mL/min*	Flow Meter Reading 1 *mL/min*	Flow Meter Reading 2 *mL/min*	Flow Meter Reading 3 *mL/min*	Flow Meter Reading 4 *mL/min*	Actual Flow Rate *mL/min*	Actual Flow Error	Set Point Value *mL/min*
0.0							
10.0	8.10	8.15	8.12	8.14	8.13	0.02	10.1
20.0	16.0	16.0	16.2	16.0	16.05	0.10	20.1
30.0	23.8	23.9	23.9	24.0	23.90	0.08	30.1
40.0	31.3	31.2	31.7	31.7	31.48	0.26	40.1
50.0	37.5	37.4	37.7	37.9	37.63	0.22	50.1
60.0	44.9	44.6	44.7	45.0	44.80	0.18	60.1
70.0	52.4	52.5	52.3	52.6	52.45	0.13	70.1
80.0	60.6	60.7	60.7	61.0	60.75	0.17	80.1
90.0	69.3	69.2	68.7	68.0	68.80	0.59	90.1
100.0	77.6	78.0	77.0	77.2	77.45	0.44	100.1

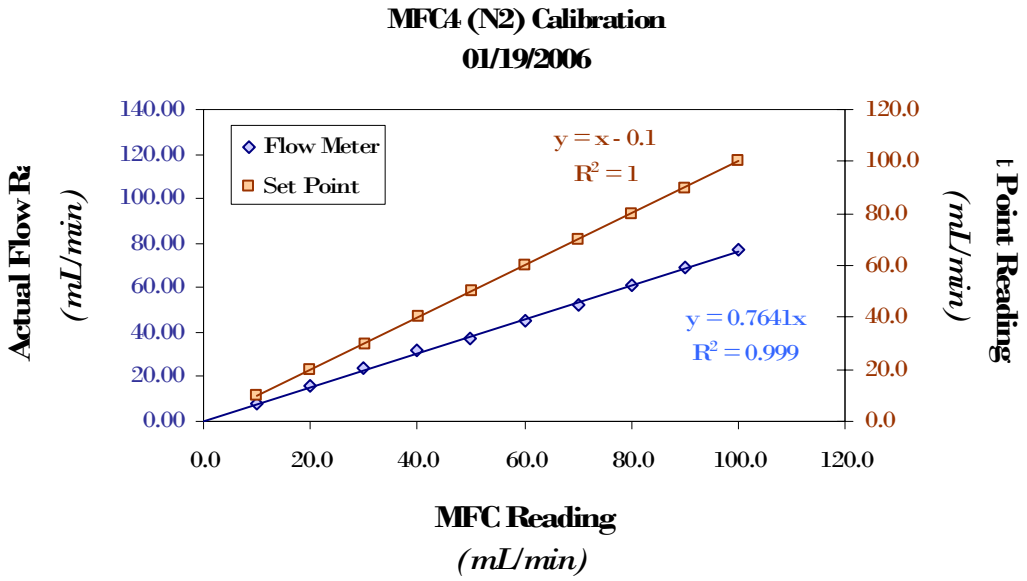

Methane

MFC Reading *mL/min*	Flow Meter Reading 1 *mL/min*	Flow Meter Reading 2 *mL/min*	Flow Meter Reading 3 *mL/min*	Flow Meter Reading 4 *mL/min*	Actual Flow Rate *mL/min*	Actual Flow Error	Set Point Value *mL/min*
0.0							
2.0							2
5.0	2.98	2.98	2.97	2.98	2.9775	0.005	5
7.0	4.16	4.13	4.16	4.17	4.155	0.0173205	7
10.0	5.96	5.94	5.98	5.96	5.96	0.0163299	10
12.0	7.16	7.11	7.19	7.18	7.16	0.0355903	12
15.0	9.06	9.13	8.94	8.9	9.0075	0.1062623	15
20.0	12.1	11.9	12	12	12	0.0816497	20
25.0	15	15.1	15	15	15.025	0.05	25
30.0	18	18	17.6	18	17.9	0.2	30
40.0	24.1	24	24	24	24.025	0.05	40

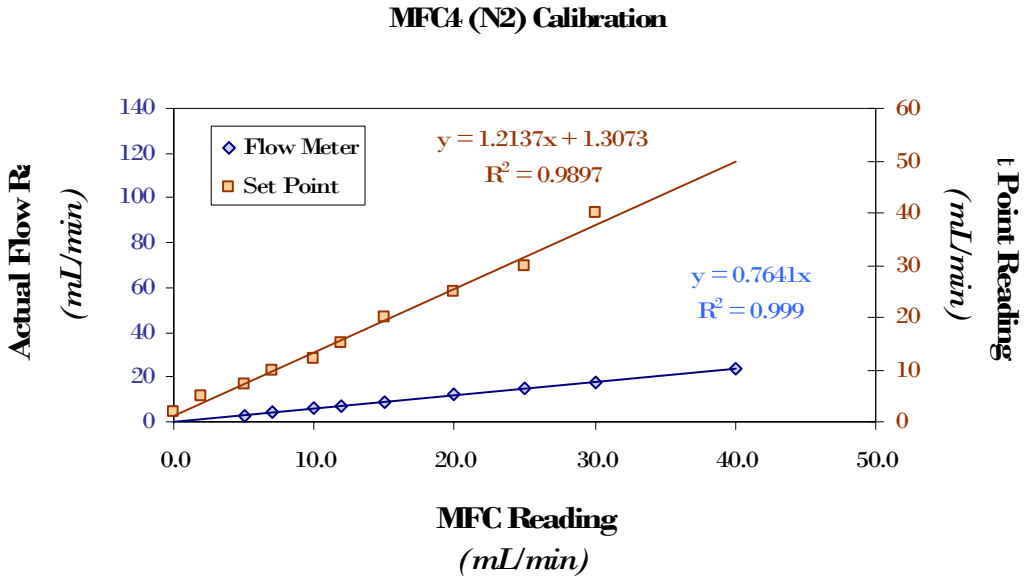

Appendix D: Reaction Route Graphs

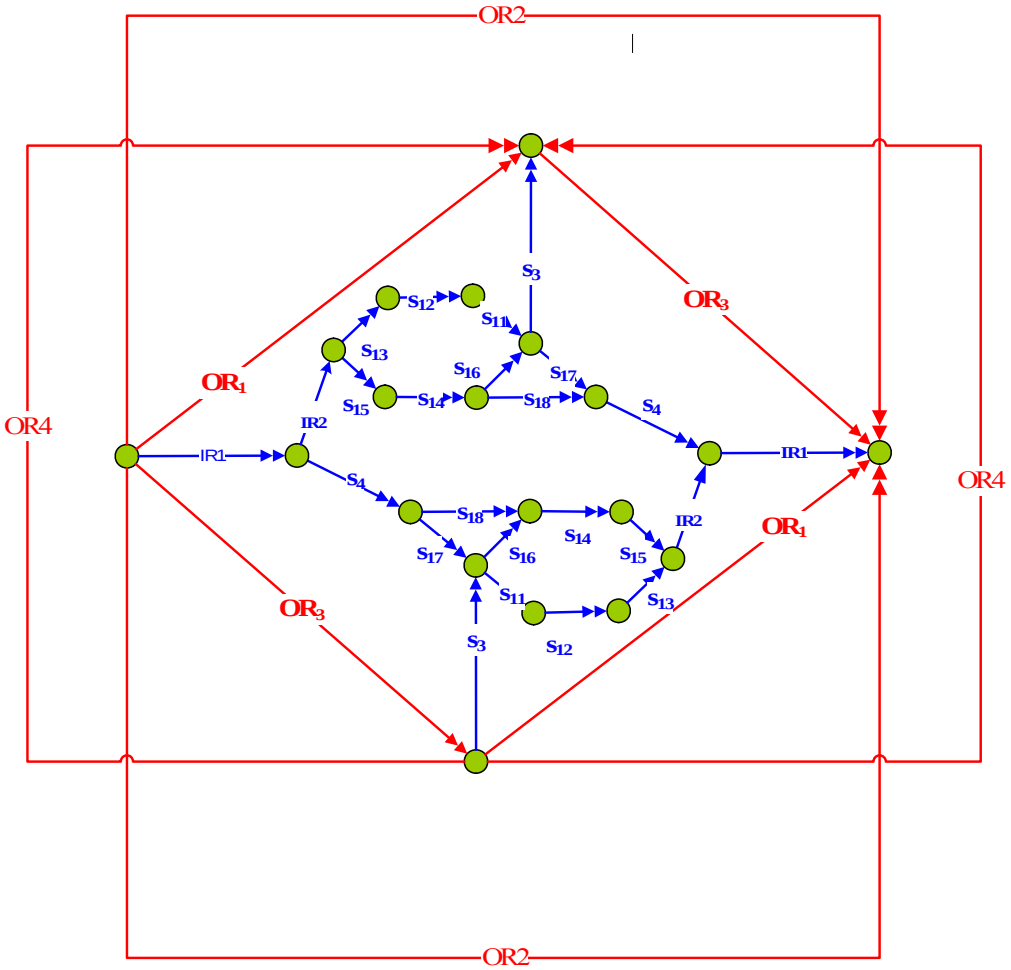

Micro-kinetic Model Mechanism

s_1: $CH_4 + S = CH_4{\cdot}S$
s_2: $H_2O + S = H_2O{\cdot}S$
s_3: $CO{\cdot}S = CO + S$
s_4: $CO_2{\cdot}S = CO_2 + S$
s_5: $HS + HS = H_2{\cdot}S + S$
s_6: $H_2{\cdot}S = H_2 + S$
s_7: $H_2O{\cdot}S + S = OH{\cdot}S + H{\cdot}S$
s_8: $OH{\cdot}S + S = O{\cdot}S + H{\cdot}S$
s_9: $CH_4{\cdot}S + S = CH_3{\cdot}S + H{\cdot}S$
s_{10}: $CH_3{\cdot}S + S = CH_2{\cdot}S + H{\cdot}S$
s_{11}: $CH_2{\cdot}S + S = CH{\cdot}S + H{\cdot}S$
s_{12}: $CH{\cdot}S + S = C{\cdot}S + H{\cdot}S$
s_{13}: $C{\cdot}S + O{\cdot}S = CO{\cdot}S + S$
s_{14}: $CH_2{\cdot}S + O{\cdot}S = CH_2O{\cdot}S + S$
s_{15}: $CH_2O{\cdot}S + S = CHO{\cdot}S + H{\cdot}S$
s_{16}: $CHO{\cdot}S + S = CO{\cdot}S + H{\cdot}S$
s_{17}: $CO{\cdot}S + O{\cdot}S = CO_2{\cdot}S + S$
s_{18}: $CHO{\cdot}S + O{\cdot}S = CO_2{\cdot}S + H{\cdot}S$

Overall Reactions

OR1: $CH_4 + H_2O = CO + 3H_2$
OR2: $CH_4 + 2H_2O = CO_2 + 4H_2$
OR3: $H_2O + CO = CO_2 + H_2$
OR4: $CH_4 + CO_2 = 2CO + 2H_2$

s_2: $H2O + S = H2O{\cdot}S$
s_5: $HS + HS = H2S + S$
s_6: $H2S = H2 + S$
s_7: $H2O{\cdot}S + S = OH{\cdot}S + H{\cdot}S$
$\underline{s_8}$: $\underline{OH{\cdot}S + S = O{\cdot}S + H{\cdot}S}$
IR1: $H2O + S = O{\cdot}S + H2$

s_1: $CH_4 + S = CH_4{\cdot}S$
$2s_5$: $2H{\cdot}S + 2H{\cdot}S = 2H_2{\cdot}S + 2S$
$2s_6$: $2H_2{\cdot}S = 2H_2 + 2S$
s_9: $CH_4{\cdot}S + S = CH_3{\cdot}S + H{\cdot}S$
$\underline{s_{10}}$: $\underline{CH_3{\cdot}S + S = CH_2{\cdot}S + H{\cdot}S}$
IR2: $CH_4 + 2HS - 2H_2 - S - CH_2S$

Xu and Froment's Mechanism + 3 Carbon Formation Steps

s_1: $CH_4 + S = CH_4{\cdot}S$
IR_1: $H_2O + S = O{\cdot}S + H_2$
s_3: $CO{\cdot}S = CO + S$
s_4: $CO_2{\cdot}S = CO_2 + S$
s_5: $HS + HS = H_2{\cdot}S + S$
s_6: $H_2{\cdot}S = H_2 + S$
s_9: $CH_4{\cdot}S + S = CH_3{\cdot}S + H{\cdot}S$
s_{10}: $CH_3{\cdot}S + S = CH_2{\cdot}S + H{\cdot}S$
s_{11}: $CH_2{\cdot}S + S = CH{\cdot}S + H{\cdot}S$
s_{12}: $CH{\cdot}S + S = C{\cdot}S + H{\cdot}S$
s_{13}: $C{\cdot}S + O{\cdot}S = CO{\cdot}S + S$
s_{14}: $CH_2{\cdot}S + O{\cdot}S = CH_2O{\cdot}S + S$
s_{15}: $CH_2O{\cdot}S + S = CHO{\cdot}S + H{\cdot}S$
s_{16}: $CHO{\cdot}S + S = CO{\cdot}S + H{\cdot}S$
s_{17}: $CO{\cdot}S + O{\cdot}S = CO_2{\cdot}S + S$
s_{18}: $CHO{\cdot}S + O{\cdot}S = CO_2{\cdot}S + H{\cdot}S$

Figure 28 Complete Reaction Route Graph Labeled with Xu and Froment's Mechanism + 3 Carbon Formation Steps and Using the 18 Step Mechanism for Micro-Kinetic Simulation

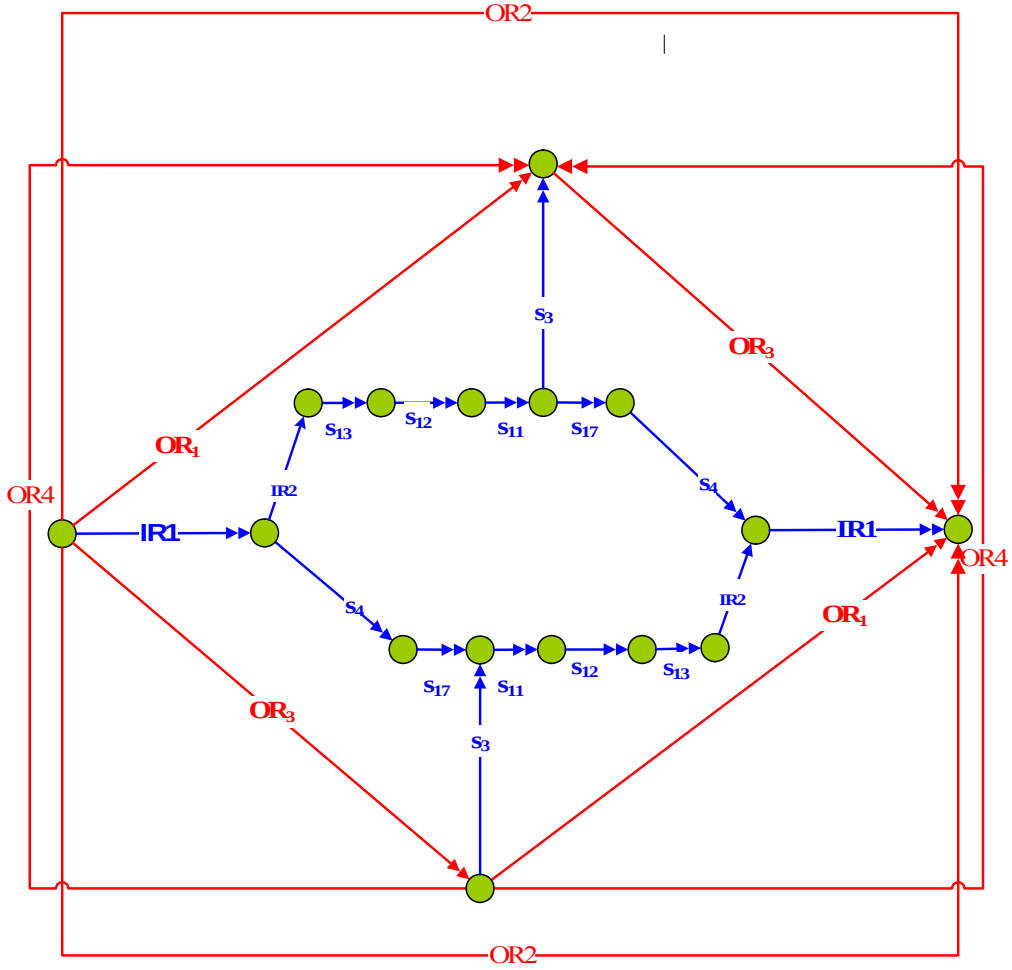

Micro-kinetic Model Mechanism

s_1: $CH_4 + S = CH_4{\cdot}S$
s_2: $H_2O + S = H_2O{\cdot}S$
s_3: $CO{\cdot}S = CO + S$
s_4: $CO_2{\cdot}S = CO_2 + S$
s_5: $HS + HS = H_2{\cdot}S + S$
s_6: $H_2{\cdot}S = H_2 + S$
s_7: $H_2O{\cdot}S + S = OH{\cdot}S + HS$
s_8: $OH{\cdot}S + S = O{\cdot}S + HS$
s_9: $CH_4{\cdot}S + S = CH_3{\cdot}S + HS$
s_{10}: $CH_3{\cdot}S + S = CH_2{\cdot}S + HS$
s_{11}: $CH_2{\cdot}S + S = CHS + HS$
s_{12}: $CHS + S = CS + HS$
s_{13}: $CS + OS = COS + S$
s_{14}: $CH_2{\cdot}S + OS = CH_2OS + S$
s_{15}: $CH_2OS + S = CHOS + HS$
s_{16}: $CHOS + S = COS + HS$
s_{17}: $COS + OS = CO_2{\cdot}S + S$
s_{18}: $CHOS + OS = CO_2{\cdot}S + HS$

Overall Reactions

OR1: $CH_4 + H_2O = CO + 3H_2$
OR2: $CH_4 + 2H_2O = CO_2 + 4H_2$
OR3: $H_2O + CO = CO_2 + H_2$
OR4: $CH_4 + CO_2 = 2CO + 2H_2$

s_2: $H2O + S = H2O{\cdot}S$
s_5: $HS + HS = H2S + S$
s_6: $H2S = H2 + S$
s_7: $H2OS + S = OHS + HS$
s_8: $OHS + S = OS + HS$
IR1: $H2O + S = O{\cdot}S + H2$

s_1: $CH_4 + S = CH_4{\cdot}S$
$2s_5$: $2HS + 2HS = 2H_2{\cdot}S + 2S$
$2s_6$: $2H_2{\cdot}S = 2H_2 + 2S$
s_9: $CH_4S + S = CH_3{\cdot}S + HS$
s_{10}: $CH_3{\cdot}S + S = CH_2{\cdot}S + HS$
IR2: $CH_4 + 2HS - 2H_2 - S - CH_2S$

Xu and Froment's Mechanism + 3 Carbon Formation Steps

s_1: $CH_4 + S = CH_4{\cdot}S$
IR_1: $H_2O + S = OS + H_2$
s_3: $CO{\cdot}S = CO + S$
s_4: $CO_2{\cdot}S = CO_2 + S$
s_5: $HS + HS = H_2{\cdot}S + S$
s_6: $H_2{\cdot}S = H_2 + S$
s_9: $CH_4{\cdot}S + S = CH_3{\cdot}S + HS$
s_{10}: $CH_3{\cdot}S + S = CH_2{\cdot}S + HS$
s_{11}: $CH_2{\cdot}S + S = CHS + HS$
s_{12}: $CHS + S = CS + HS$
s_{13}: $CS + OS = COS + S$
s_{14}: $CH_2{\cdot}S + OS = CH_2OS + S$
s_{15}: $CH_2OS + S = CHOS + HS$
s_{16}: $CHOS + S = COS + HS$
s_{17}: $COS + OS = CO_2{\cdot}S + S$
s_{18}: $CHOS + OS = CO_2{\cdot}S + HS$

Figure 29 Reduced Reaction Route Graph with Removal of Steps s_9, s_{10}, and s_{12}

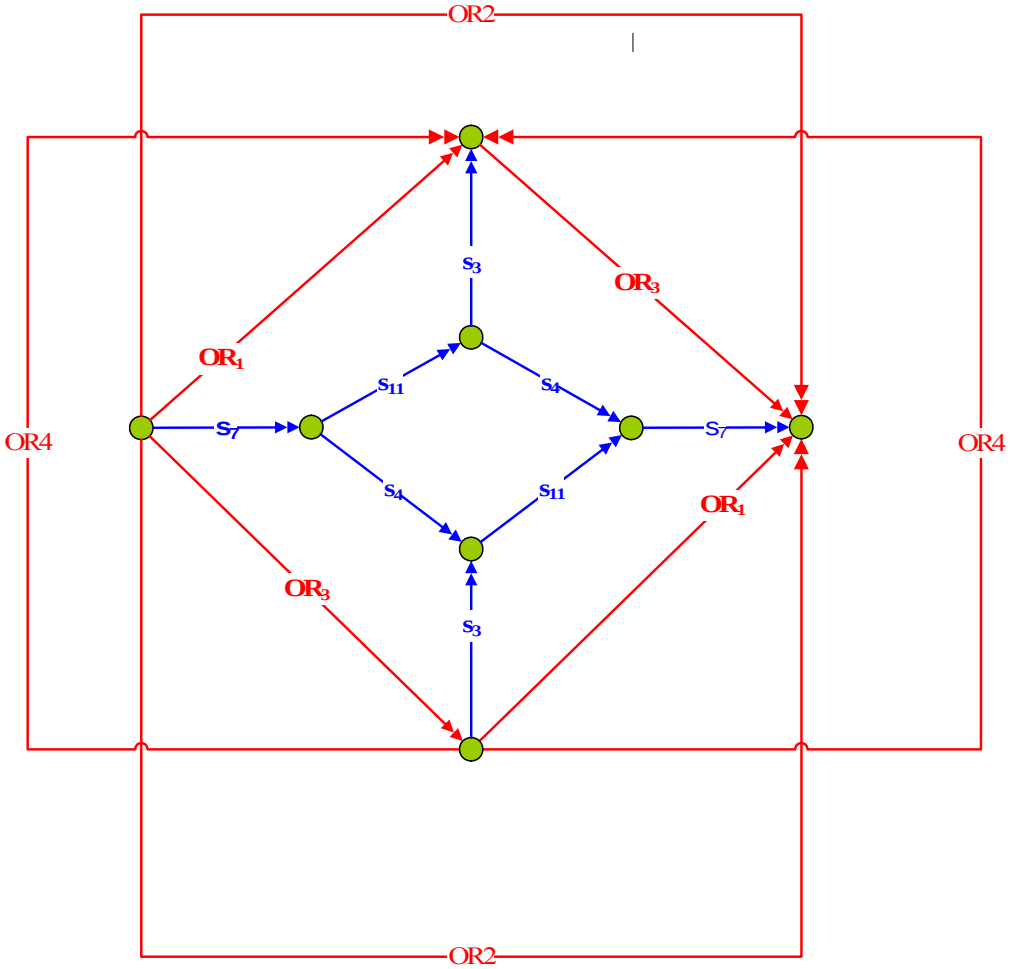

Micro-kinetic Model Mechanism

s_1: $CH_4 + S = CH_4{\cdot}S$
s_2: $H_2O + S = H_2O{\cdot}S$
s_3: $CO{\cdot}S = CO + S$
s_4: $CO_2{\cdot}S = CO_2 + S$
s_5: $HS + HS = H_2{\cdot}S + S$
s_6: $H_2{\cdot}S = H_2 + S$
s_7: $H_2O{\cdot}S + S = OH{\cdot}S + H{\cdot}S$
s_8: $OH{\cdot}S + S = O{\cdot}S + H{\cdot}S$
s_9: $CH_4{\cdot}S + S = CH_3{\cdot}S + H{\cdot}S$
s_{10}: $CH_3{\cdot}S + S = CH_2{\cdot}S + H{\cdot}S$
s_{11}: $CH_2{\cdot}S + S = CH{\cdot}S + H{\cdot}S$
s_{12}: $CH{\cdot}S + S = C{\cdot}S + H{\cdot}S$
s_{13}: $C{\cdot}S + O{\cdot}S = COS + S$
s_{14}: $CH_2{\cdot}S + O{\cdot}S = CH_2O{\cdot}S + S$
s_{15}: $CH_2O{\cdot}S + S = CHO{\cdot}S + H{\cdot}S$
s_{16}: $CHO{\cdot}S + S = CO{\cdot}S + H{\cdot}S$
s_{17}: $CO{\cdot}S + O{\cdot}S = CO_2{\cdot}S + S$
s_{18}: $CHO{\cdot}S + O{\cdot}S = CO_2{\cdot}S + H{\cdot}S$

Overall Reactions

OR1: $CH_4 + H_2O = CO + 3H_2$
OR2: $CH_4 + 2H_2O = CO_2 + 4H_2$
OR3: $H_2O + CO = CO_2 + H_2$
OR4: $CH_4 + CO_2 = 2CO + 2H_2$

s_2: $H2O + S = H2O{\cdot}S$
s_5: $HS + HS = H2S + S$
s_6: $H2S = H2 + S$
s_7: $H2OS + S = OHS + HS$
$\underline{s_8}$: $\underline{OHS + S = OS + HS}$
IR1: $H2O + S = O.S + H2$

s_1: $CH_4 + S = CH_4{\cdot}S$
$2s_5$: $2H{\cdot}S + 2H{\cdot}S = 2H_2{\cdot}S + 2S$
$2s_6$: $2H_2{\cdot}S = 2H_2 + 2S$
s_9: $CH_4{\cdot}S + S = CH_3{\cdot}S + H.S$
$\underline{s_{10}}$: $\underline{CH_3{\cdot}S + S = CH_2{\cdot}S + H.S}$
IR2: $CH_4 + 2HS - 2H_2 - S - CH_2S$

Xu and Froment's Mechanism + 3 Carbon Formation Steps

s_1: $CH_4 + S = CH_4{\cdot}S$
IR$_1$: $H_2O + S = O{\cdot}S + H_2$
s_3: $CO{\cdot}S = CO + S$
s_4: $CO_2{\cdot}S = CO_2 + S$
s_5: $HS + HS = H_2{\cdot}S + S$
s_6: $H_2{\cdot}S = H_2 + S$
s_9: $CH_4{\cdot}S + S = CH_3{\cdot}S + H.S$
s_{10}: $CH_3{\cdot}S + S = CH_2{\cdot}S + H.S$
s_{11}: $CH_2{\cdot}S + S = CH{\cdot}S + H{\cdot}S$
s_{12}: $CH{\cdot}S + S = C{\cdot}S + H{\cdot}S$
s_{13}: $C{\cdot}S + O{\cdot}S = COS + S$
s_{14}: $CH_2{\cdot}S + O{\cdot}S = CH_2O{\cdot}S + S$
s_{15}: $CH_2O{\cdot}S + S = CHO{\cdot}S + H.S$
s_{16}: $CHO{\cdot}S + S = CO{\cdot}S + H.S$
s_{17}: $CO{\cdot}S + O{\cdot}S = CO_2{\cdot}S + S$
s_{18}: $CHO{\cdot}S + O{\cdot}S = CO_2{\cdot}S + H{\cdot}S$

Figure 30 Final Reduced Graph